FIELD and LABORATORY TESTS of LATERALLY LOADED ROWS of LIME-CEMENT COLUMNS

Razvan Ignat

Licentiate Thesis

Department of Civil and Architectural Engineering

Division of Soil and Rock Mechanics

KTH, Royal Institute of Technology

Stockholm, 2015

TRISTA-JOB LIC 2028

ISSN 1650-951x

PREFACE

The work presented in this thesis was conducted between February 2012 and April 2015 at Skanska Teknik, Geotechnical Department, and the Division of Soil and Rock Mechanics, Department of Civil and Architectural Engineering, Royal Institute of Technology, Stockholm, Sweden. The work was supervised by Professor Stefan Larsson, Head of the Division of Soil and Rock Mechanics, with assistance from Dr Sadek Baker and Dr Sven Liedberg.

I would like to express my gratitude to the Development Fund of the Swedish Construction Industry (SBUF), the Swedish Transport Administration (TV), Cementa and Skanska, whose financial support made this research project possible. Sincere thanks go to Johan Jandelius at Skanska Foundation, Ivar Nöre and Patrick Andersson at Geometrik and Ingemar Forsgren at Ingefors Geoteknik AB for their commitment and contribution in the execution of the field tests.

The warmest of acknowledgement I would like to give to my supervisors Professor Stefan Larsson, Dr Sadek Baker and Dr Sven Liedberg for their encouragement and great support through this project. I would also like to thank all my colleagues at Skanska Teknik and KTH for their support during those years.

Finally, I would like to thank my family – my beloved wife Heam, for her unconditional support and understanding, my sons Victor and Julian, for all the joy, love and happiness they bring to my life, and the rest of my family for their help in making this work possible.

Stockholm, May 2015

Razvan Ignat

SUMMARY

Due to the increased need for infrastructure in areas with poor soil condition there is increasing interest for new methods and new applications of existing methods in order to provide safe and cost-effective foundation structures. One such method that has been used internationally with good results when excavations are to be performed in locations with thick soft clay deposits is to install column-type ground improvement on the passive side in interaction with a retaining structure. This has proven to significantly reduce the excavation induced deflections behind the retaining structure, reduce structural forces and improve safety against basal heave failure. Although this application has been used with good results internationally, there are very few cases in Sweden where this application has been used. Due to uncertainties regarding behavior of laterally loaded lime-cement columns the shear strength of laterally loaded lime-cement columns installed in the passive zone is significantly reduced according to the current design praxis, which implies that the effect of ground improvement conducted in the passive zone will be very limited.

In order to increase the application of the method to include construction where deep mixing columns are laterally loaded such as excavation support, permanent slopes where ground improvement is conducted in shear and passive zone and high embankments, reliable design model for laterally loaded columns needs to be developed and implemented.

The objective of this research project is to increase knowledge and understanding of the behavior of laterally loaded lime-cement columns installed in shear and passive zones. This licentiate thesis presents the first part of the research project and focuses on investigating strength and stiffness properties of laboratory stabilized soil and the execution of a full-scale field test where the behavior of laterally loaded rows of lime-cement columns has been documented.

The most important findings and conclusions from this study are:

- Behavior of lime-cement columns subjected to extension loading is very similar to an overconsolidated material.
- Failure due to extension loading will occur along a weak zone in the sample, i.e. the weakest link theory where the weakest link determines the strength of the chain.
- Field tests show that column-type ground improvement of the clay installed as rows of overlapping columns in the passive zone of the sheet pile wall will significantly increase the capacity of the structure and reduce excavation and loading induced deformations in the soil both on the active and passive side of the sheet pile wall.
- Excavation and load induced stress increment is transferred mainly to the column rows that forms a “strut-like effect” below the bottom of the excavation.
- Interaction between the column rows and the clay between the rows increased with decreasing distance between the rows.
- For a distance between the rows of 3.0 m, failure occurred only in the clay between the rows and resulted in a brittle failure mechanism.

SAMMANFATTNING

Ett större behov av infrastruktur i områden med dåliga markförhållanden har medfört ökat interesse för nya metoder och nya appliceringar av befintliga metoder i avsikt att erbjuda säkra och kostnadseffektiva konstruktioner. En metod som internationellt har använts med goda resultat för djupa schakter i områden där lösa lerlager med stor mäktighet förekommer är jordförstärkning genom djupstabilisering med pelare (oftast cement) i passiv zonen av olika typer av stödkonstruktioner. Detta har visat sig att signifikant minska schakt inducerade deformationer bakom stödkonstruktionen, minska resulterande krafter i stödkonstruktionen samt öka säkerheten mot bottenupptryckning. Även om denna metod har använts med goda resultat internationellt, finns det väldigt få dokumenterade fall i Sverige där metoden använts. På grund av osäkerhet relaterad till materialbeteende och brottmekanismer för kalk-cement pelare som utsätts för lateralt och drag belastning, en väsentlig reduktion av hållfastheten tillämpas för pelare installerade i skjuv- och passiv zon i enlighet med den nuvarande dimensioneringspraxisen, vilket medför att effekten av förstärkning i skjuv och passiv zon blir mycket begränsad.

För att öka möjligheten att djupstabilisering med kalk-cement pelare tillämpas i fall där pelarna utsätts för lateral och drag belastning såsom stabilisering av djupa schakter, stabilisering av slänter och höga bankar i passiv zone, en tillförlitlig modell för dimensionering är nödvändigt.

Målet med denna forskning projekt är att öka kunskapen och förståelsen kring kalk-cement pelares beteende och verkningssätt i passiv och direkt skjuvzon. I denna licentiat avhandling presenteras resultat av den första delen av forskning projektet med fokus på undersökning av hållfasthet och styvhetsegenskaper av laboratorier stabiliserade prover samt utförande av ett fält försök där beteendet av lateralt belastade skivor av kalk-cement pelare har dokumenterats.

De viktigaste upptäckterna och slutsatser från denna studie är:

- Beteendet hos dragbelastad kalk-cement stabiliserad lera är mycket lik den för ett överkonsoliderat material.
- Materialbrott under dragbelastning sker i lokala svaga zoner, d.v.s. materialets hållfasthet bestäms av den svagaste länken.
- Fält försök visar att kalk-cement pelarstabilisering utförd som överlappande skivor i passiv zon av en spontkonstruktion signifikant ökar konstruktionens kapacitet mot brott och minskar schakt och last inducerade deformationer i jorden både inom aktiv och passiv sida om sponten.
- Schakt och last inducerade tillskottsspänningar överförs till största del till pelarskivorna som fungerar som stämp under schaktbotten.
- En minskat centrum avstånd mellan pelarskivorna ökar samverkan mellan den stabiliserade jorden och leran mellan skivorna.
- För fallet men ett centrumavstånd av 3.0 m mellan pelarskivorna skedde brottet endast i leran mellan skivorna och resulterade i ett mycket spröd brott förlopp.

LIST OF PUBLICATIONS

Paper I

Ignat R., Baker S., Larsson S., Liedberg S., 2015. Two- and three-dimensional analyses of excavation support with rows of dry deep mixing columns. Computers and Geotechnics, Vol. 66, p. 16-30.

I and Larsson initiated the case study. I made the calculations and wrote the paper, supervised and assisted by Baker, Larsson and Liedberg.

Paper II

Ignat R., Baker S., Larsson S., 2015. Field test of braced excavation supported with rows of dry deep mixing columns. Accepted for publication and presentation at Deep Mixing 2015, San Francisco, June 2-5, 2015. http://dfi.org/dfieventlp.asp?13237

I conducted the field tests and wrote the paper. Larsson and Baker supervised the work and assisted with comments on the paper.

LIST OF NOTATIONS

Roman letters

c_v	Coefficient of consolidation at $\sigma'_{p\,vert}$
E_{50}	Young's secant modulus at 50% of ultimate strength
E_{ini}	Young's tangent modulus
k	Permeability at $\sigma'_{p\,v}$
K_0	At rest earth pressure coefficient, σ'_h/σ'_v
M_0	Oedometer modulus below $\sigma'_{p\,v}$
M_L	Oedometer modulus between $\sigma'_{p\,v}$ and σ'_L
q	Deviator stress, equal to difference of σ'_1 and σ'_3
q_{peak}	Peak deviator stress
q_u	Unconfined compression strength
$q_{u\ 28d}$	Unconfined compression strength at 28 days
q_{ult}	Evaluated ultimate load
s_{col}	Distance between columns
s_{row}	Distance between column rows
s_u	Undrained shear strength
$s_{u\ cone}$	Undrained shear strength evaluated from fall-cone tests
$s_{u\ comp}$	Undrained shear strength evaluated from CK_0UC tests
$s_{u\ ext}$	Undrained shear strength evaluated from CK_0UE tests
$s_{u\ CPT}$	Undrained shear strength evaluated from CPT tests
$s_{u\ DSS}$	Undrained shear strength evaluated from direct simple shear tests
$s_{u\ KPS}$	Undrained shear strength of lime-cement columns evaluated from KPS tests
$s_{u\ Vb}$	Undrained shear strength evaluated from field vane tests
$s_{uc\ peak}$	Maximum shear strength under compression loading
$s_{ue\ peak}$	Maximum shear strength under extension loading
$s_{uc\ res}$	Large strain (critical state) undrained shear strength under compression loading
s'	Average value of the principle stresses σ'_1 and σ'_3 or the average value of σ'_v and σ'_h in the axial symmetric case
S_t	Sensitivity

t	Difference of $\sigma_1^{'}$ and $\sigma_3^{'}$ divided by two or the difference between σ'_v and σ'_h divided by two in the axial symmetric case
w_n	Natural water content
w_L	Liquid limit

Greek letters

c'	Effective cohesion intercept
$\Delta\sigma_h$	Horizontal earth pressure change
$\triangle u$	Excess pore water pressure
δ_h	Horizontal displacement
δ_v	Vertical displacement
ε_a	Axial strain
ε_{vol}	Volumetric strain from the start of the test to $\sigma_{p\,vert}^{'}$
$\varepsilon_{x\,3D}$	3D horizontal strain
$\varepsilon_{x\,2D}$	2D horizontal strain
$\emptyset'$	Friction angle
γ	Shear strain
γ	Unit weight of the soil
ρ	Density
σ'_{v0}	Vertical effective in situ stress
σ'_{h0}	Horizontal effective in situ stress
σ_a	Axial stress in triaxial testing
σ_h	Total horizontal stress
$\sigma_L^{'}$	Effective stress above $\sigma_{p\,vert}^{'}$ where the oedometer modulus starts to increase
$\sigma_{p\,v}^{'}$	Vertical effective preconsolidation pressure
σ_r	Radial stress in triaxial testing
$\sigma_v^{'cons}$	Vertical effective consolidation pressure
σ_v	Total vertical stress
τ_{max}	Maximum Shear stress

Abbreviations

CPT	Cone penetration test
CRS	Constant rate of strain
CIUC	Isotropic consolidated samples compressed under undrained conditions
CIUE	Isotropic consolidated samples expose to extension under undrained conditions
CK_0UC	K_0 consolidated samples compressed under undrained conditions
CK_0UE	K_0 consolidated samples expose to extension under undrained conditions
CUDSS	Consolidated samples exposed to direct simple shear under undrained conditions
KPS	Column penetration test
OCR	Overconsolidation ratio. The ratio between the vertical preconsolidation pressure and the actual vertical effective stress
SPW	Sheet pile wall
UCT	Unconfined compression test

CONTENTS

1 INTRODUCTION

1.1 Background

Ground improvement by deep mixing with lime-cement columns has been used successfully in Sweden for the last 40 years, mainly for reduction of settlements and to some extent to improve stability of road and railway embankments. The economic benefits of the method makes it the most used ground improvement method in Sweden, Norway and Finland but the method is also used to a large extent in Japan, China, the USA, Australia, the UK and several other European countries. Development of the method in Sweden has led to the use of columns of increasing strength and stiffness properties and application of the method has increased from mainly for reduction of settlements to include stability of embankments, stability of temporary and permanent slopes and foundations for different types of constructions. Internationally, the deep mixing method has also been used with good results as reinforced retaining structures when excavations are to be performed in locations with thick soft clay deposits, and one relatively new application is to install column-type ground improvement on the passive side in interaction with sheet pile walls.

The use of this application has been documented for a few field cases, Tanaka (1993), O'Rourke et al. (1997b), O'Rourke and McGinn (2006), Ou et al. (2008). The most important findings were that by improving the soil in the passive zone, the passive earth pressure that can be developed in front of the retaining structure is increased. This has proven to significantly reduce excavation induced deflections behind the retaining structure, reduce structural forces (bending moment in the retaining structure, strut and anchor forces) and improve safety against basal heave failure. Although this application has been used with good results internationally, there are very few cases in Sweden where it has been used.

The current design model implemented in the Swedish design guidelines, TK Geo (2013), Larsson (2006), is based on the assumption that the improved soil volume behaves as a composite material and the governing failure mode is a shear failure through the columns and the soil between the columns. The material properties of the stabilized soil volume are calculated as the weighted strength and stiffness properties of the columns and the soil between the columns. Full interaction between the columns and the soil is usually assumed and the difference between the two materials stress-strain behavior is not taken into consideration. When utilized in shear and passive zone, the strength properties of the columns should also be, according to the design guidelines, significantly reduced which means that the effect of ground improvement conducted in shear and passive zones will be very limited.

In order to increase the application of the method to include constructions where deep mixing columns are laterally loaded, such as excavation support, permanent slopes where ground improvement is conducted in shear and passive zones and high embankments, a reliable design model for laterally loaded columns needs to be developed and implemented.

1.2 Previous Research

Since column-type ground improvement began to be used to increase the stability of embankments during the 1990s, several research studies focusing on the behavior of laterally loaded columns have been conducted. The majority of these studies, which include analytical, numerical and small scale model tests, investigated laterally loaded columns due to embankment loading.

Kivelö (1998) presented an analytical model for calculating the stability of embankments where the shear resistance of the columns depends on the location along a slip surface, the loading condition of the columns and the soil conditions. The different failure modes that can arise in the columns are based on studies performed by Brinch Hansen (1948) and Broms (1972) on laterally loaded piles. Broms (1999) investigated the possibility of progressive failure and analyzed the failure of two embankments where ground improvement by deep mixing with lime-cement columns was performed in Sweden.

Both internal and external stability of single columns under embankment loading have been investigated by Kitazume & Maruyama (2006, 2007 and 2008) by means of 1g, small-scale model tests. The performed tests and analyses showed that a bending failure of the columns and a tilting failure pattern in the embankment are the most probable internal and external failure modes, respectively.

The failure mechanism of single columns under embankments has been analyzed through numerical analyses in several case studies and research projects by Navin (2005), Navin & Filz (2006), Han et al. (2005 and 2007), Huang et al. (2006), among others. The most important findings of these studies was that for a majority of cases stability analyses conducted with limit equilibrium methods will significantly overestimate the factor of safety of the structure compared to numerical analyses.

Larsson (1999) and Larsson & Broms (2000) conducted small-scale laboratory tests where they showed that at the same area replacement ratio a shear wall pattern with overlapping columns is much more effective than singular columns when subjected to lateral loading. Larsson et al. (2012) performed numerical analyses of several conducted small-scale tests of laterally loaded lime-cement columns where the columns were modeled using a concrete damage plasticity model that was able to simulate a stiffness and strength degradation followed by the emergence of shear cracks in the columns due to loading. The results showed good agreement between the experimental and numerical stress-deformation relationship and that the strength of the overlapping zone between the columns has an important effect on the shear resistance of the columns.

Adams (2008, 2009, 2011) investigated several different cases of the stability of levees supported by deep-mixed shear walls through numerical analyzes and showed that the factor of the safety for a slip failure is substantially higher for a shear wall pattern compared to isolated columns at the same area replacement ratio. Based on these studies, Filz et al. (2011) presented a simplified analytical solution for calculation of the safety factor for external and internal stability of levees supported by deep mixing shear walls with overlapping columns.

Yang et al. (2011) investigated the behavior of an embedded improved soil raft (soil cement columns that form a continuously improved composite ground and act like struts below the excavated ground level) to help restrain the movements of a retaining wall by conducting numerical analyses of a hypothetical case and simulation of a reported case history. The authors examined the mechanisms of how the mass properties of the improved soil are mobilized and how application of different material properties in the horizontal direction within a column and the geometrical arrangement of the columns, affect the degree of mobilization of the mass properties of the raft compared to the elemental properties. Based on these results, Yang et al. suggested that soil-cement columns used to improve the stability of excavations should be constructed with overlap rather than just in contact with each other.

1.3 Research Objectives

The objective of this research project is to increase knowledge and understanding of the behavior of laterally loaded lime-cement columns in shear and passive zones. This project also aims to investigate the material strength and stiffness properties when subjected to shear and extension loading and present a reliable design method based on performed laboratory and field tests that can adequately predict the effect of lime-cement column ground improvement conducted in the passive zones of a construction.

The focus in the first part of the project, which is presented in this licentiate thesis, was on investigating strength and stiffness properties of laboratory improved soil and the performance of a full scale field test where the behavior of laterally loaded rows of lime-cement columns has been documented.

The ability of a simplified 2D numerical model to reflect the behavior of a 3D mechanical system consisting of rows of overlapping columns subjected to lateral loading has also been investigated using numerical analyses. The second part of the research project will focus on the development of a conceptual design methodology for lime-cement column improvement in shear and passive zones.

In order to accomplish this, the following objectives were set for this thesis:

- Conduct laboratory tests on lime-cement improved clay samples in order to increase the knowledge and understanding of the material behavior during compression and extension loading.
- Through numerical analyses, predict an expected behavior of a retaining structure interacting with rows of overlapping lime-cement columns installed in the passive zone where first excavated and then loaded to failure.
- Conduct two full-scale tests where a retaining structure interacting with rows of overlapping lime-cement columns installed in the passive zone which was first excavated and then loaded to failure.
- Determine the strength and stiffness properties of the clay at the site of the full-scale tests for different loading situations in order to, in the next part of the research project, perform analyses of the conducted full scale tests.

1.4 Outline of Thesis

This licentiate thesis is written as a compilation thesis and consists of six chapters, briefly described below, and two appended papers.

Chapter 1 - Introduction

The background to the project, a summary of previously conducted research and the objectives of this research project are presented in this chapter.

Chapter 2 - Geotechnical conditions of test site

In this chapter, the site of the full-scale tests is described. The results of laboratory tests conducted on the soft clay and evaluated material properties of the clay are also presented in this chapter

Chapter 3 - Laboratory tests on stabilized clay

In this chapter, a description and the results of the performed unconfined compression tests and triaxial tests together with evaluated material strength and stiffness properties are presented.

Chapter 4 - Finite element analyses of lime-cement column rows supported excavation

Chapter 4 contains a short description of the conducted numerical analyses together with a summary of the results and the conclusions drawn from this study.

Chapter 5 - Field tests

In this chapter, the execution of the field tests is described and selected results are presented.

Chapter 6 - Conclusion and future work

The major conclusions from this study are presented in this chapter along with suggestions for future work related to the study.

2 GEOTECHNICAL CONDITIONS AT TEST SITE

2.1 General Site Description and Soil Profile

Two individual full-scale tests were performed in the eastern part of Sweden, about 70 km northwest of Stockholm in the proximity of the city of Enköping. The site chosen for the tests is an unexploited open field with an area of about100x200 m situated about 100-120 m north of the Enköping creek. The area is divided by two trenches running through the area. The trenches are approximately 1.5 m wide and 0.5 m deep and their function is to divert rain water from the surrounding higher areas to the creek. The area is relatively flat, with an elevation above sea level at the site that varies between +5.9 and +6.2 m.

The geotechnical site investigation was concentrated to the location of the test areas. Both test areas, with dimensions of about 20x30 m, were located in the south central part of the site about 35 m from each other, where the largest thickness of the soft clay layer could be found. Closest to the ground surface, the soil consists of a 1.2-1.5 m thick layer of dry crust followed by a soft post-glacial clay layer, silt and sand above moraine closest to the bedrock. The thickness of the clay layer beneath the dry crust varies between 7-9 m and is generally increasing towards the creek located south of the site. The first 2 meters of the soft clay has been classified as gyttja-bearing clay and streaks/shots of sulphide soil occur to a depth of about 5 m in both test areas. From about 6-7 m depth the clay alternates with thin horizontal layers of silt and sand, which is typical for the region. The undrained shear strength of the clay evaluated from field vane tests is between 9-13 kPa to about 5 m depth and thereafter increases by approximately 1 kPa/m. The clay is normally or slightly overconsolidated and the Overconsolidation ratio, *OCR*, generally decreases with depth. The thickness of the frictional soil beneath the clay varies between 3-7 m and the level of the bedrock was found at 14-22 m beneath the ground level.

Fig. 1: Location of the test site

2.2 Field Tests

The in-situ tests consisted of cone penetration tests, *CPT*, and field vane tests, *Vb*, performed in order to determine the thickness of the clay layer, the undrained shear strength, s_u, and to investigate the presence of permeable layers of frictional soil within the clay layer. Soil/rock drilling tests, *Jb2*, were performed in order to locate the level of the bedrock. Disturbed samples were collected with a helical auger, *Skr*, and undisturbed samples were extracted using the Swedish standard piston sampler (SIS 2007) from 2, 5 and 7m depth for laboratory testing. Pore pressure measurements were conducted in the clay at the same depths and locations as the undisturbed samples that were extracted. The free groundwater table was measured in open pipes installed at a depth of 1.0 m into the frictional soil below the clay.

2.3 Routine Laboratory Tests

Classification and determination of density, ρ, natural water content, w_n, liquid limit, w_L, sensitivity, S_t, and undrained shear strength determined by fall-cone tests, $s_{u\,cone}$, of the clay were performed on undisturbed samples collected from the field test.

In both test area 1 and test area 2, the depth of the soft clay below the dry crust is about 7.0-8.5 m. The clay in test area 1 has a w_n equal to 75-82 % and a ρ of 1.50-1.55 t/m^3 from the top of the clay layer down to a depth of 5 m. Between 5 and 7 m depth the value of w_n decreases to about 57% at 7 m of depth while the ρ increases to about 1.75 t/m^3. Throughout the entire profile has w_n been determined to be higher than w_L. The variation of w_n follows, however, a similar trend as w_L, see Fig. 2a. Evaluated s_u from both field and laboratory tests is presented in Fig. 2 b together with S_t. At the top of the clay, S_t is about 20 and increases with depth and at both 5 and 7 m of depth the clay is classified according to the Swedish classification system as highly sensitive, S_t >30, with a value of about 50 at 7 m depth.

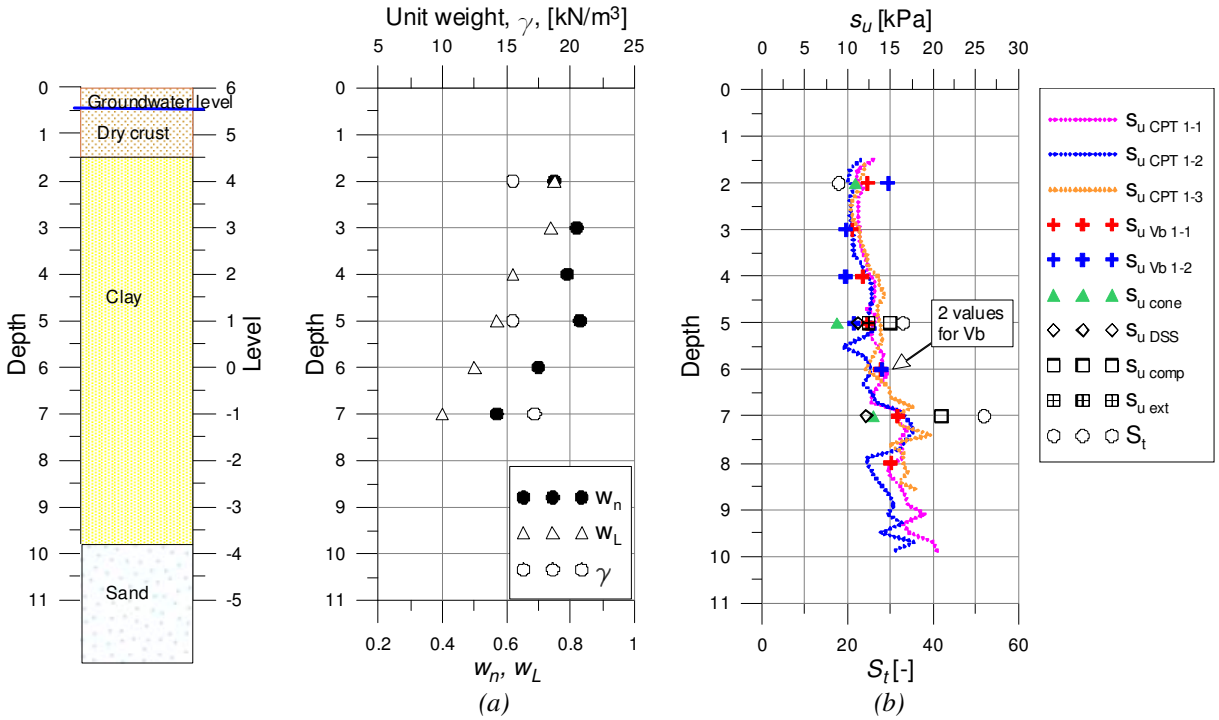

Fig 2: Soil properties test area 1:
(a) Water content, liquid limit and unit weight;
(b) Undrained shear strength and sensitivity

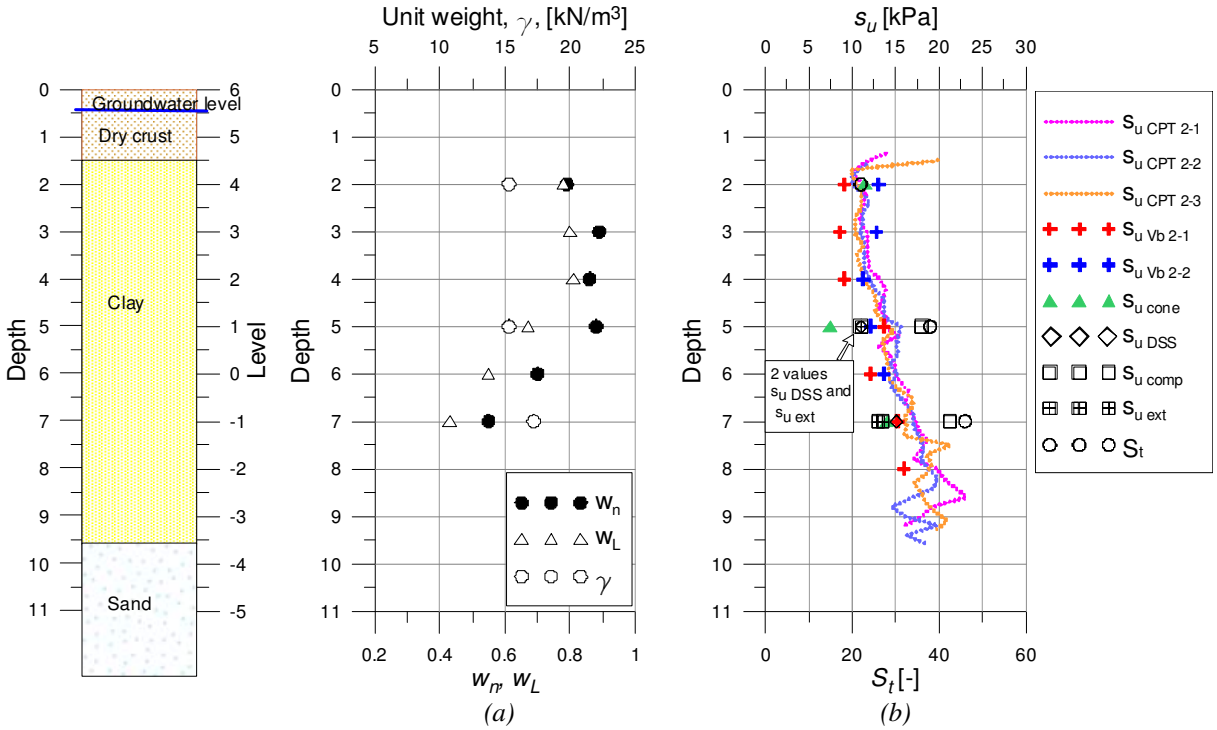

Fig 3: Soil properties test area 2:
(a) Water content, liquid limit and unit weight
(b) Undrained shear strength and sensitivity

The properties of the clay at the location of test area 2 are very similar to those at test area 1, and are presented in Fig. 3. Between 2 and 5 m depth, w_n, w_L and S_t are slightly higher in test area 2 compared to test area 1, but below this depth equal values of w_n and ρ were obtained for both test areas while S_t was slightly lower for test area 2. Evaluated s_u from field tests for test area 2 is also very similar to s_u evaluated for test area 1.

2.4 Compression Tests

Constant rate of strain oedometer tests, *CRS* tests, were conducted on four samples from 5 and 7 m depth in order to determine the behavior of the clay for 1D loading. The *CRS* tests were conducted according to Swedish Standard SS027126 with a deformation rate of 0.0024 mm/min. From the *CRS* tests the vertical preconsolidation pressure, $\sigma'_{p\,v}$, was estimated according to Swedish practice described by Sällfors (1975), Larsson (1981), Larsson (1986). The vertical in situ effective stress, $\sigma'_{v\,0}$, was calculated from the unit weight of the soil, γ, and the pore water pressure measurements in the field.

Evaluated parameters obtained from the *CRS* tests conducted on undisturbed samples from 5 and 7 m of depth are presented in Tables 1 and 2 for each test area. Samples from 2 m of depth were disturbed and no reliable results were obtained from CRS tests conducted on samples from this depth, very likely due to the vicinity to the dry crust and the somewhat organic content.

Table 1: Results of CRS tests conducted at Test area 1

Depth	$\sigma'_{p\,v}$ [kPa]	σ'_L [kPa]	M_0 [kPa]	M_L [kPa]	k [m/s]	c_v [m²/s]	OCR	ε_{vol} [%]
5 m	60	79	1715	215	5.0e-10	6.0e-7	1.5	3.0
7 m	65	122	3420	700	4.8e-10	1.0e-7	1.3	1.9

Table 2: Results of CRS tests conducted at Test area 2

Depth	$\sigma'_{p\,v}$ [kPa]	σ'_L [kPa]	M_0 [kPa]	M_L [kPa]	k [m/s]	c_v [m²/s]	OCR	ε_{vol} [%]
5 m	58	85	1680	275	6.0e-10	7.2e-7	1.5	3.4
7 m	60	117	2730	500	5.5e-10	9.0e-8	1.2	2.2

where:

$\sigma'_{p\,v}$ = Vertical preconsolidation stress
σ'_L = Effective stress above $\sigma'_{p\,v}$ where the oedometer modulus begins to increase
M_0 = Oedometer modulus below $\sigma'_{p\,v}$
M_L = Oedometer modulus between $\sigma'_{p\,v}$ and σ'_L
k = Permeability at $\sigma'_{p\,v}$
c_v = Coefficient of consolidation at $\sigma'_{p\,v}$
ε_{vol} = Volumetric strain from the start of the test to $\sigma'_{p\,v}$

2.5 Shear Tests

Naturally consolidated soft clays are usually prestressed for different normal stresses in different directions and due to the actual at rest earth pressure coefficient, K_0, consolidation history, exhibit anisotropic undrained shear strength, as described by Larsson (1977), Ladd (1991), Ladd & Foott (1974), Mayne (1985), Mayne & Kulhawy (1982). In order to evaluate the strength anisotropy of the soft clay, K_0 consolidated undrained compression shear tests, *CK₀UC*, K_0 consolidated extension shear tests, *CK₀UE*, and consolidated undrained simple shear tests, *CUDSS*, were conducted on clay samples from 5 and 7 m depth.

The soil behavior in the form of shear strength and stress paths can be normalized to the vertical consolidation stress applied prior to shearing of the specimen, $\sigma_v'^{cons}$, according to the *SHANSEP* method (Stress History And Normalized Soil Engineering Properties) proposed by Ladd & Foot (1974). The *SHANSEP* technique implies that the sample is K_0 consolidated far beyond $\sigma'_{p\,v}$, in order to measure the behavior of normally consolidated clay, and then unloaded at different stress situations to study the overconsolidated behavior. This method is recommended for mechanically overconsolidated and truly normal consolidated clays with low sensitivities. However, Ladd & Foott (1974) and Ladd (1991) did not recommend this technique for use on highly sensitive quick clays and naturally cemented soils because the structure of such soils will be significantly altered during consolidation to stresses above $\sigma'_{p\,v}$. For those cases, the recompression technique, where the soil is reloaded to the vertical effective in situ stress, σ'_{v0}, before shearing is recommended, provided that the test can be performed on high quality samples with a minimum of disturbance effects.

2.5.1 Testing procedure

The triaxial tests were conducted according to European Standard ISO/TS 17892-9:2005, and the Swedish Geotechnical Society guidelines for Triaxial testing (2012). The samples were saturated before consolidation and the Skempton pore pressure coefficient, B, measured before consolidation of the samples began, varied between 0.97-0.99, indicating that full saturation of the samples were achieved.

Due to the high sensitivity of the clay, the majority of the samples were consolidated for an effective stress situation approximately equal to σ'_{v0}. Consolidation was conducted according to the simplified recompression method with a "one-step" consolidation step described by Lacasse & Berre (1988). The samples were first consolidated isotropically to a stress level equal to the in situ effective horizontal stresses, σ'_{h0}, before the axial stress, σ_a, was increased until the in situ deviatoric stress, $\sigma_v - \sigma_h$, was reached. No filter paper strips were used, resulting in a required consolidation time that varied between 24-36 h.

The active tests were performed by increasing σ_a, and keeping the radial stress, σ_r, constant while the passive tests were performed by decreasing σ_a while σ_r was kept constant. The tests were conducted to a total axial strain, ε_a, during shearing of about 12% and both compression and extension tests were performed with an axial strain rate equal to 0.7% /h, corresponding to a rate of shear strain of 1.0%/h. The cross-sectional area of the sample was corrected during the consolidation and shearing stages under the assumption that the specimen deforms as a cylinder with constant diameter throughout its height. This correction method was proposed by La Rochelle et al. (1988) for a barreling type failure. The effect of the membrane on the measured strength of the specimen depends on several factors such as elastic properties, initial diameter and thickness of the membrane, and can have a large impact especially in the case of very soft soils at large strains and with stiff membranes. Calculation of the membrane correction factor, based on method proposed by Head (1998), shows that the membrane correction factor that should be imposed on the deviator stress is less than 1 kPa for strains less than 5% and was therefore considered to be negligible.

Consolidated undrained simple shear tests were performed according to Swedish Standard SS 027127 and the Swedish Geotechnical Society guidelines for direct shear tests (2004). The samples were consolidated to a stress level equal to σ'_{v0} and were conducted at a strain rate of 0.1 mm/h. The undrained shear strength, $s_{u\,DSS}$, was evaluated as the maximum obtained shear stress, τ_{max}, or alternatively the shear stress at 15% shear strain if τ_{max} was not reached at this shear strain level.

The stress conditions for the conducted undrained compression, extension and direct simple shear tests are shown in Tables 3 and Table 4.

Table 3: Stress conditions for samples from 5 m depth

Sample	Depth	Test	σ'_{v0} [kPa]	σ'^{cons}_{v} [kPa]	$K_{0\,kons}$
1A	5 m	CK_0UC	39	36	0.56
1B	5 m	CK_0UC	39	41	0.63
1C	5 m	CK_0UC	39	48	0.70
1D	5 m	CK_0UE	39	39	0.61
1E	5 m	CK_0UE	39	37	0.61
1F	5 m	*CUDSS*	39	38	-
1G	5 m	*CUDSS*	39	36	-

Table 4: Stress conditions for samples from 7 m depth

Sample	Depth	Test	σ'_{v0} [kPa]	σ'^{cons}_{v} [kPa]	$K_{0\,kons}$
2A	7 m	CK_0UC	50	41	0.69
2B	7 m	CK_0UC	50	62	0.63
2C	7 m	*CIUC*	50	73	1.00
2D	7 m	CK_0UE	50	49	0.63
2E	7 m	CK_0UE	50	52	0.63
2F	7 m	*CUDSS*	50	50	-
2G	7 m	*CUDSS*	50	50	-

2.5.2 Test results

Examination of the samples after conclusion of the tests showed that the failure mode for the majority of the compression tests was a combination of shear plane and barreling failure, Fig. 4 a, but a single plane shear failure developed in one of the tests conducted on samples at 5 m depth, Fig. 4 b. For the extension tests the same failure mode, Fig. 4 c, was obtained in all tests.

(a) (b) (c)

Figure 4: Failure modes after triaxial tests on clay samples
(a) Combined shear and barreling failure for compression tests
(b) Shear failure for compression test sample, 5 m depth
(c) Typical tension failure for extension tests

Results for the *CK₀UC* and *CK₀UE* in terms of deviator stress - axial strain relationship, excess pore pressure–axial strain behavior and effective stress paths plotted in *s'-t* space (where $s' = (\sigma_1' + \sigma_3')/2$ and $t = (\sigma_1 - \sigma_3)/2$) are shown in Fig. 5-7 for both compression and extension tests. Although consolidation was not performed according to the *SHANSEP* method, normalization of s_u and effective stress paths to $\sigma_v'^{cons}$ from *CRS* was performed in order to study how s_u depends on type of loading and *OCR*.

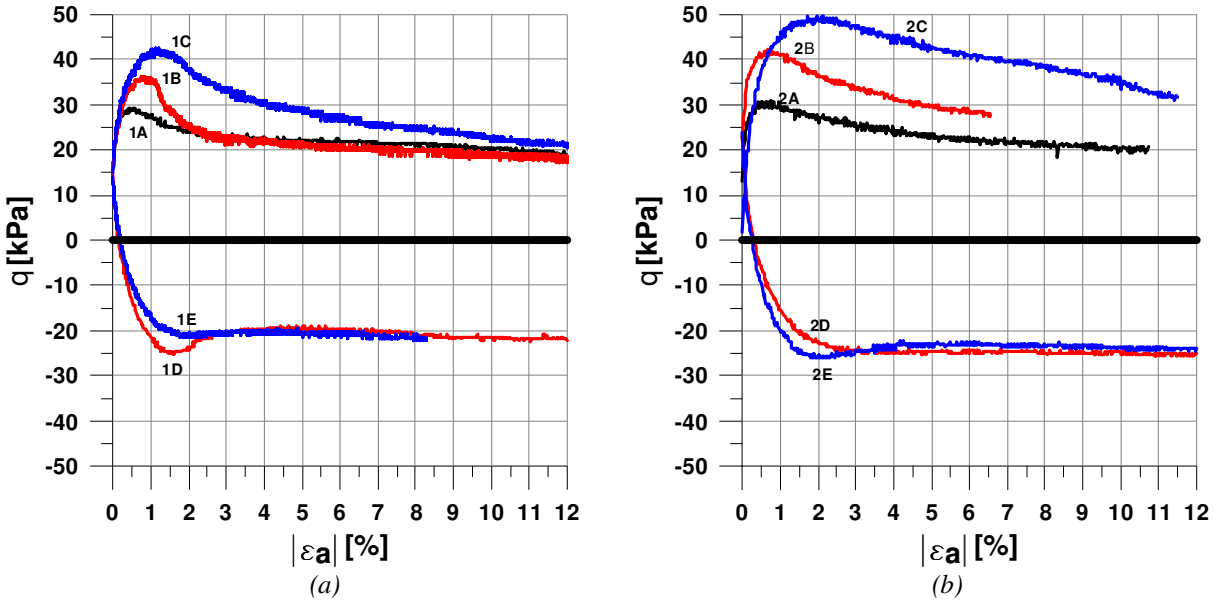

(a) (b)

Figure 5: Results of CK₀UC and CK₀UE tests on clay samples.
(a) Deviator stress versus axial strain samples, 5 m depth
(b) Deviator stress versus axial strain samples, 7 m depth

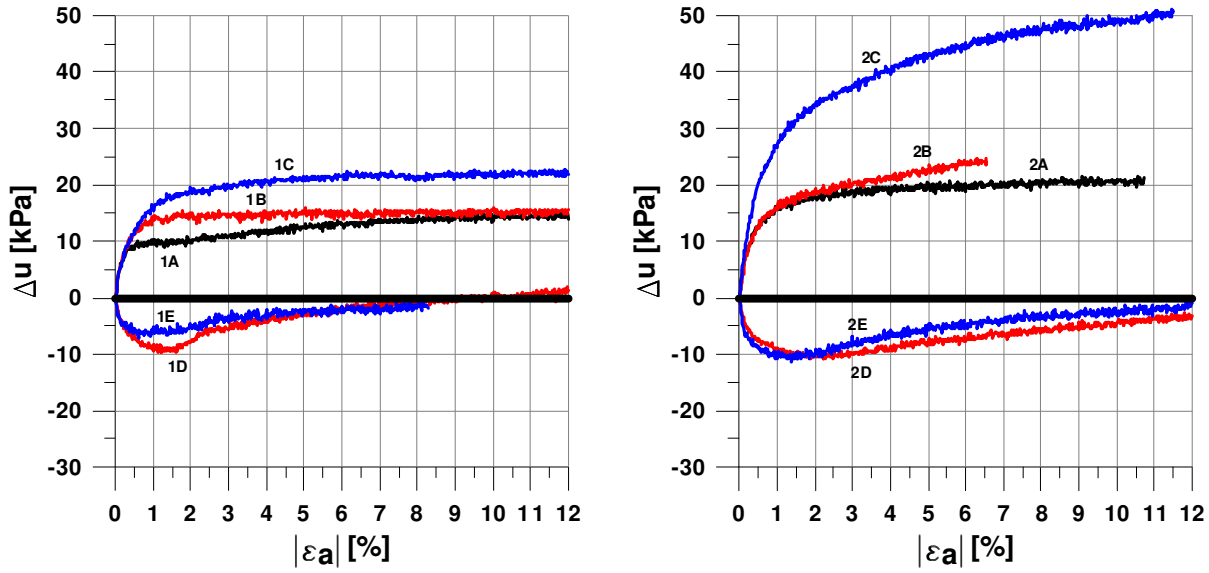

(a) *(b)*

Figure 6: Results of CK_0UC and CK_0UE tests on clay samples.
(a) Excess pore pressure versus axial strain samples, 5 m depth
(b) Excess pore pressure versus axial strain samples, 7 m depth

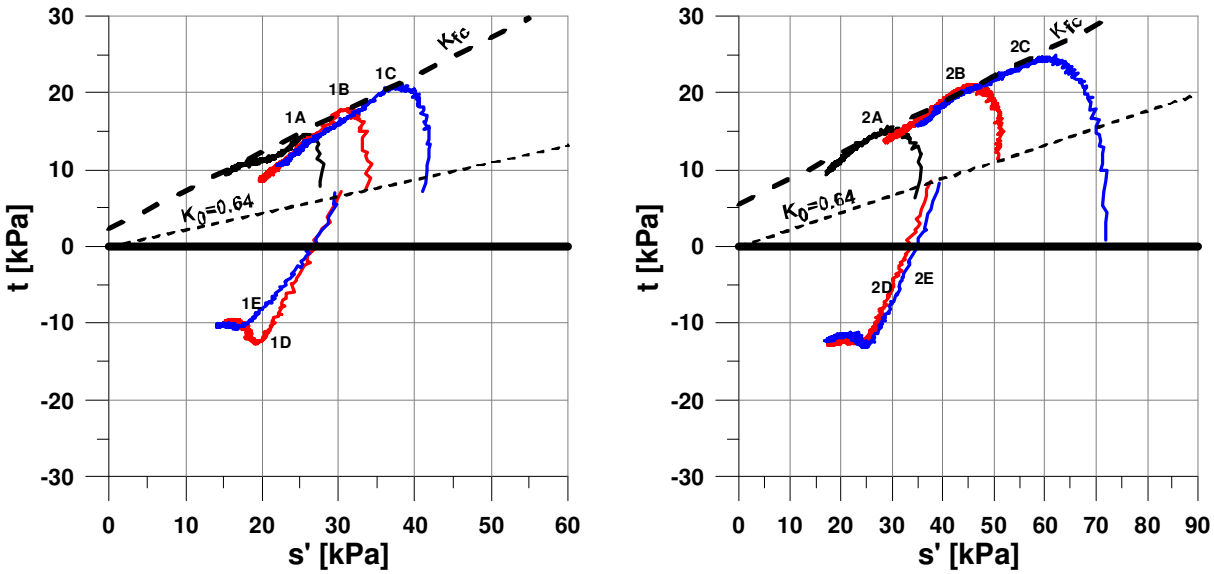

(a) *(b)*

Figure 7: Results of CK_0UC and CK_0UE tests on clay samples; stress paths in s'-t plane
(a) 5 m depth
(b) 7 m depth

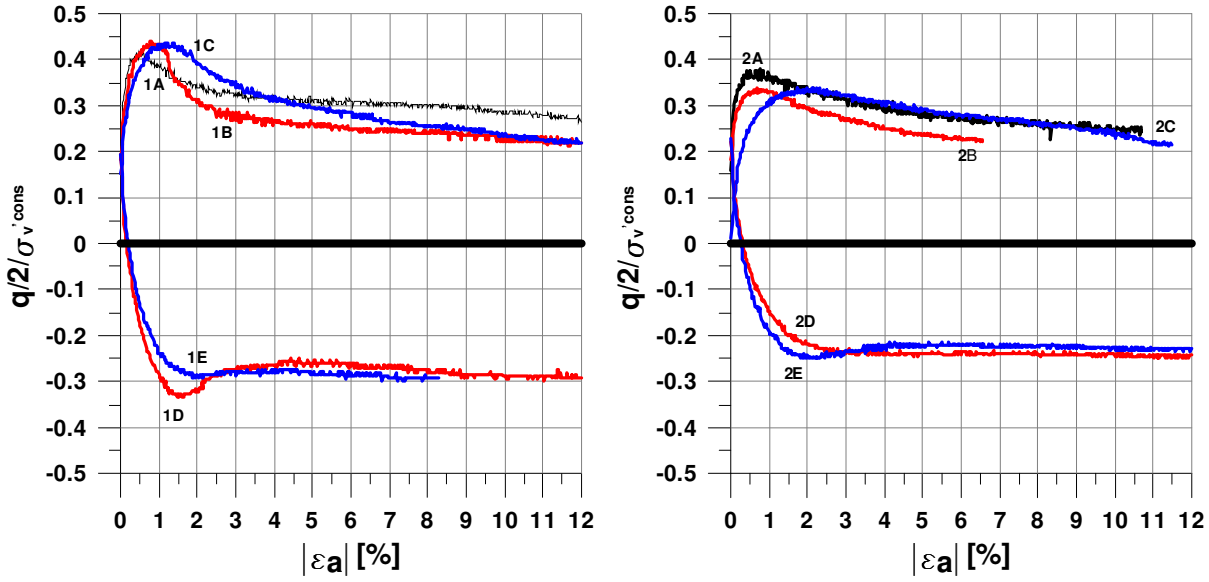

(a) *(b)*

Figure 8: Results of CK_0UC and CK_0UE tests on clay samples; normalized deviator stress to effective consolidation stress versus axial strain
(a) 5 m depth
(b) 7 m depth

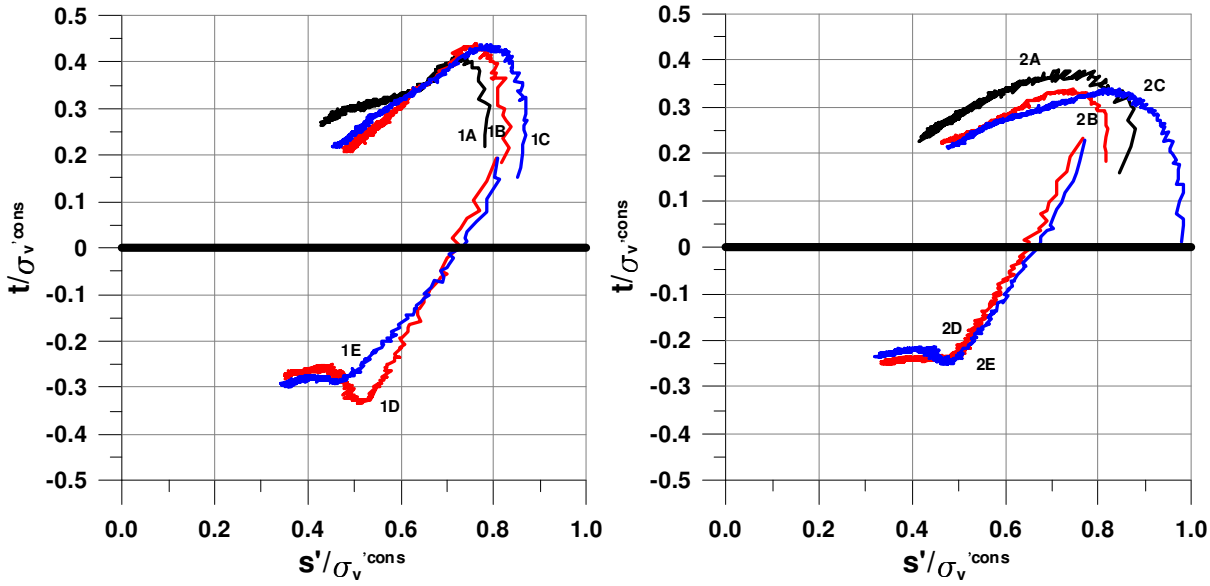

(a) *(b)*

Figure 9: Results of CK_0UC and CK_0UE tests on clay samples; normalized stress paths in s'-t plane
(a) 5 m depth
(b) 7 m depth

The deviator stress-strain relationship shows that for all compression tests with the exception of sample 2C, the peak deviator stress, q_{peak} was obtained at ε_a equal to 0.5-1.0% and there is a clear indication of strain softening beyond q_{peak}. There is also a clear indication that an increasing confining pressure resulted in larger excess pore pressure and also a higher s_u and ε_a at q_{peak}. In the extension tests, q_{peak} was obtained at ε_a equal to 1.5-2.5% and the tests showed no clear indication of a decrease in q after the peak. The tests showed that the clay follows a stress path typical for normally consolidated clay. During compression tests, the excess pore pressure, Δu, will increase rapidly until q_{peak} is reached and the rate of Δu is much lower thereafter.

This results in a decrease in effective stresses and a distinct turn to the left occurs when the stress path reaches the failure line. In all extension tests, a decrease in Δu occurred initially. Subsequently, after q_{peak}, Δu began to increase and was at critical state, $du/d\varepsilon = 0$ and $dq/d\varepsilon = 0$, close to zero. The development of Δu in the extension tests is typical for soft normal consolidated clays and similar results have been reported by Balasubramaniam & Li (1977) for triaxial extension unloading tests performed on soft Bangkok clay.

The Young's modulus evaluated as secant modulus at 50% of q_{peak}, E_{50}, shows a clear difference between the 5 and 7 m clay in the compression tests, with about 50% higher E_{50} values for the 7 m samples. The ratio between the secant modulus and the undrained shear strength, E_{50}/s_u, varies between 190 - 445 in the compression tests and 280 - 345 in the extension tests. In the compression tests, there is a clear indication of decreasing E_{50}/s_u with increased $\sigma_v'^{cons}$.

Material parameters evaluated from the compression and extension shear tests are presented in Tables 5 and 6.

Table 5: Material parameters evaluated from CK_0UC tests

Sample	Depth	ε_{vol} [%]	OCR	s_u [kPa]	$s_u/\sigma_v'^{cons}$	E_{ini} [kPa]	E_{50} [kPa]	E_{50}/s_u
1A	5 m	1.7	1.7	14.9	0.42	5200	4150	280
1B	5 m	4.4	1.4	18.1	0.44	6700	4150	230
1C	5 m	2.1	1.2	21.3	0.44	7400	4100	190
2A	7 m	2.6	1.6	15.6	0.38	11700	6950	445
2B	7 m	3.5	1.0	21.1	0.34	8300	6150	290
2C	7 m	7.7	1.0	25.0	0.34	9600	6050	240

Table 6: Material parameters evaluated from CK_0UE tests

Sample	Depth	ε_{vol} [%]	OCR	s_u [kPa]	$s_u/\sigma_v'^{cons}$	E_{ini}	E_{50}	E_{50}/s_u
1D	5 m	1.4	1.6	12.6	0.34	11300	3700	290
1E	5 m	2.7	1.6	11.0	0.30	8700	3050	280
2D	7 m	2.8	1.2	13.0	0.25	11000	3800	290
2E	7 m	2.7	1.2	13.2	0.25	14500	4550	345

The results of the *CUDSS* tests are presented in Fig. 10 together with the ratio between s_u and $\sigma_v'^{cons}$. Sample 2F shows a lower s_u than expected, possibly as a result of disturbance during sampling. This can be seen from the relative high volumetric strain during consolidation to the in situ stresses.

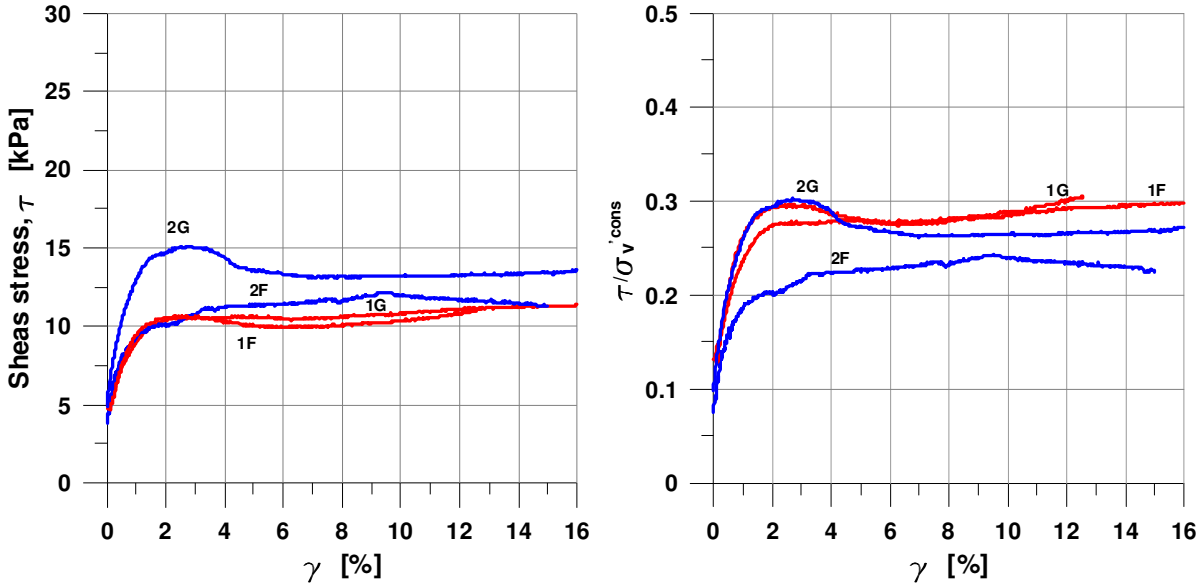

(a) *(b)*

Figure 10: Results of the CUDSS tests;
(a) Shear stress versus shear strain
(b) Normalized shear stress versus shear strain

Table 7: Results of the CUDSS tests

Sample	Depth	ε_{vol} [%]	*OCR*	s_u [kPa]	$s_u/\sigma_v'^{cons}$
1F	5 m	3.1	1.5	11.6	0.30
1G	5 m	1.2	1.5	11.0	0.30
2F	7 m	3.9	1.3	12.2	0.24
2G	7 m	2.5	1.2	15.1	0.30

3 LABORATORY TESTS ON STABILIZED CLAY

3.1 Scope of Laboratory Tests

In order to predict the behavior of the field test and to be able to conduct an accurate study of the results, it is important to have a good knowledge of the geotechnical properties of lime-cement improved soil regarding strength and stiffness under different loading conditions. In order to achieve this, unconfined compression tests, *UCT*, triaxial isotropic consolidated undrained active tests, *CIUC*, and triaxial isotropic consolidated undrained passive tests, *CIUE*, were conducted on laboratory-mixed samples.

3.2 Sample Preparation

The dry binder content used was 120 kg/m^3 and consisted of 50% quicklime, QL 0-0.1 KÖ, and 50% Portland cement, CEM II/A-LL 42.5 R, that is similar to the dry binder content used in the field tests. The procured clay was stored in sealed plastic bags at 7°C from the time it was collected in the field until mixing in the laboratory. The binders were mixed with the soil for 5-7 minutes and the mixture was immediately thereafter, gradually filled in to 50 mm diameter plastic tubes using compaction performed by hand stamp every 30 mm. The tubes were filled to a height of 170 mm and were then sealed before storage in a climate room at 7°C, corresponding to the ground temperature of the soil in Sweden. Both *UCT* and *CIUC/CIUE* tests were conducted on samples with a height to diameter ratio of 2:1, 100 mm height and 50 mm diameter. Before the tests were conducted, the specimens were cut and smoothed to obtain parallel end surfaces, see Fig. 11. In general, the 5 m samples exhibited fewer imperfections and felt both more homogenous and less brittle than the 7 m samples, which was due to the differences in the structure of the clay at the different depths.

(a) *(b)*

Figure 11: Laboratory-mixed samples before testing
(a) 5 m depth
(b) 7 m depth

3.3 Unconfined Compression Tests

In Sweden, *UCT* is the standard method used to evaluate strength and stiffness properties of laboratory improved soil. In order to evaluate the strength increase over time, testing is usually performed at three different time intervals, where 14, 28 and 90 days after mixing are standard, Larsson (2006), but other time configurations are also used. In this study, *UCTs* were performed 28, 56 and 84 days after mixing. The tests were performed at a strain rate of 1mm/min until either failure or ε_a equal to 10% was reached. In order to minimize friction at the end surfaces, the endplate was lubricated with silicone grease.

The results of the *UCTs* are presented in Table 8 and Fig. 12-13.

Table 8: Results of UCTs on laboratory samples from 5 and 7 m depth.

Depth [m]	Curing time [days]	Mean Unconfined Compressive Strength, q_u, [kPa]	Mean Secant Young's Modulus, E_{50}, [MPa]	E_{50}/q_u	Mean Axial Strain at failure, εa, [%]
5	28	253	13.5	53	3.9
5	84	323	14.7	46	3.6
7	28	349	15.3	44	4.2
7	56	445	29.8	67	3.0
7	84	598	55.1	92	2.1

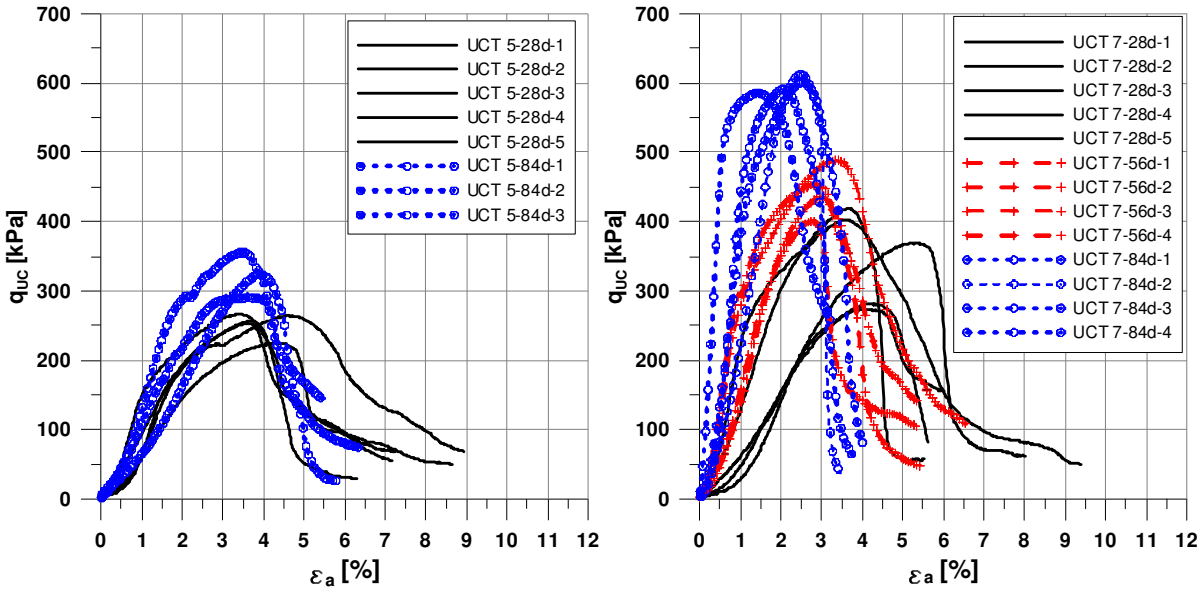

(a) (b)

Figure 12: Unconfined compression strength versus axial strain for laboratory samples with curing time 28, 56 and 84 days:

(a) 5 m depth

(b) 7 m depth

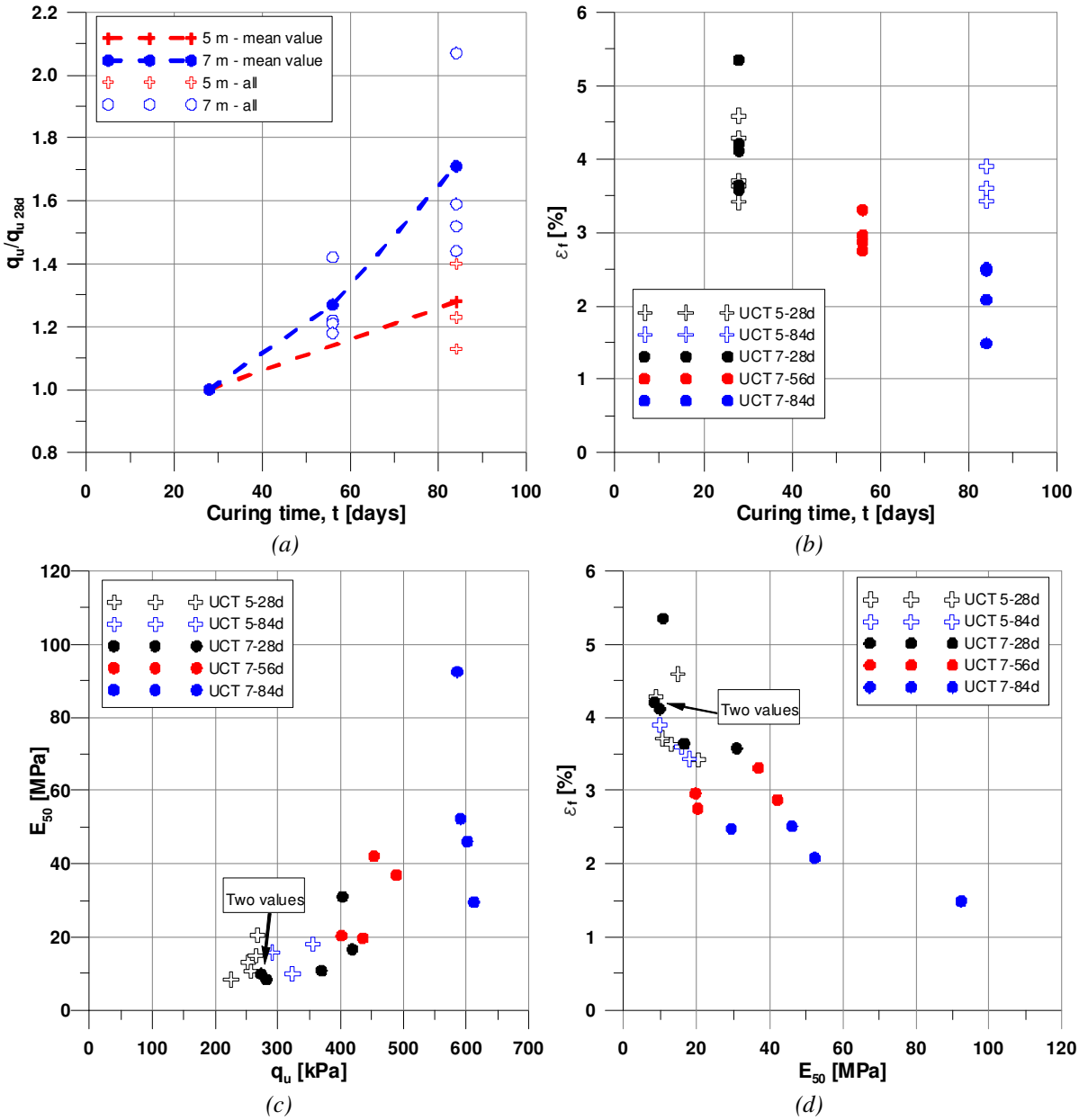

Figure 13: Results of UCT on lime/cement stabilized clay

(a) Normalized unconfined compression strength versus curing time

(b) Axial strain at failure versus curing time.

(c) Secant Young's modulus, E_{50}, versus unconfined compression strength

(d) Axial strain at failure versus Secant Young's modulus, E_{50}.

Although the same amount of dry binders were used in both cases, the improved clay from 5 m depth shows a different behavior compared with the samples prepared from 7 m depth regarding strength and stiffness properties. Generally, the unconfined compressive strength after 28 days, $q_{u\ 28d}$, is lower for the 5 m samples compared to the 7 m samples, even if ε_a at failure is of the same magnitude. Furthermore, contrary to the 7 m samples which exhibit a large increase in strength and decrease in strain at failure with curing time, after 84 days of curing the 5 m samples exhibit, a very limited strength increase and about the same failure strain as the samples that had been cured for 28 days, see Fig. 12 and 13 a-b.

The Young's modulus evaluated as the secant modulus of the columns at 50% of q_u , E_{50}, is presented in Fig. 13 c-d. Regarding the 7 m samples, there is a clear strength increase and decrease in axial strain at failure with curing time, and this obviously leads to a clear increase in E_{50} with curing time and q_u .

For the 5 m samples, both strength increase and strain at failure show very limited increments with curing time and, as expected, no increase in E_{50} with curing time could be observed.

The reason for the large difference obtained in the properties of the stabilized soil from the different depths is believed to be due to the difference in the structure of the clay and agrees with results presented by Åhnberg et al. (1995) that show that laboratory tests on lime-cement stabilized clay with high sulfide or gyttja content indicates both lower strength and a slower strength and stiffness increase with time compared to stabilized clays with no organic content.

3.4 Triaxial Tests

In order to estimate the strength and stiffness properties for conditions more similar to the in-situ conditions, two series of isotropic consolidated undrained compression, *CIUC*, and isotropic consolidated undrained extension test, *CIUE*, were performed on laboratory mixed samples, 28-30 days after mixing. As for the *UCT*, one series of tests was performed with samples prepared with clay only from 5 m depth while the second series of tests was conducted with samples prepared with clay from 7 m depth. The curing time before testing was chosen such that it largely coincides with the time at which the lime-cement columns in the field test will be subjected to loading until failure.

Earlier conducted triaxial tests on stabilized soils with different types of binder by Åhnberg (1995, 2006, and 2007), Balasubramaniam & Buensucesco (1989), Balasubramaniam et al. (1989), Bergado & Balasubramaniam (2005), Baker (2000), Kivelö (1998), Tatsouka and Kobayashi (1983), have shown that the behavior of lime, cement or a combination of both improved clay, consolidated to stresses below the quasi preconsolidation pressure, is in general similar to that of a stiff overconsolidated clay. Decreasing and negative excess pore pressures for high and medium strength samples consolidated at low confining pressures have been reported for the majority of conducted undrained compression tests.

Åhnberg (2004), investigated the effect of different back pressures and strain rates for triaxial testing of stabilized clay and showed that for consolidated undrained triaxial tests the level of back pressure, and thereby the degree of saturation that is achieved in the sample, has a significant impact on the measured undrained shear strength and the differences between the shear strength obtained at tests with low respectively high backpressure increase with increasing stress level, i.e. the depth.

3.4.1 Testing procedure

Before consolidation, saturation of the sample was conducted by stepwise increase of back pressure and cell pressure over a time period of about 6-8 h and the back pressure applied in the performed tests varied between 400-500 kPa. A *B-value* (Skempton pore pressure coefficient), measured before consolidation of the samples was conducted, of 0.93-0.98 was obtained. Full saturation in the samples, was not achieved for three of the samples for which a *B-value* lower than 0.95 was obtained.

The samples were isotropic consolidated to a stress situation close to σ'_{v0} of the actual depth from where the clay was obtained (5 and 7 m depth), but even higher $\sigma_v'^{cons}$, corresponding to a higher in-situ depth, were used in some of the tests. No filter paper strips were used, allowing drainage under consolidation stage only at the bottom of the samples, where the pore pressure was measured. Each sample was consolidated for about 16 h before the shearing process began a time frame that was sufficient to reach the targeted effective stresses and fitted with the planned testing schedule.

The *CIUC* tests give information about the material strength and stiffness properties when subjected to compression loading but, in this application, columns installed on the passive side of a retaining structure, the lime/cement columns will be subjected to mainly shear and tension loading and thereby material properties and stress-strain behavior under extension loading are important. Also, during the field tests the lime-cement columns in the field will be subjected to different loading conditions:

- a. During the excavation stages, σ_v will decrease due to removal of soil while σ_h will remain constant or increase depending on the stiffness of the retaining structure and degree of mobilization of a passive earth pressure. This loading situation will be close to a triaxial extension test conducted in such a way that σ_r is kept constant/increased while σ_a is decreased.
- b. During the loading stage, σ_v will remain constant while σ_h will increase due to mobilization of passive strength until a failure mechanism emerges. This loading situation will be close to a triaxial extension test conducted in such a way that σ_r is increased and σ_a is kept constant.

Loading performed in *CIUC* tests was done by increasing σ_a while σ_r was kept constant and the tests were performed strain controlled at a rate of ε_a equal to 0.7% /h, corresponding to a shear strain rate of 1.0%/h. Loading performed in *CIUE* tests was done by increasing σ_r while σ_a was kept constant and the tests were performed using a constant rate increment of the radial stress. The stress conditions for the conducted tests are shown in Tables 9 and 10.

Table 9: Stress conditions in the undrained shear tests for samples from 5 m depth

Sample	Depth	Test	σ'_{v0} [kPa]	σ'^{cons}_{v} [kPa]
LC1A	5 m	*CIUC*	39	40
LC1B	5 m	*CIUC*	39	65
LC1C	5 m	*CIUC*	39	145
LC1D	5 m	*CIUC*	39	41
LC1E	5 m	*CIUC*	39	41
LC1F	5 m	*CIUE*	39	39
LC1G	5 m	*CIUE*	39	38
LC1H	5 m	*CIUE*	39	42

Table 10: Stress conditions in the undrained shear tests for samples from 7 m depth

Sample	Depth	Test	σ'_{v0} [kPa]	σ'^{cons}_{v} [kPa]
LC2A	7 m	*CIUC*	50	40
LC2B	7 m	*CIUC*	50	65
LC2C	7 m	*CIUC*	50	95
LC2D	7 m	*CIUC*	50	45
LC2E	7 m	*CIUC*	50	60
LC2F	7 m	*CIUE*	50	51
LC2G	7 m	*CIUE*	50	35
LC2H	7 m	*CIUE*	50	51

3.4.2 Test results

As expected, different failure modes occurred for the *CIUC* and *CIUE* tests. These are illustrated in Fig. 14. A single shear plane failure was the general failure mode for *CIUC* tests on improved samples from both 5 and 7 m depth, while all *CIUE* tests resulted in a failure where the sample was elongated and failure occurred along a horizontal plane. The location of the failure plane differed for each sample, indicating that for extension loading, failure takes place along a weakness plane that depends on the quality and homogeneity of the actual sample tested.

(a) *(b)* *(c)* *(d)*

Figure 14: Pictures of failure modes after triaxial tests on stabilized clay samples
(a) Shear plane failure compression test; sample from 5 m depth
(b) Shear plane failure compression test; sample from 7 m depth
(c) Tension failure extension test; sample from 5 m depth
(d) Tension failure extension test; sample from 7 m depth

3.4.3 Deviator stress-axial strain behavior

The stress-axial strain relationship for both compression and extension tests is illustrated in Fig. 15. In general, the laboratory improved soil exhibits a ductile behavior in compression, with ε_a compression at peak deviator stress, q_{peak}, of about the same size as the *UCT*, 2.8 – 4.5%. Several of the compression tests indicate an initial yielding of the samples at a stress level corresponding to 50-75% of q_{peak}, above which level there is a significant decrease of the elastic modulus. This stress-strain behavior is not typical of medium or high strength stabilized soils and the stress-strain behavior in the conducted tests is rather similar to a strain hardening material with an expanding yield surface. In the majority of *CIUC* tests there is almost no reduction of the residual undrained shear strength, $s_{uc\,res}$, compared to the peak undrained shear strength, $s_{uc\,peak}$ $(= q_{peak}/2)$, except for two samples that also exhibit higher strengths and for which $s_{u\,res}$, is about 85% of $s_{u\,peak}$. The mean triaxial compressive strength is slightly lower compared to the *UCT*s, about 87% of $q_{u\,28d}$, for both 5 and 7 m samples. The difference in obtained compressive strength can, according to Åhnberg (2006), be explained by differences in the degree of sample saturation and different strain rates being applied in the different tests during shearing of the samples.

For extension loading, the peak undrained shear strength, $s_{ue\,peak,}$ was evaluated to 93% for the 5 m samples and 68% for the 7 m sample of $s_{uc\,peak}$. In the *CIUE* tests, the material exhibits a more brittle behavior with ε_a at q_{peak} in the order of 50% of ε_a in compression, about 1.5-2.5%. Also, in contrast to the *CIUC* tests a very small scatter in the magnitude of q_{peak} was obtained.

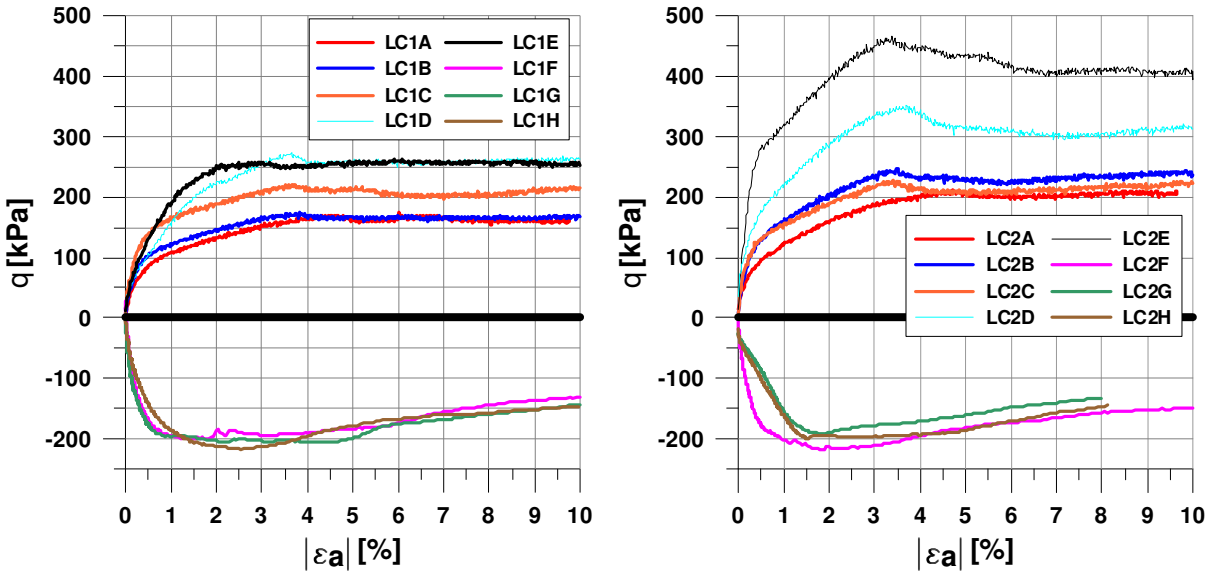

Figure 15: Results of CIUC and CIUE tests; deviator stress versus axial strain
(a) 5 m depth
(b) 7 m depth

3.4.4 Excess pore water pressure development

The excess pore pressure- axial strain relationship for both the *CIUC* and the *CIUE* tests is presented in Fig. 16. The low increase in pore pressure for samples LC1D, LC2G and LC2H indicates that full saturation of those samples was not accomplished. The overall behavior in all conducted tests was similar to an overconsolidated stiff soil with positive Δu generated at the start of the shearing test followed by, prior to q_{peak} being reached, a decrease in Δu. In the *CIUC* tests, which were performed at different consolidation stresses, the results show that there is a clear relationship between Δu and $\sigma_v'^{cons}$, with increasing Δu generated at the start of the test for samples consolidated at a higher $\sigma_v'^{cons}$. In samples of higher strength consolidated at low $\sigma_v'^{cons}$, negative Δu develops due to dilation prior to failure indicating that these samples are heavily overconsolidated.

In the *CIUE* tests, Δu shows up to about 2% axial strain a behavior similar to the *CIUC* tests, with initial positive Δu development followed by a decrease in Δu before q_{peak} was reached. At larger $\varepsilon_{a,}$ generated Δu in the *CIUE* tests shows a different behavior compared to the *CIUC* tests. This is believed to be caused by the boundary conditions of the conducted tests. To illustrate this, the development of σ_r, σ_a, ε_a, and Δu during the shearing stage are presented for samples LC1F and LC1G in Fig. 17, and the same behavior was observed in all the *CIUE* tests.

At the start of the test, σ_r is increased at a constant rate while σ_a remained constant, according to the imposed test conditions. During the initial shearing stage, ε_a increased at a constant rate (until it reached a value of about 0.7%) and increased at a much faster rate thereafter. This corresponds to the stress level where the material yielding criterion has been reached. As the yielding criterion was reached, illustrated by line (1) in Fig. 17, the strain rate began to increase rapidly and at the same time Δu began to decrease. After this stage, σ_r continued to increase, but at a significantly larger strain rate, until a failure criterion was obtained at q_{peak}, illustrated by line (2) in Fig. 17. As the failure criterion was reached, the imposed conditions could no longer be fulfilled due to large deformations of the sample, and resulted in a slight decrease in σ_r. Due to the sample continuing to deform (the sample was elongated), eventually σ_a could no longer be kept constant and began to increase. This caused an increase in Δu, illustrated by line (3) in Fig. 17. At this stage, due to the imposed boundary conditions, the test changed from being a loading extension test to a loading compression test.

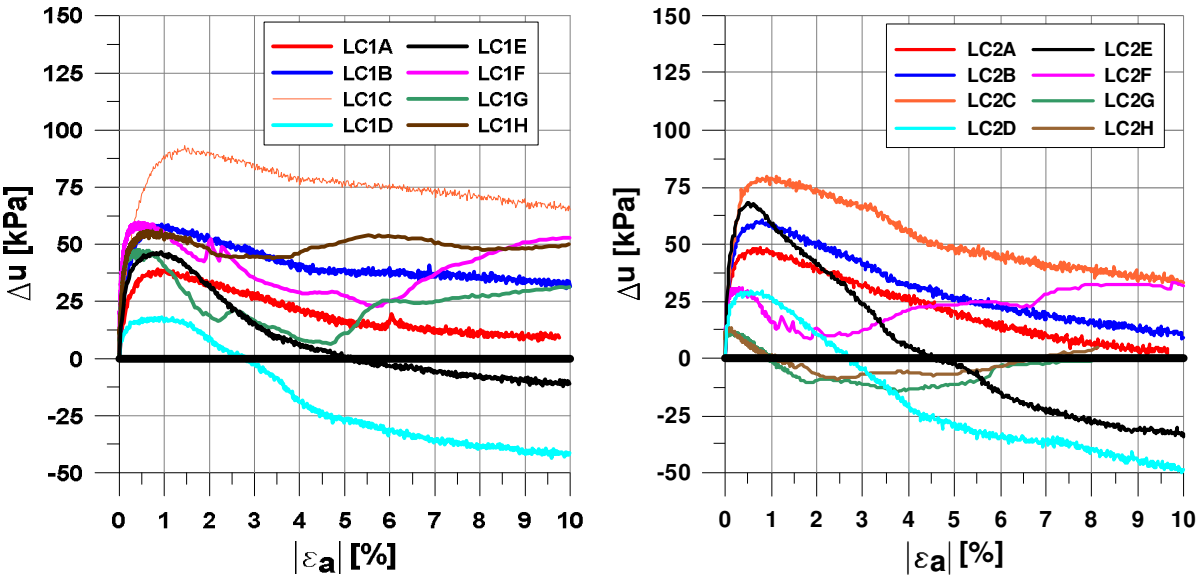

(a) *(b)*

Figure 16: Results of CIUC and CIUE tests; excess pore pressure versus axial strain.
(a) 5 m depth
(b) 7 m depth

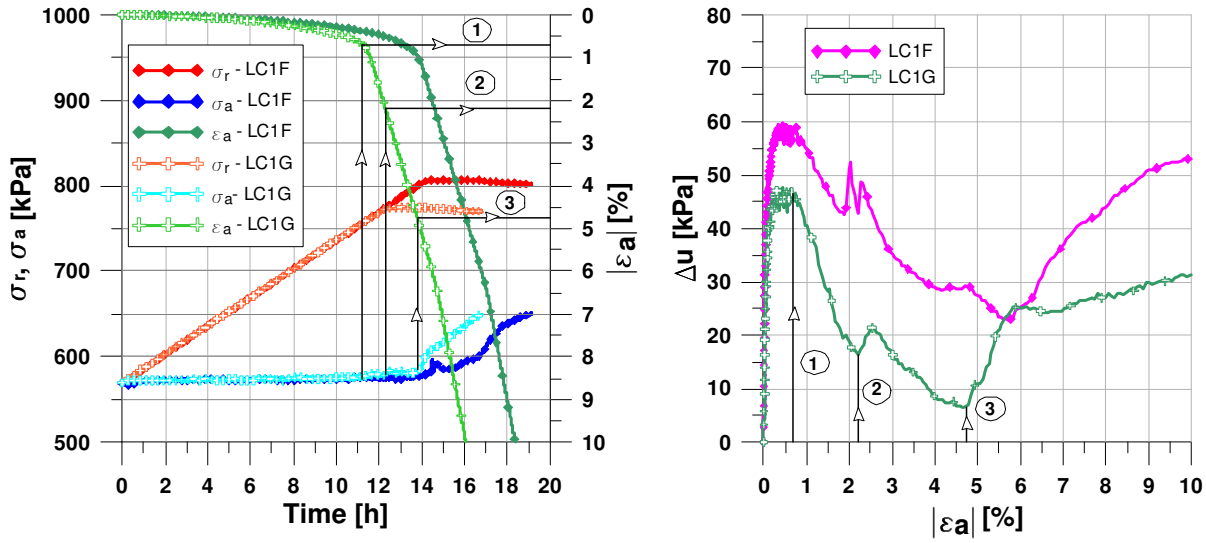

(a) *(b)*

Figure 17: Stress, strain and excess pore pressure behavior during shearing stage for CIUE tests
(a) Development of radial stress, σ_r, axial stress, σ_a, axial strain, ε_a
(b) Development of excess pore pressure, Δu

The effect of the increase in σ_a after failure due to the boundary conditions of the test (that in the *CIUE* test corresponds to the minor principal stress), is that q_{peak} decreases and the material behavior after failure, according to the strain-stress relationship will be rather similar to a strain softening material.

3.4.5 Effective stress paths

The overconsolidated behavior observed regarding development of Δu is also confirmed by the effective stress paths both for *CIUC* and *CIUE* tests, presented in the *s'-t* graphs in Fig. 18. In samples consolidated at higher $\sigma_v'^{cons}$, high Δu are generated during the initial shearing stage and there is a clear inclination to the left of the effective stress path towards the drained effective failure line, indicating a slightly overconsolidated behavior, before the stress path changes to the right as Δu begin to decrease. In samples consolidated at low $\sigma_v'^{cons}$, the stress paths are by contrast inclined to the right almost from the very start of the shear test due to smaller increase in Δu and thereby increasing mean effective stresses, and the failure line is approached more gradually. The initial yielding under compression loading observed in the stress-strain behavior coincides in the presented *s'-t* graphs with the intersection point between the effective stress path and the effective failure line.

The difference in stress path between the 5 and 7 m samples in the *CIUE* tests is believed to be caused by the 7 m samples (LC2G and LC2H) not being fully saturated. Due to the low pore pressure generated, the effective mean stress, *s'*, will be overestimated causing the stress path to deviate from the effective failure line.

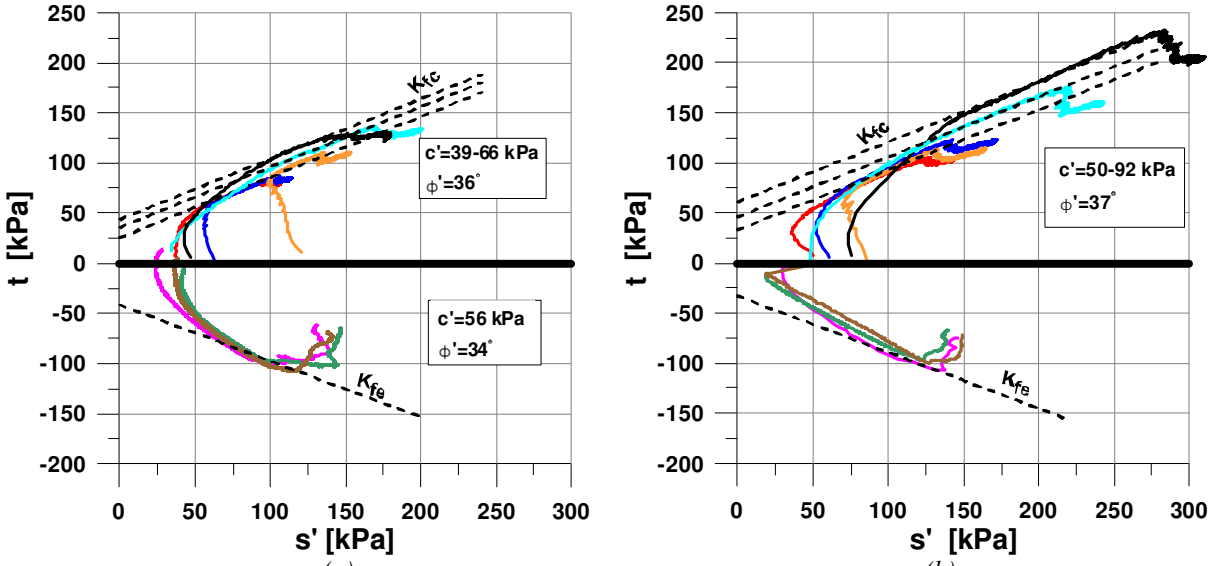

(a) *(b)*

Figure 18: Results of CIUC and CIUE tests; stress paths in s'-t plane
(a) 5 m depth
(b) 7 m depth

3.4.6 Evaluation of material properties

Drained strength parameters were evaluated based on the effective stress paths. In the CIUC tests, the obtained effective friction angle, ϕ', was evaluated to 36°-37° and no increase in magnitude could be observed with increasing q_{peak}. On the other hand, a much larger scatter in the results was obtained for the effective cohesion intercept, c', that was found to vary between 39-66 kPa for the 5 m samples and 50-92 kPa for the 7 m samples. The results also show that c' is strongly linked to q_{peak} and the ratio c'/q_{peak} was found to vary between 0.18 - 0.25. Almost all the tests were conducted at low $\sigma_v'^{cons}$ in order to reflect the actual conditions in the field, and the results are in good agreement with results reported earlier by Kivelö (1998), Åhnberg (2006), Balasubramaniam & Buensucesco (1989) and Tatsouka & Kobayashi (1983).

In the *CIUE* tests, ϕ' was slightly lower compared to the *CIUC* tests and a ϕ' value of 34° was evaluated. The cohesion intercept evaluated from the *CIUE* tests was also lower and was found to vary between 45-56 kPa. The ratio c'/q_{peak} evaluated from the *CIUE* tests was of about the same magnitude, 0.21-0.28, as for *CIUC* tests.

In the *CIUC* tests, E_{50}, is of the same magnitude as values reported earlier by Baker (2000) and Åhnberg (1995) for lime-cement stabilized samples, of 50-200× q_{peak}, and the tests indicate that E_{50} increases with increasing s_u but also with increasing $\sigma_v'^{cons}$.

In general, E_{50} evaluated from the *CIUE* tests (unloading modulus) was considerably higher compared to the modulus evaluated from the *CIUC* tests. The mean ratio between unloading and loading modulus, $E_{50\,e}/E_{50\,c}$, for the 5 m samples was evaluated to be 2.2 and the ratio E_{50}/q_{peak} between *CIUE* and *CIUC* tests had about the same value, 2.3. Also, in contrast to the *CIUC* tests the stress-strain relationship remained linear until close to q_{peak} was reached.

Table 11: Material parameters evaluated from CIUC tests.

Sample	Depth [m]	q_{peak} [kPa]	E_{50} [MPa]	ε_a [%]	E_{50} / q_{peak}	c' / q_{peak}
LC1A	5	179	16.9	3.9	94	0.22
LC1B	5	175	30.4	3.6	174	0.22
LC1C	5	224	41.4	4.2	185	0.18
LC1D	5	275	17.4	3.5	63	0.20
LC1E	5	264	25.4	2.8	96	0.25
LC2A	**7**	213	12.0	4.5	56	0.23
LC2B	**7**	247	29.3	3.5	119	0.20
LC2C	**7**	230	34.2	3.4	149	0.22
LC2D	**7**	354	30.1	3.6	85	0.20
LC2E	**7**	469	77.1	3.2	164	0.20

Table 12: Material parameters evaluated from CIUE tests.

Sample	Depth [m]	q_{peak} [kPa]	E_{50} [MPa]	ε_a [%]	E_{50} / q_{peak}	c' / q_{peak}
LC1F	5	199	60.4	1.4	304	0.28
LC1G	5	204	78.2	2.2	381	0.27
LC1H	5	217	36.5	2.5	168	0.26
LC2F	**7**	218	60.5	1.8	278	0.21
LC2G	**7**	199	(16.9)*	1.8	(85)*	(0.23)*
LC2H	**7**	200	(20.8)*	1.5	(104)*	(0.23)*

* Results are believed not to be representative due to samples not being fully saturated.

4 NUMERICAL ANALYSES OF AN EXCAVATION SUPPORTED BY LIME-CEMENT COLUMN ROWS

4.1 Background and Scope of Numerical Analyses

As part of planning and preparation for the field tests, finite element analyses were conducted, in order to study the behavior of laterally loaded rows of lime-cement columns installed in the passive zone of a retaining structure. A few case studies and numerical analyses of the deep mixing column type of ground improvement in deep excavations have been published by Tanaka (1993), O'Rourke & O'Donell (1997), Ou et al. (1996, 2008, 2013), Yang et al (2011). In the majority of the numerical analyses that have been presented, 2D "plane strain" models or 3D analyses where the improved soil is modeled as a composite material with weighted strength and stiffness properties have been used. Excavation and loading of a sheet pile wall where the soil on the passive side of the wall is improved by deep mixing columns is a three-dimensional mechanical system in which the retaining structure, the columns and the soft soil between the columns interact. If the columns and the soil in-between are modeled as a composite material, the interaction between the columns and the soil with respect to stress distribution, shear stresses and deformations cannot be fully studied. Aside from the distance between the column rows and distance between the columns within the row, even the strength properties of the overlapping zone which often are lower than the strength of the columns, as demonstrated by Yoshida (1996) and Yoshizawa et al. (1997), is believed to have a important significance on the behavior of laterally loaded deep mixing columns.

The scope of the conducted numerical analyses was to investigate how a 2D model will predict the ultimate limit state behavior regarding failure load, failure mechanism, stress-strain relationship, and deformations up to failure load, compared to a 3D model when the columns are subjected to lateral forces. Also a method to model the vertical overlap between the columns in a 2D plane strain model is compared to a 3D model. A large number of both 3D and 2D analyses where the effect of different center distance between the column rows, s_{row}, center distance between columns in each row, s_{col}, and strength and stiffness properties of the overlapping zone between the columns were conducted.

4.2 Geometrical Model and Material Properties

At the time when these finite element analyses were conducted only an overall site investigation and no laboratory test were yet performed at the location of the test sites. Input values of the geometrical model and material properties chosen for the soft clay and stabilized soil in this study, are therefore theoretical, and are not fully consistent with the laboratory test results presented above and geometrical layout of the later conducted field tests. The strength and stiffness parameters chosen for the stabilized soil are typical for dry deep mixing lime-cement columns in Sweden while properties of the structural elements (sheet pile, anchors, wale beam) was chosen as typical for Scandinavian country's construction projects involving excavation works. Only a brief presentation of the geometrical model, material properties and analyses set-up is presented here and the boundary and model conditions and also material properties of the soil, lime-cement columns and retaining structure are presented in Paper I.

The soil was assumed to consist of 1 m of stiff dry crust overlaying 10.5 m of normally consolidated very soft clay over very stiff frictional soil and a groundwater table situated at the top of the soft clay, 1 m below the ground surface. The retaining structure was a steel sheet pile wall with a length of 7 m. The length of the sheet pile wall was chosen such that a rotational stability failure governed the failure mechanism of the wall. The sheet pile wall was horizontally anchored backward with steel wire anchors 1 m below the ground surface with a center-to-center distance of 3 m. The improved soil consists of dry deep mixing columns with a diameter of 0.6 m, installed as overlapping columns perpendicular to the sheet pile wall. The column rows had a width of 7.0-7.2 m and a length of 10 m starting from the upper edge of the soft soil. In order to avoid boundary effects, the length of the model was chosen to be 35 m and its width, due to symmetrical effects, to be 3 m, Fig. 19. The simulated

width of the excavation was chosen to be 15 m, while the unexcavated side was chosen to be 20 m from the side boundary of the model.

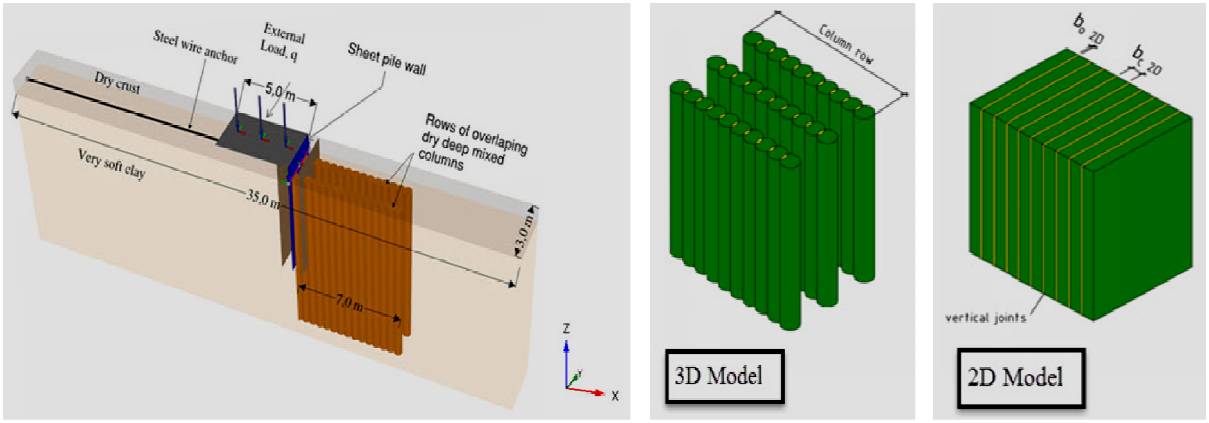

(a) *(b)* *(c)*

Figure 19: Geometric model for conducted numerical analyses
(a) 3D model geometry
(b) Row of overlapping columns; 3D model
(c) Composite material with vertical joints representing column overlap; 2D model

In order to compare the 3D and the 2D methodologies, the effect of a strength reduction in the overlapping zone between the columns in the rows was taken into account in the 2D model by defining vertical joints in the composite soil volume. The weighted material properties of the composite soil volume were calculated based on the area replacement ratio of the columns and the area replacement ratio of the overlap zones, which was chosen equal to the corresponding 3D area replacement ratio. The finite element program PLAXIS 3D 2012 was used in this study and the analysis was performed as undrained effective stress analysis with undrained strength parameters since the excavation and the loading were executed rapidly and the consolidation process is therefore very limited.

4.3 Analyses Set-up

The analyses were performed by defining calculation phases for each working sequence in order to model how a stage excavation inside a braced sheet pile wall and a loading procedure is usually conducted in reality. The excavation was performed in two steps to a final excavation depth of 4 m below the ground surface, before a uniformly distributed surface load, q, was applied behind the sheet pile wall. After the last excavation stage, a uniform distributed load, q, was applied and increased in constant increments of 10 kPa until a failure collapse mechanism was reached. Due to the excavations, the earth pressure acting on the sheet pile wall increased and the column rows were subjected to an increasing lateral loading and a simultaneously decrease in overburden pressure on the passive side of the retaining structure. In this way, the development of the emerging failure mechanism and the stress-strain relationship in the columns when subjected to laterally loading until failure could be analyzed.

4.4 Summary of Results and Conclusions from Numerical Analyses

Here, only some of the results and conclusions obtained from this study are presented, and for full results, analyses and discussion the reader is referred to the appended paper (Paper I).

In general, the results show that the 2D model can predict an ultimate load (evaluation of the ultimate load is described in detail in Paper I), q_{ult}, that agrees well with the corresponding 3D analyses regardless of s_{row} and s_{col} for full overlap strength. Also, by introducing vertical joints in the composite soil volume, the 2D model can effectively predict the load-induced shear stress in the column rows, as illustrated in Fig. 20.

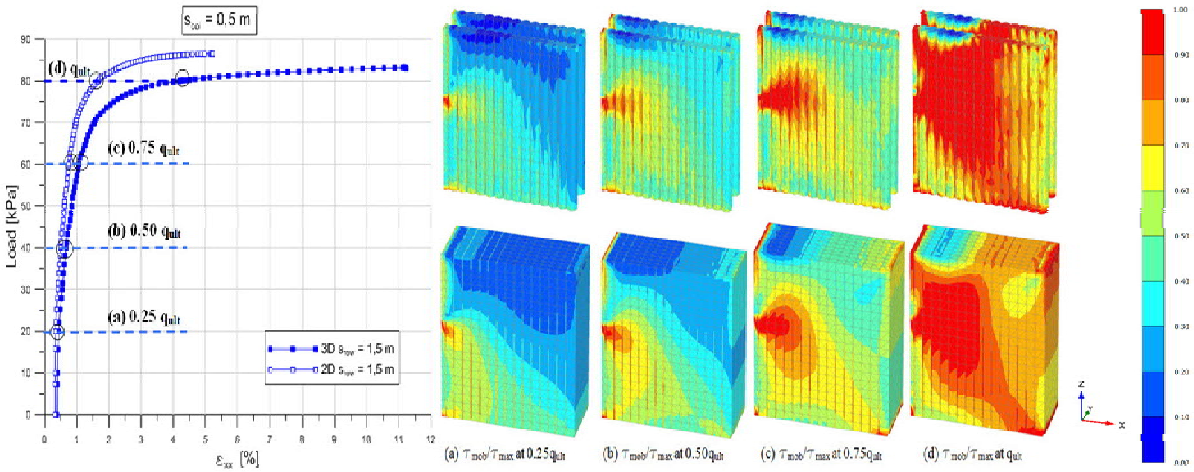

Figure 20: Load-strain curve of 3D and 2D calculations with s_{row} = 1.5 m and s_{col}= 0.5 m. Snapshots of ratio between mobilized shear stress and maximum shear stress at 25, 50, 75 and 100% of q_{ult}.

Similar results are obtained if the reduction of strength and stiffness properties in the overlap zone between the columns is less than 50%. For a width of overlap zone between columns of 0.2 m, s_{col} =0.4 m, the strength properties of the overlap zone will have a significant effect on the predicted ultimate load. For a very poor overlap quality, 75% reduction of overlap strength, the 2D model generally predicts a lower ultimate load for a high area improvement ratio and a significantly higher ultimate load for a low area improvement ratio compared to a 3D model.

For full overlap strength, the 2D model will underestimate both the deformation in the stabilized soil and the displacement of the retaining structure compared to the deformation predicted by the 3D model. The ratio between the 3D and 2D predicted horizontal strain in the stabilized soil beneath the excavation at the same load level and the horizontal displacement in the sheet pile wall are compared and shown in Fig. 21. The horizontal strain ratio, $\varepsilon_{x\,3D}/\varepsilon_{x\,2D}$, between the 3D and 2D analyses as a function of q is presented up to the level $q = q_{ult}$. After the excavation and before the load is applied, there is no significant difference regarding s_{row}. After the load is applied, $\varepsilon_{x\,3D}/\varepsilon_{x2D}$ increases at first almost linearly in all studied cases. In all cases there is a distinct non-linear increase in $\varepsilon_{x\,3D}/\varepsilon_{x2D}$ when q exceeds 65-90% of the evaluated q_{ult}.

When the strength and stiffness properties of the column overlap are reduced, the results of predicted strains and deformation of the sheet pile wall show different trends in the 2D and 3D analyses, see Fig. 22. For a high area ratio improvement, s_{row}= 1.0 m, $\varepsilon_{x\,3D}/\varepsilon_{x2D}$ is constant until approximately 80-90 % of q_{ult} is reached. Above this load level, $\varepsilon_{x\,3D}/\varepsilon_{x2D}$ increases as q is further increased for an overlap strength equal to the column strength ($s_{u\,o} = s_{u\,c}$), but $\varepsilon_{x\,3D}/\varepsilon_{x2D}$ decreases as the overlap strength is reduced. The results also show that for an equal reduction in overlap strength, $\varepsilon_{x\,3D}/\varepsilon_{x2D}$ decreases faster when the overlap area is increased (s_{col} decreases). For a low area improvement ratio, s_{row} = 3.0 m, the overall trend is that $\varepsilon_{x\,3D}/\varepsilon_{x2D}$ increases when q is increased, i.e. the 3D analysis predicts larger strains at q_{ult} regardless of overlap strength.

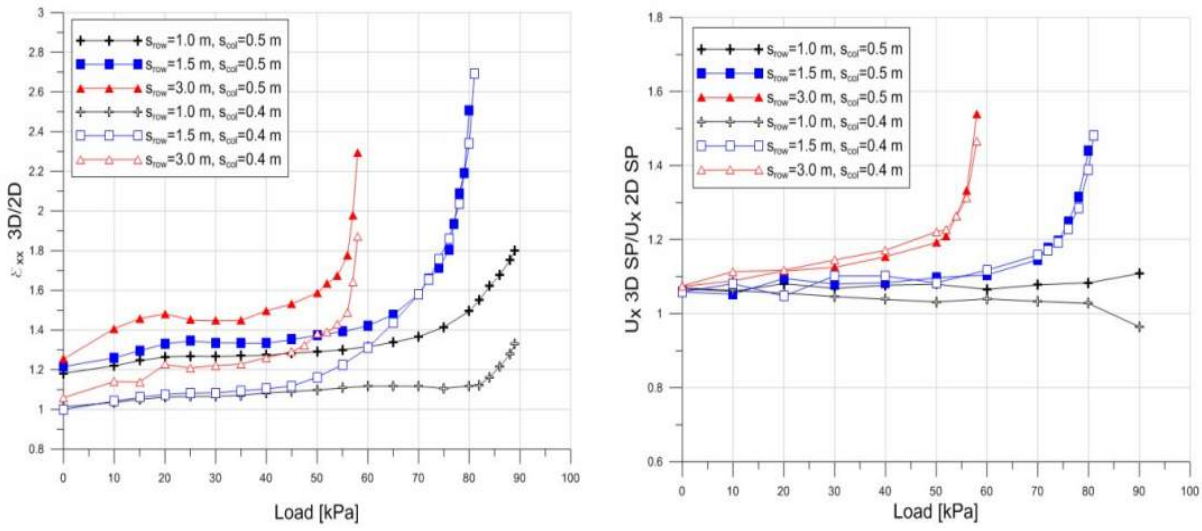

(a) *(b)*

Figure 21: Results of calculated deformations for full overlap strength

(a) Horizontal strain ratio, $\varepsilon_{x\,3D}/\varepsilon_{x\,2D}$,

(b) Ratio between the maximum horizontal deformations of the sheet pile wall

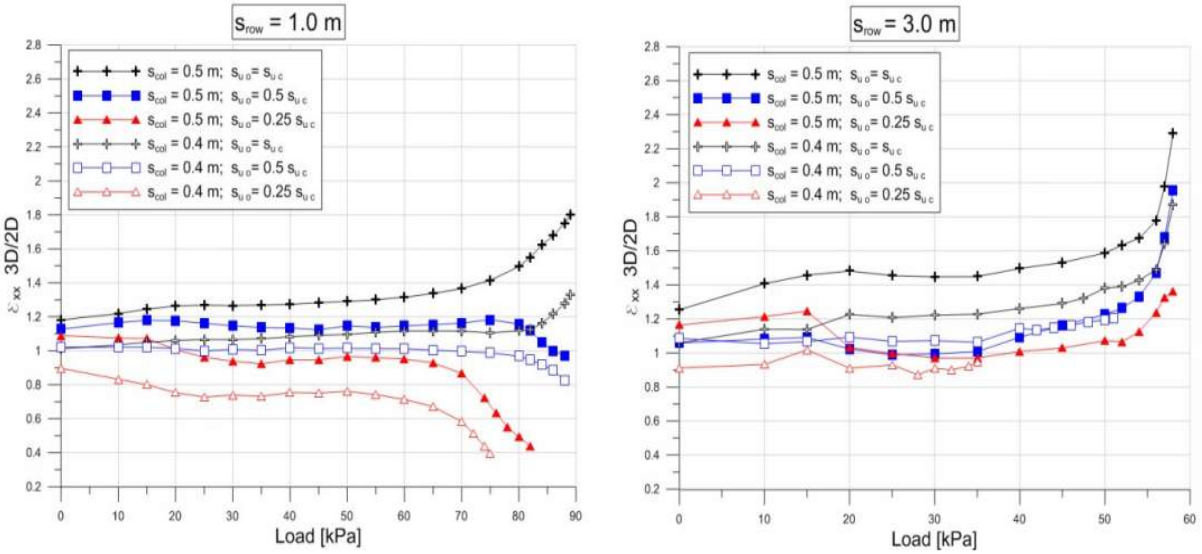

(a) *(b)*

Figure 22: Results of calculated deformations for reduced overlap strength

(a) Horizontal strain ratio, $\varepsilon_{x\,3D}/\varepsilon_{x\,2D}$, s_{row}= 1.0 m

(b) Horizontal strain ratio, $\varepsilon_{x\,3D}/\varepsilon_{x\,2D}$, s_{row}= 3.0 m

The following conclusions could be deduced from the conducted finite element analyses:

- By taking into consideration the effect of the overlap zone between columns installed in a row pattern, a 2D plane strain model shows reasonably good agreement regarding obtained deformations compared to a 3D model, as long as the stress level in large parts of the stabilized soil does not reach the stated yielding criteria.
- Development of shear stresses in the overlap zones and columns in the rows due to loading, show good agreement between the 2D and the 3D model.
- The area improvement ratio has a significant influence on how well the prediction of calculated deformations agrees between the two models. In addition to the area replacement ratio, the quality of the overlap zone between columns impacts strongly on the predicted deformation but also the predicted ultimate load and the failure mechanism that occurs.

5 FIELD TESTS

Two full-scale tests where excavation and loading until failure of two individual retaining structures consisting of sheet pile walls and rows of overlapping lime-cement columns installed in the passive zone of the walls were performed. The full-scale tests were conducted between March and June 2014.

5.1 Test Set Up

The geometrical layout of both test areas was identical with the exception of the distance between the rows of lime-cement columns. For the first test site, Test 1, the distance between the rows, s_{row}, was 3.0 m while for the second test site, Test 2, s_{row} was 1.5 m. The distance between the two tests was about 40 m.

The geometrical layout of Test site 1 is shown in Fig. 23. Each test areas consists of two steel sheet pile walls, SPW, of type VL604, with a crest length of almost 20 m installed parallel to each other such that the width of the excavation pit is equal to 12 m. The SPWs were installed to a depth of 7 m below the ground surface on the loading side and to 7.5 m on the opposite side and the length of the SPW was chosen such that a rotational stability failure was the expected failure mechanism. The SPWs were braced with steel struts, HEB 300, at a level of 1 m below the ground surface installed with a center- to- center distance of 3.0-3.5 m. The load transfer between the SPWs and the struts was ensured by installing steel whale beams, HEB 260. The size of the excavated area at the bottom of the excavation pit was 14x12 m. Excavation between the SPWs to the planned level of 4.5 m below the ground surface was performed with open slopes. In order to improve the stability of the slopes, ground improvement with singular lime-cement columns was conducted 0-5 m behind the slope crest.

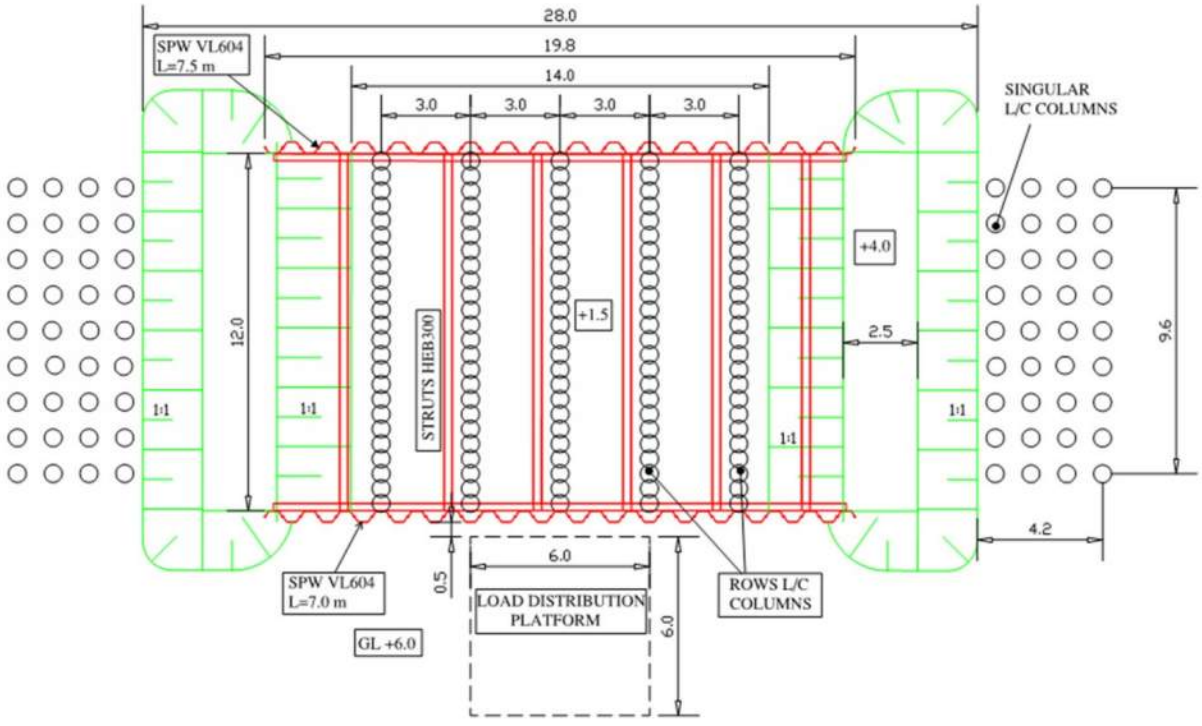

Figure 23: Plan view of geometrical layout for Test 1

5.2 Lime-cement Columns

5.2.1 Installation

Installation of the column rows were performed in April 2014 using the dry deep mixing procedure, where binder as a dry powder was mixed with the in situ clay. The binder content was 120 kg/m^3, 50% quicklime, QL 0-0.1 KÖ, and 50% Portland cement, CEM II/A-LL 42.5 R. For test 1, 5 rows of overlapping columns were installed and 9 rows of overlapping columns for test 2. Each row comprised 24 columns with a diameter of 0.6 m and a center- to- center distance of 0.5 m giving an improvement ratio, a_s, of 17.5% for test 1 and 35% for test 2. The columns were installed approximately 0.2-0.3 m into the frictional soil underneath the soft clay layer. The length of the columns installed for Test 1 was between 7.5-9.5 m with an average length of 8.8 m, while the columns installed for Test 2 had a length of 8.0-10.4 m with an average length of 9.0 m. The singular columns used to improve the stability of the open end slopes were installed in a rectangular pattern with a center- to- center distance of 1.2 m to a depth of 6.5 m below the ground surface. The columns were manufactured with a rotational speed of the mixing tool of 175 rev/min and a retrieval speed of 20 mm/rev and were installed before the installation of the SPWs. In order to ensure connection between the SPWs and the column rows, the SPWs in both test areas were installed 4-12 hours after the installations of the columns close to the center of the last column in each row, see Fig. 24.

(a) (b)

Figure 24: Pictures of Installation of Lime-cement columns
(a) Installation of SPW in newly installed columns, Test area 1
(b) Excavated column row 2.5 m below ground surface, Test area 2

5.2.2 Quality control of installed lime/cement columns

Quality control of the installed columns was conducted on one column in each row by column penetration tests, KPS. The KPS tests were conducted 10-12 days after installation of the columns and were performed according to the Swedish design guideline, TK Geo (2014) and Larsson (2006). Predrilling in the center of the columns was performed in order to facilitate the verticality of the KPS-probe. The KPS-probe was equipped with a CPT-probe (cone penetration test probe) allowing bar friction from the penetration resistance, $q_{c\,KPS}$, to be distinguished. The undrained shear strength of the columns, $s_{u\,KPS}$, evaluated according to the Swedish design guideline, TK Geo (2013) is presented in Fig. 25. The results from both Test 1 and Test 2 show similar results with relatively low shear strength of about 100-200 kPa between 2.5 and 5 m depth and the lowest strength is obtained at about 3.5 m depth. The shear strength increases thereafter to about 7 m depth, below which $s_{u\,KPS}$ was measured to vary between 300-400 kPa.

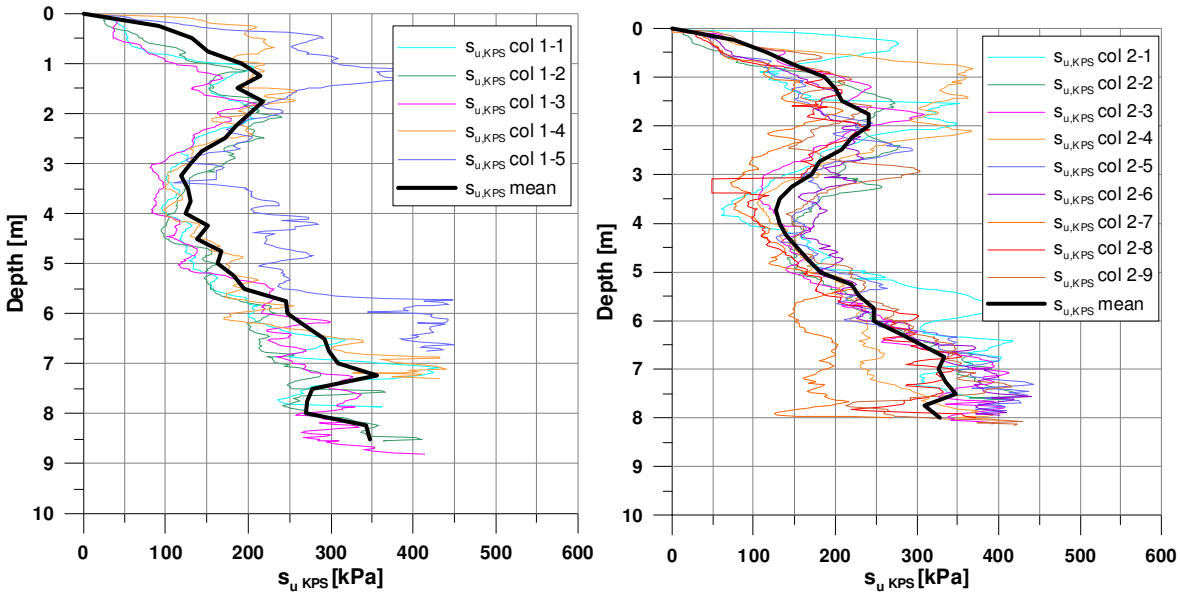

Figure 25: Results of KPS tests
(a) Test area 1
(b) Test area 2

The evaluated $s_{u\,KPS}$ corresponds well with the profile of the soft clay where streaks of sulphide soil occur between 2 and 5 m depth, see Fig. 24 b, and layers of silt/sand occur below 6-7 m. At 5 m, there is a good agreement of evaluated s_u between the field tests and the laboratory tests on improved samples, while at 7 m s_u evaluated from laboratory tests is lower compared to the field test results.

5.3 Test Procedure

The general working procedure from the start of excavation work was planned identical for both tests and is described below:

1. Excavation to a depth of 2.0 m below the ground surface.
2. Installation of whale beams and strut beams at a level of 1.0 m below the ground surface.
3. Installation of strain gauges on the strut beams.
4. Excavation to a depth of 4.0 m below the ground surface in the entire test area.
5. Excavation to a depth of 4.5 m below the ground surface with the exception of an area of about 0.5 m around the instruments
6. Construction of a stiff load distribution platform and mounting of steel containers on the load distribution platform
7. Stepwise loading until a failure mechanism is obtained

For both tests, excavation was carried out with a long-range excavator with a weight of about 30 tons and a digging arm with a reach of 16 m. Due to the long reach of the machine, all the excavation work could be conducted from the opposite side of the instrumented sheet pile wall. In order not to damage the instruments installed in the passive zone of the sheet pile wall, excavation closer to the instruments than 0.5 m was conducted with an 8-ton excavator equipped with a small dozer and by hand between the instruments. All the excavated masses were continuously moved 20-40 m away from the test area.

5.4 Loading Procedure

The load was applied after the excavation to full depth had been performed. Loading was performed by filling two containers, with a size of 6.3x2.6x2.50 (L x B x H). The containers were reinforced with a frame of HEB100 beams welded on the containers at two levels. Each container was centrically positioned on steel frames that were placed above a load distribution platform, LDP, with a size of 6x6 m, see Fig. 26. The load cells intended to monitor the applied load were installed beneath the steel frames and positioned in such a way that an equal load distribution should be obtained for all four load cells under one container.

The following procedure was used for the construction of the LDP (steps 1-5 below) and mounting of the containers in their final positions:

1. A 0.3 m thick layer of stony gravel 0-90 was placed on a geotextile at the ground level over an area of 6x6 m. The gravel was compacted using a manually operated roller with 6 overpasses.
2. 7 reinforced wooden carpets measuring 6.0x0.9x0.20 m and weighting 700 kg each were placed on the layer of gravel.
3. 4 steel plates measuring 4.0x2.0x0.03 m and weighting 2000 kg each were placed on the stock carpets
4. Two layers of steel plates, 0.4x0.3x0.02 + 0.13x0.13x0.02, on which the load cells were placed on were welded to the large steel plates.
5. The steel frames were lifted into position on the load cells, parallel to the direction of the wall
6. Load cells were put in place, 4 under each steel frame.
7. The containers were lifted into position on the steel frames.

Figure 26: Pictures of LDP construction and load container; Test 1

Figure 27: Pictures of LDP construction and mounted container; Test 2

Because the load required to induce a failure of the structure for Test 2 was expected to be higher than for Test 1, a stiffer LDP was constructed for Test 2 by increasing the layer of gravel to 0.35 m and installing two crosswise layers of reinforced wooden carpets instead of one. Also, to reduce the risk of tipping the containers at failure, the steel frames and containers were rotated 90°, see Fig. 27. Loading of soil masses in the containers was conducted with a long-range excavator. The excavator could reach the containers from a distance of 16 m which was considered far enough for safety resons. The load was increased stepwise with a time interval of about 1-3 hours between every new load step under continuous monitoring of the measuring instruments. For Test 1, excavated clay masses were used as filling material in the containers while for Test 2 the containers were filled with gravel material, 0-32 mm, in order to attain a higher load.

The weight of the LDP (compacted gravel, wooden carpets and steel plates) was equivalent to a distributed load of 9 kPa for Test 1 and 11 kPa for Test 2. The load measured in the load cells includes the dead weight of the steel frame the containers are placed upon, the dead weight of the containers, and the weight of the material loaded in the containers. The load for each container was calculated as the average load measured by the 4 load cells under each steel frame.

The total load applied was calculated as:

$$q_L = \frac{(G_{c1}+G_{c2})}{A_{LDP}} + q_{LPD}$$

where

q_L = Total distributed load behind the sheet pile wall [kPa]

G_{c1} = Average load for load cells under container 1 [kN]

G_{c2} = Average load for load cells under container 2 [kN]

A_{LDP} = Area of load distribution platform [m^2]

q_{LPD} = Load of the distribution platform [kPa]

5.5 Instrumentation

5.5.1 Location of instruments

The aim of the instrumentation was to collect extensive data on the performance of the structure with focus on excavation and loading induced deformations and stresses in the soil and structural forces acting on the SPW. In order to study the behavior of the stabilized soil, instrumentation of the test areas was performed on both the active and passive side of the SPW. Measurement instruments were installed at the same locations for both tests areas in order to compare the obtained results. The location of all instruments in plane is shown in Figs. 28 and 29.

A total of 6 inclinometers were installed in each test area, two on the active side and four on the passive side. Two of the inclinometers on the passive side were installed in the center of the columns while the remaining two were installed between the column rows at a distance of 1.5 and 4.0 m from the center line of the SPW. On the active side, the inclinometers were installed 0.5 m from the center line of the SPW and positioned in front of the instrumented column row and between the column rows.

Six earth pressure cells, with integrated pore pressure transducers were installed in each test area. Position in plane was chosen similar to that of the inclinometers with two cells installed on the active side and four on the passive side. Two of the cells on the passive side were installed in the lime-cement columns and the remaining two were installed between the column rows at a distance of 1.0 and 3.5 m from the center of the SPW. All cells on the passive side were installed at a depth of 5.5 m, which is between the planned bottom of excavation and the toe of the SPW. The cells on the active side were installed 0.5 m from the center of the SPW at a depth of 5.5 and 6.5 m.

Additional pore water pressure measurements were performed by means of 6 pore pressure transducers installed in the clay in each test area. Two of the transducers were installed on the active side, 0.5 m from the center of the sheet pile wall, at a depth of 3.0 and 5.5 m below the ground surface. The remaining four were installed in the clay between the column rows on the passive side of the sheet pile wall, 1.0 m and 3.5 m from the center of the wall at a depth of 5.5 and 7.0 m.

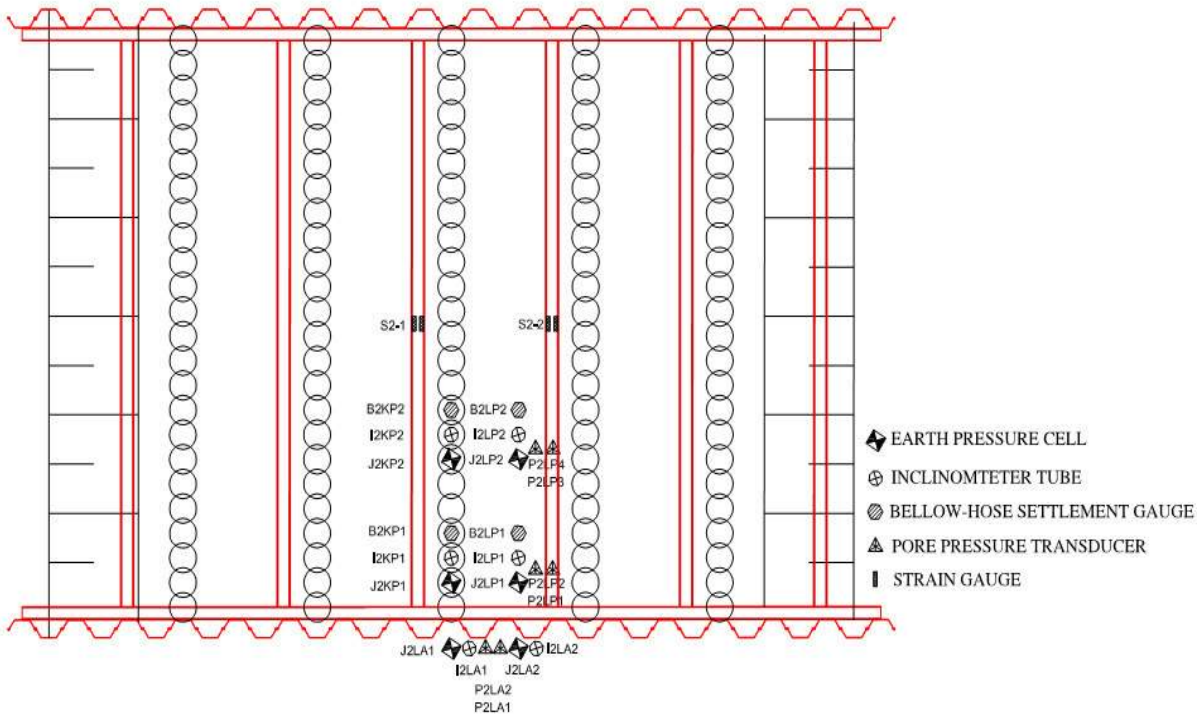

Figure 28: Instrumentation plan, Test 2

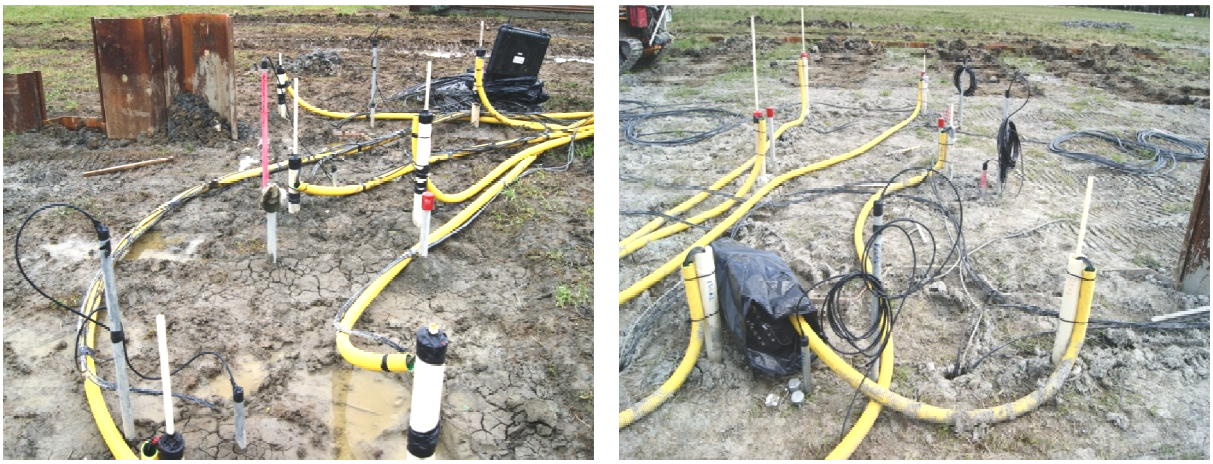

(a) *(b)*

Figure 29: Pictures after completion of instrumentation
(a) Test 1
(b)Test 2

Excavation induced vertical displacements in the soil/columns on the passive side of the SPW were measured through four bellow-hoses installed in each test area. Two of the instruments were installed in the center of the columns and two in the clay between the rows at a distance of 2.0 and 4.5 m from the center of the SPW. Normal forces in the strut beams were measured with strain gauges installed on two of the struts located in front of the loading area in each test area.

All measurements, with the exception of the vertical deformation measurements performed with bellow-hose settlement gauges, were collected automatically by connecting the measuring devices to GSM data loggers, allowing data to be both stored and transmitted wirelessly to a server for near real-time viewing.

5.5.2 Inclinometers

The inclinometers installed were of type Geometrik MI100 with centering device for tracked casings and a measuring range of 100mm/m in one direction. The inclinometer tubes have an outside diameter of 70 mm with a length of 3.0 m. The tubes are jointed with a pin connection and the outside diameter of the joint is 75 mm. The tube bottoms were installed in the dense sand/moraine layer. All inclinometers had a spacing between the inclination transducers of 1.0 m.

Installation of the inclinometer tubes in the lime cement columns was conducted within 48-72 hours after installation of the columns by pre-drilling a borehole with a 70 mm diameter ODEX drill bit in the center of the columns. In order not to risk damaging the columns, cautious drilling with simultaneously water flushing was conducted. The boreholes were drilled to about 0.5 m beneath the bottom of the column into the frictional soil layer and the inclinometer tubes were installed directly after the drilling.

5.5.3 Earth pressure cells

The earth pressure cells installed were manufactured by Glötzl, type PE/P (16.02.04.11.2), and equipped with integrated pore pressure transducers. The measuring range of the instrument is 0-500 kPa for earth pressure and 0-300 kPa for pore pressure. In order not to damage the sensors, all cells were installed after the installation of the columns and the SPW. Installation of cells in the columns was performed in the center of each column within 24 hours after installation of the columns.

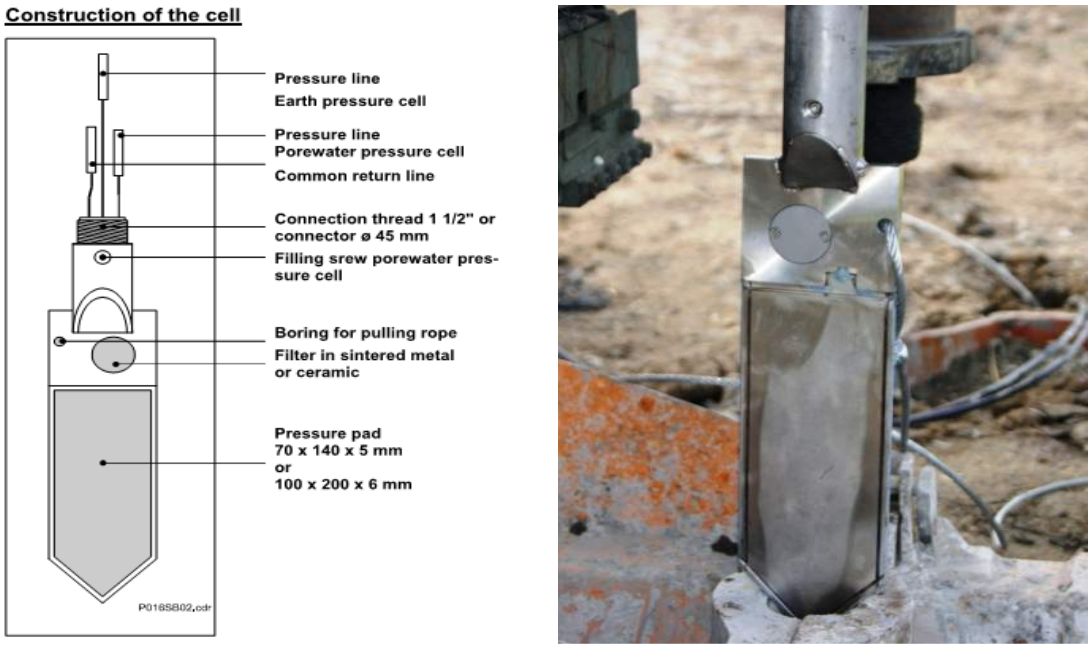

(a) (b)

Figure 30: (a) Technical description of earth pressure cell type PE/P from Glötzl
(b)Picture of earth pressure cell during installation

The cells are of push in type and are usually installed by connecting steel rods and pushed in to the desired depth. When the cell has been pushed in to the desired level the rod is retracted, leaving the cell in place. The steel rods used to push the cells into the soil are relatively slender and if the cells have to be installed at larger depth or through firm soil this has proven to cause difficulties. Damage to the sensors can occur due to bending/torsion of the pressure pad during installation. To reduce the risk of damaging the cells during installation, a borehole was created at the location of every cell to a depth of 0.5 m above the desired installation level using a soil screw sampler with 100 mm in diameter. The earth pressure cell were then submerged into the created borehole with steel rods and then pushed in to the soil the remaining 0.5 m to the desired level. A steel cable was attached to the cells in order to be able to retrieve them after the tests.

5.5.4 Pore pressure sensors

Each test area was instrumented with 6 pore pressure sensors. The sensors are manufactured by Keller, type PR36, and are equipped with BAT MkIII filter tips. The measuring range of the instruments was 0-200 kPa. Installation of pore pressure sensors was completed two weeks before the start of the full-scale tests, giving enough time for equalization of the pore pressure in the soil resulting from the installation process.

5.5.5 Bellow-hose settlement gauges

The bellow-hoses were installed 24-72 hours after the installation of the columns. Each bellow-hose was equipped with gauges with a vertical center distance of 1.0 m and the last gauge was installed at a depth of 0.5 m in the frictional soil below the clay layer/columns. Due to installation in the stiff frictional soil, the last gauge in every bellow-hose was considered to be fixed (no vertical displacements) and served as a reference point for the measurements. Measurements were conducted manually, see Fig. 31 a, and the vertical deformation in the soil layer below the excavation was calculated as the relative movement between each gauge and the last gauge installed in the frictional soil. Each measurement was repeated twice in order to avoid reading errors. Measurements were performed before and after every excavation step, before start of loading and after the tests were completed.

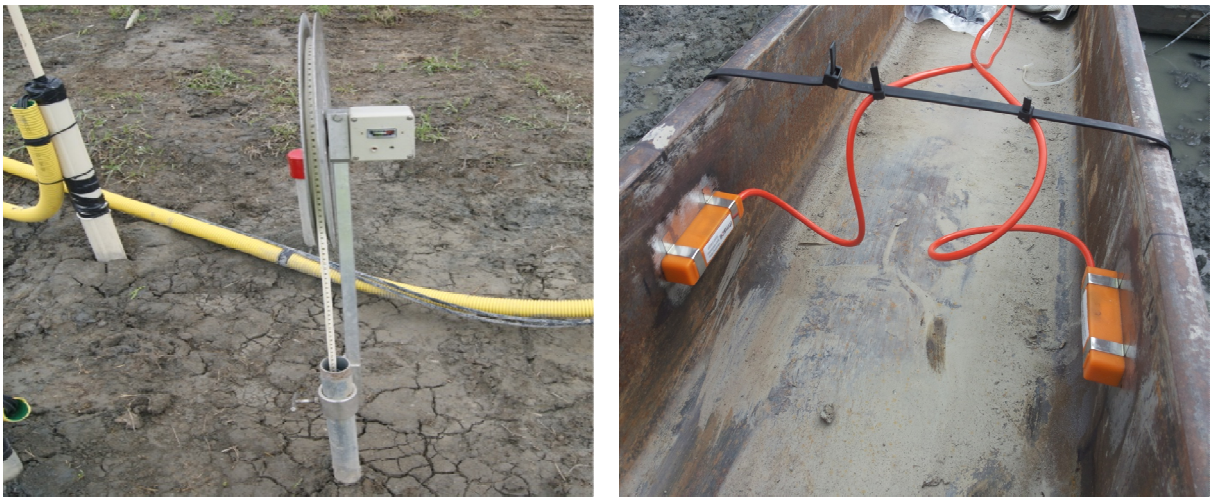

(a) *(b)*

Figure 31: *(a) Picture of measurement of bellow-hose*
(b)Picture of installed strain gauges on strut beams

5.5.6 Strain gauges

Two strut beams in every test area were instrumented with four strain gauges each, see Fig. 31 b. The strain gauges were manufactured by ITM Soil, of type vibrating wire spot weldable strain gauge with integral thermistor, ST1. The strain gauges were welded to the beam flanges, two on every flange. The measuring range of the instruments was 0-3000 microstrains with a temperature range of -20 to +80°C and a measuring accuracy of ± 0.5%. The reported strut force was the calculated mean value between the four strain gauges attached to the beam flanges.

5.5.7 Load cells

The load applied behind the SPW was monitored by means of 8 load cells, 4 under each container, manufactured by Glötzl, of type KLN250 AI and equipped with piezoelectric transducers. The measuring range of each load cell was 0-250 kN with a maximum load of 300 kN and a measuring accuracy of ± 0.5 %.

(a) *(b)*

Figure 32: *(a) Load cell type Glötzl*
(b) Load cell installed under steel frame

5.8 Test Execution - Test 1

Excavation to the first level of 2.0 m below the ground surface was conducted from 13 to 14 May 2014. Directly after the excavation was completed, installation of the whale beams, strut beam followed by instrumentation of the strut beams was initiated and was completed on 20 May. The next excavation step, to a depth of 4.0 m began on 21 May and was completed a day later. Final excavation to 4.5 m below the ground surface was conducted on 26 May and the LDP was constructed during the same day. Load containers were lifted into place upon the load frames on 27 May and loading of the containers began the same day at 13:30. The load was stepwise increased, according to Table 13, and the last load step was applied at 18:40.

Table 13: Applied load Test 1

Time schedule	Container load at end of load cycle [kN]		Total load [kPa]
	Load cells under steel frame 1	Load cells under steel frame 2	Containers + Load platform
Start	6.0	4.0	9.3
Containers lifted into place: 11:45-12:10	99.5*	34.5	12.7
Load step 1: 13:30-14:10	191.3	109.0	17.3
Load step 2: 14:50-15:05	229.0	160.4	19.8
Load step 3: 16:05-16:20	305.1	275.6	25.1
Load step 4: 17:20-17:50	503.2	538.0	37.9
Load step 5: 18:30-18:40	550.5	588.5	40.6

**The weight of the containers differed because container 1 had double base plates of steel installed.*

From the start of loading until the end of third load step, only small linear changes of horizontal displacements, excess pore pressures, earth pressures and strut forces were measured. Under the fourth load step the load was therefore increased from 581 kN to 1041 kN. After the last load step, the total load, including the dead weight of the LDP, reached 1460 kN which is equivalent to a distributed load of 40.6 kPa. The load in the containers remained constant at a value of 1139 kN from the end of the last load cycle until 20:50. Between 20:50 and 21:00 the load, measured in the load cells, dropped to 950 kN and this corresponds to the time of failure. The failure mechanism was a rotational stability failure of the sheet pile resulting in a large heave of the soil at the bottom of the excavation and settlements on the active side of the SPW. After failure the load remained constant at about 950 kN until backfilling of the excavated area began at about 23:30.

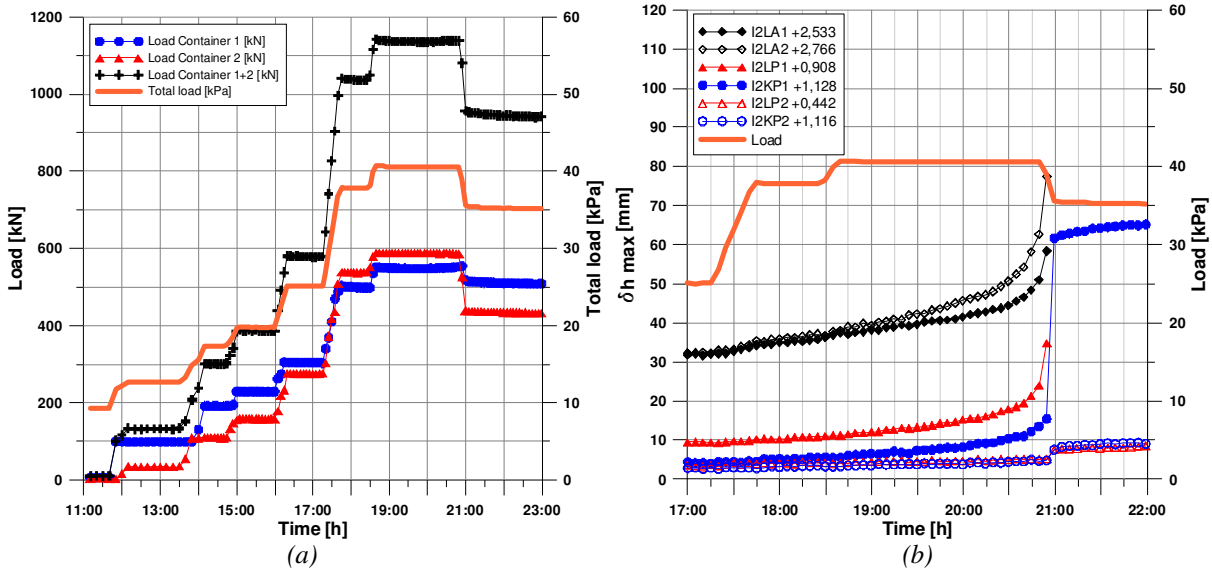

Figure 33: (a) Stepwise load increase to failure; Test 1
(b)Maximum horizontal displacements and external load at failure; Test 1

Readings from the inclinometers installed in the active zone (I2LA1 and I2LA2), and in the passive zone located 1.5 m from the SPW (I2LP1 and I2KP1) showed that the horizontal displacements, δ_h, begin to increase linearly just after load step 4 was applied at 17:20 and continued until about 20:30, see Fig. 33. Just prior to the load drop, δ_h began to accelerate both in the active zone and in inclinometers installed in the passive zone 1.5 m from the SPW. The inclinometers installed in the passive zone, 4.0 m from the SPW (I2LP2 and I2KP2) showed that $\delta_h$remained constant to failure occurred at 20:55. Continued readings of δ_h from the inclinometers installed in the active zone and the inclinometer in the clay in the passive zone 1.5 m from the SPW could not be performed after 20:55 due to the large failure obtained. The results indicated that a brittle failure with a very rapid progress (less than 15 minutes) and small deformations prior to the failure occurring. The failure mechanism was a rotational stability failure of the SPW, resulting in large vertical displacements both at the bottom of the excavation (heave) and at ground level on the active side of the SPW (settlements), se Fig. 34. A slip surface developed at failure with a starting point located about 6 m from the SPW, just behind the applied load, on the active side, and with the toe of the slip surface located about 3-3.5 m from the SPW on the passive side. The largest change in inclination in the inclinometers located in the active zone was measured between the two gauges closest to the toe of the SPW indicating that the slip surface occurred just below the SPW.

Figure 34: Loading and failure of sheet pile wall Test 1

5.9 Test Execution - Test 2

Excavation to the first level of 2.0 m below the ground surface began on 15 May 2014 and was completed on 19 May. Similar to Test 1, installation of whale beams and strut beams began directly after the excavation and were completed on 28 May. Instrumentation of the strut beams and connection to the data loggers was completed on 2 June. Excavation to the final level of 4.5 m below the ground level was conducted in one single step and was completed on 3 June. Construction of the LDP, installation of load cells and mounting of steel frames and containers were performed on the next day.

The loading of the containers began in the morning of 9 June and was stepwise increased, according to Table 14 and Fig. 35.

Table 14: Applied load Test 2

Time schedule		External load at end of cycle [kN]		Total load [kPa]
		Load cells under steel frame 1	Load cells under steel frame 2	Containers + Load platform
Start (containers on place)		101*	36	14.8
06/09/2014	Load step 1: 08:30-09:10	257.1	225.0	24.4
06/09/2014	Load step 2: 11:15-11:35	371.6	358.4	31.3
06/09/2014	Load step 3: 15:15-16:00	519.4	575.6	41.4
06/09/2014	Load step 4: 17:20-17:50	640.6	711.9	48.6
06/09/2014	Load step 5: 19:50-20:10	673.2	765.7	51.0
06/09/2014	Load step 6: 20:50-21:00	710.1	800.1	52.9
06/09/2014	**Unloading 22:20-22:40**	588.2	644.0	45.2
06/10/2014	Load step 7: 09:30-09:50	741.2	776.8	54.0
06/10/2014	**Unloading 13:20-13:50**	488.5	501.0	38.5
06/10/2014	**0.5 m Excavation 14:30-18:00**			
06/11/2014	Load step 8: 07:35-08:00	809.8	817	56.2

**The weight of the containers differed because container 1 had double base plates of steel installed.*

After the last load increment conducted on 9 June (load step 1-6), the containers were filled close to the maximum and the total load, including the dead load of the LDP, was 1906 kN, equivalent to a distributed load of 53 kPa. About 1 hour after step 6 was applied at 22:00, no indication of an emergent failure (accelerating deformations, rapid increase in excess pore water pressure/strut load) could be detected from the measurements. Due to the late hour and the risk of a fast brittle failure similar to Test 1 occurring during the night, it was decided to partly unload the containers for the night and continue the test the next morning. All measuring equipment was left running and monitored during the night.

The containers were filled again to about the same load during the next morning (load step 7). Four hours after the load was applied again, only slightly increasing pore pressure and horizontal displacement were measured and no indication of an impending failure could be observed. Because a large additional load increase was not possible, due to containers being almost overfull, the only possibility to induce failure of the structure was to conduct an additional excavation. After unloading about 30% of the load from the containers, an additional excavation of 0.5 m, to a final excavation depth of 5.0 m, was conducted. To protect the instruments, no excavation was performed closer than 0.5 m from the measuring equipment. After the additional excavation has been completed horizontal displacements, pore water pressure and strut forces were monitored for a period of about 14 hours before full load (load step 8) was finally applied.

Final loading of the containers was conducted in one load step between 07:35 and 8:00 the following morning. The load registered in the load cells was 1627 kN and the total load behind the SPW which includes the weight of LDP, was 2020 kN, equivalent to a distributed load of 56 kPa. The first cracks at the excavation bottom, starting from the SPW towards the center of the excavation began to develop about 10-15 minutes after the load was applied, see Fig. 36. The length and width of the cracks increased rapidly and reached a length of about 2.5-3 m within another 15 minutes. At this stage, an inclination of the SPW could be observed at the position of the LDP with a simultaneous vertical displacement of the soil (heave) at the bottom of the shaft and settlement of the soil beneath the LDP. Ten to fifteen minutes after final loading was conducted, a decrease in the load was registered by the load cells. The load decrease accelerated after 08:30 as a result of parts of the load on top of the overfull containers sliding over the top due to settlement of the ground surface and change in inclination of the containers, whereby the load decreased from 1627 kN to 1420 kN at 08:50. Between 08:50 and 08:52 the load dropped to 1180 kN and continued to decrease to 1034 kN at 08:58, after which the load remained constant until the excavation pit was backfilled.

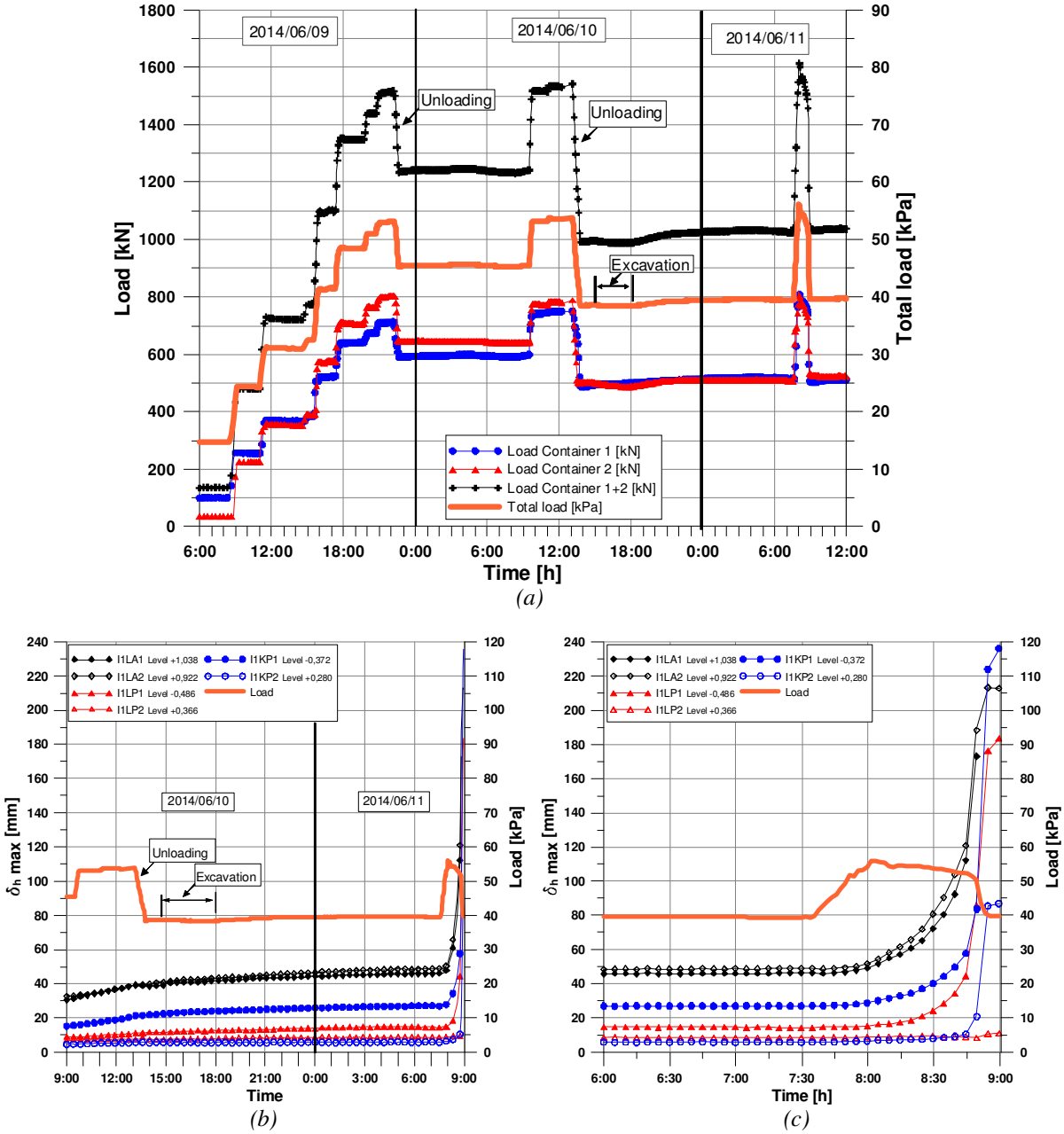

Figure 35: *(a) Stepwise load increase to failure; Test 2*
(b)Maximum horizontal displacements and external load at failure; Test 2
(c) Detail of maximum horizontal displacements and external load at failure; Test 2

Readings from the inclinometers installed in the active zone (I1LA1 and I1LA2), and in the passive zone located 1.5 m from the SPW (I1LP1 and I1KP1) showed that δ_h began to increase immediately after loading was finished, see Fig. 35. The increment of δ_h, was fairly linear up to about 08:20 at which point δ_h began to accelerate. The inclinometers installed in the passive zone, 4.0 m from the SPW (I1LP2 and I1KP2) showed that δ_h remained constant up to about 08:45. After 08:45, an accelerating increment of δ_h was measured in the column while δ_h in the clay remained constant. The failure mechanism was similar to Test 1 with a rotational stability failure of the SPW resulting in heaving at the bottom of the excavation and settlements of the ground surface beneath the LDP, see Fig. 36. In contrast to Test 1, the failure of Test 2 was considerably less brittle with stepwise increasing deformations and a progress of about 40 minutes from beginning to t end.

Figure 36: Loading and failure of SPW; Test 2

5.10 Field Tests Results

Selected results from both tests areas are shown below. Measurement results have been divided in to several graphs in order to distinguish between excavation and load induced displacements, stresses and forces in the structure.

5.10.1 Horizontal displacements – Test 1

Horizontal displacements in the soil measured 0.5 m behind the SPW (active zone), I2LA2, are presented in Fig. 37. Horizontal displacements measured in the column wall, I2KP1, and the soil between the column walls, I2LP1, at the same distance in front of the SPW (passive zone), 1.5 m, are presented in Figs. 38 and 39.

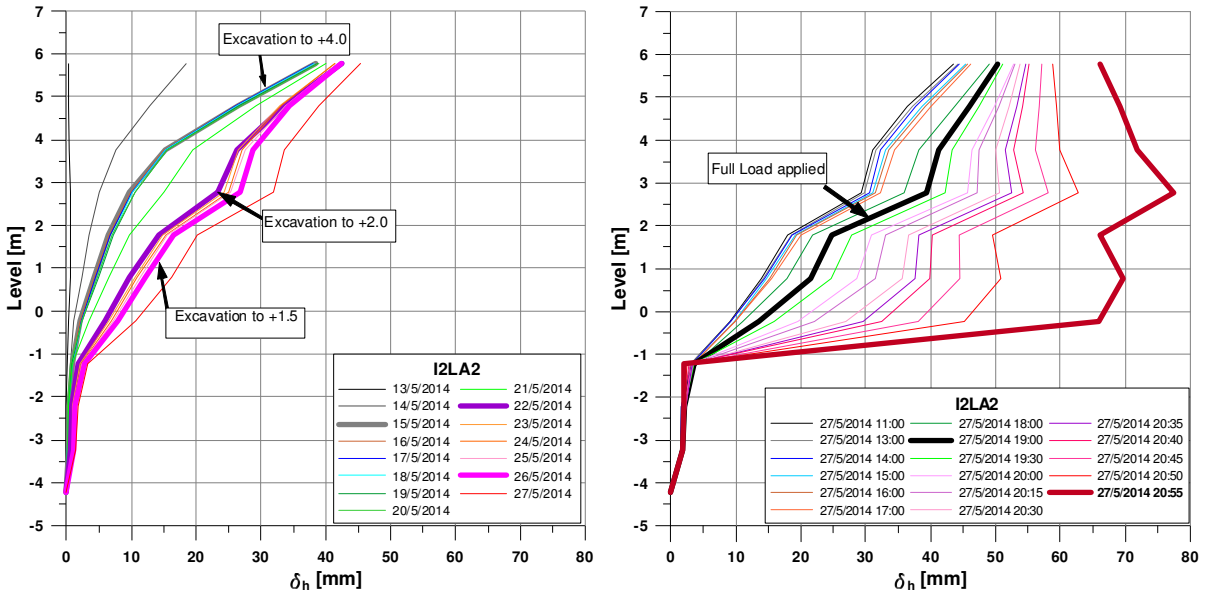

(a) (b)

Figure 37: (a) Test 1: Excavation induced horizontal displacements in active zone (0.5 m from SPW)
(b) Test1: Load induced horizontal displacements in active zone (0.5 m from SPW)

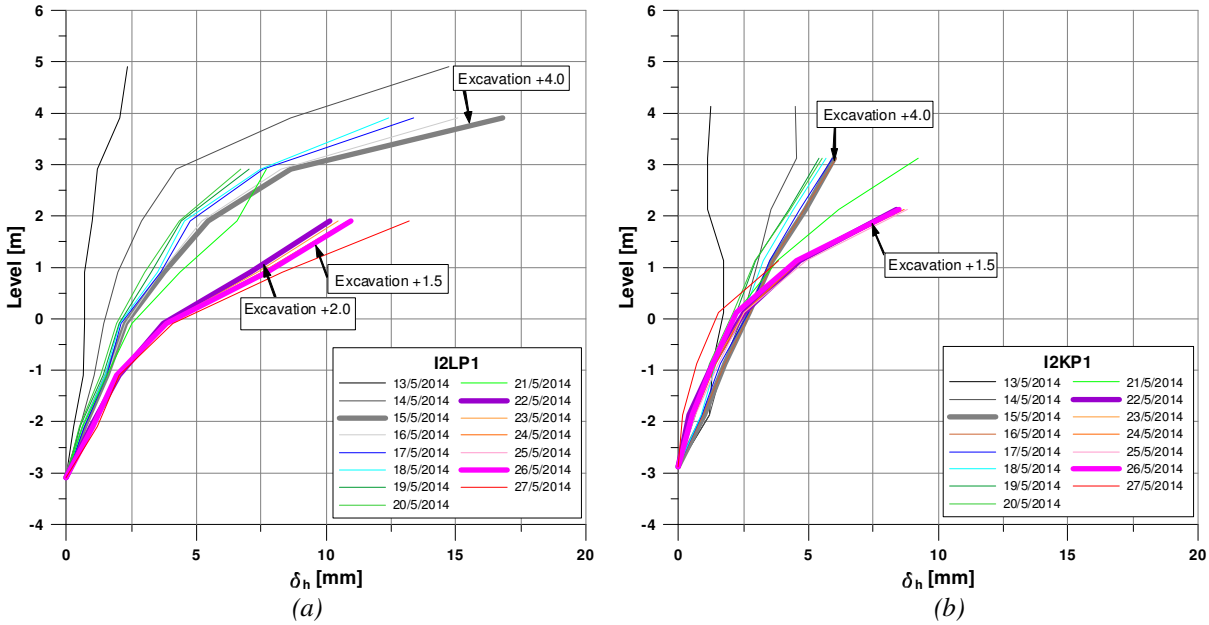

(a) (b)

Figure 38: (a) Test 1: Excavation induced horizontal displacements in clay passive zone (1.5 m from SPW)
(b) Test 1: Excavation induced horizontal displacements in column passive zone (1.5 m from SPW)

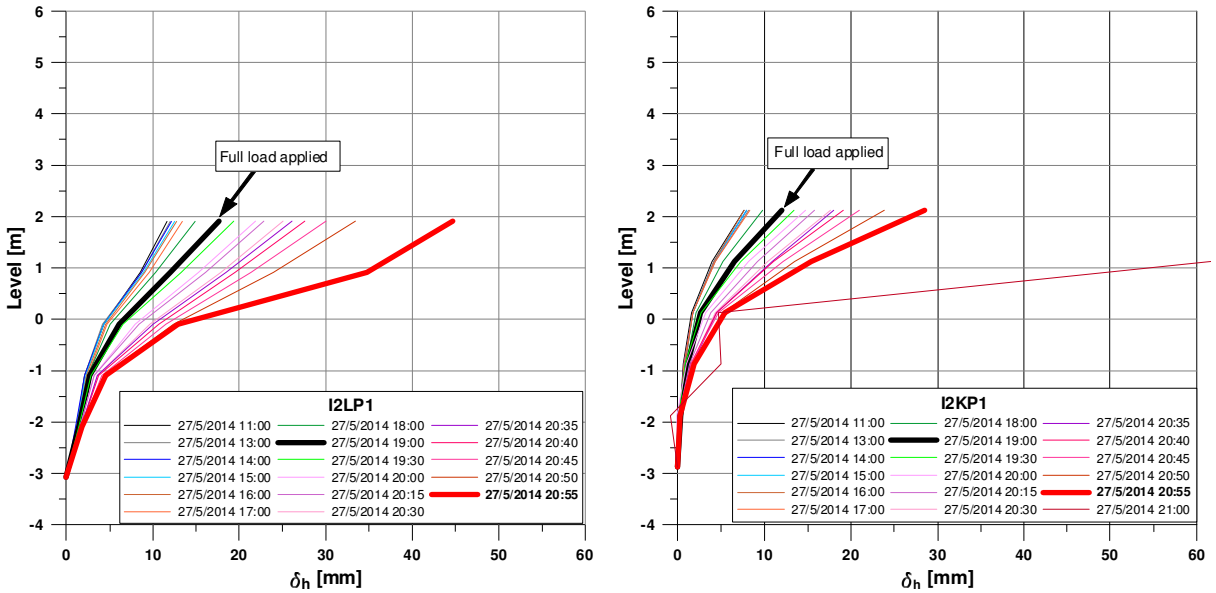

(a) *(b)*

Figure 39: *(a) Test 1: Load induced horizontal displacements in clay passive zone (1.5 m from SPW)*
(b) Test 1: Load induced horizontal displacements in column passive zone (1.5 m from SPW)

5.10.2 Horizontal displacements – Test 2

Horizontal displacements in the soil measured 0.5 m behind the SPW (active zone), I1LA2, are presented in Figs. 40 and 41. Horizontal displacements measured in the column wall, I1KP1, and the soil between the column walls, I1LP1, at the same distance in front of the SPW (passive zone), 1.5 m, are presented in Figs. 42, 43 and 44. Horizontal displacements measured in the column wall, I1KP2, and the soil between the column walls, I1LP2, at the same distance in front of the SPW (passive zone), 4.0 m, during the last day of loading are presented in Fig. 45.

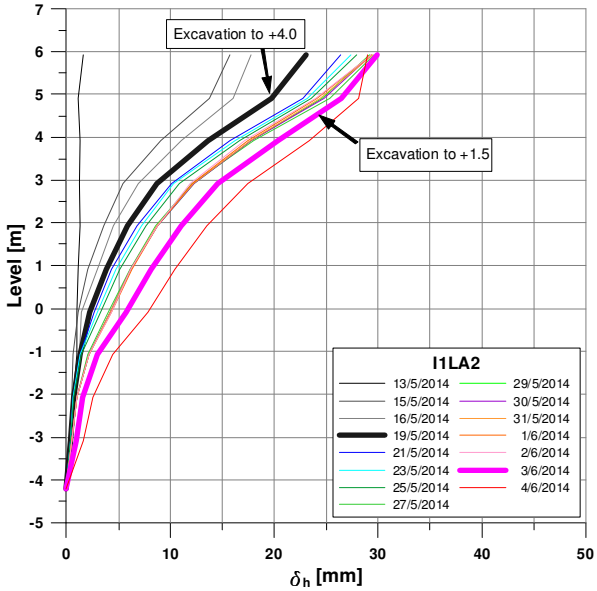

Figure 40: Test 2: Excavation induced horizontal displacements in active zone (0.5 m from SPW)

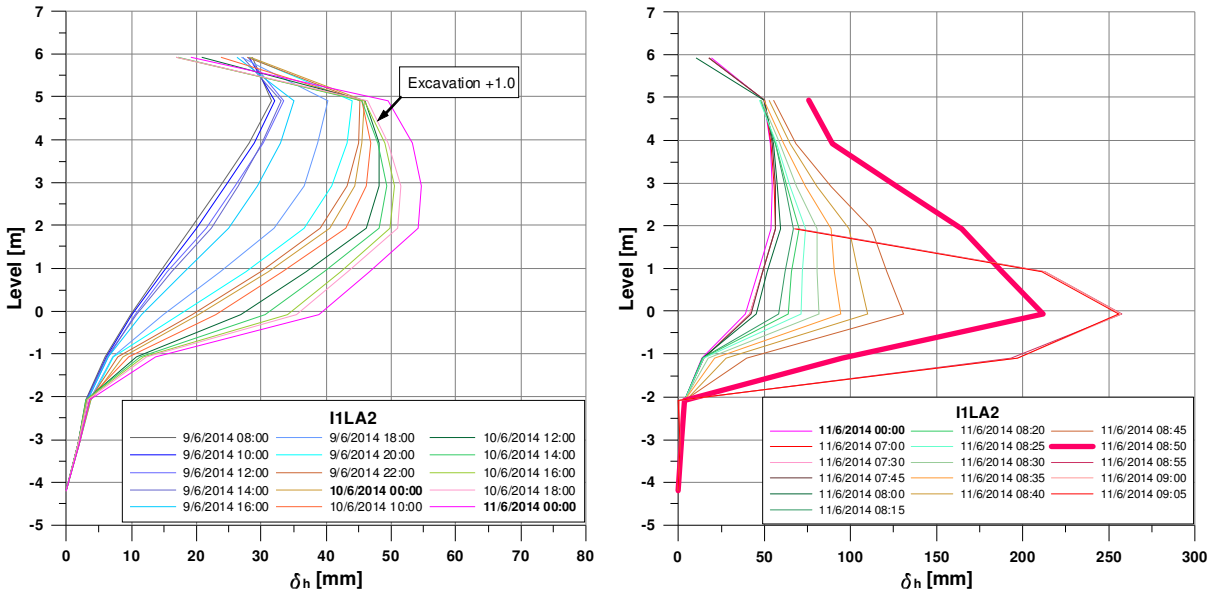

(a) *(b)*

Figure 41: *(a) Test 2: Load induced horizontal displacements in active zone (0.5 m from SPW); Day 1+2*
(b) Test 2: Load induced horizontal displacements in active zone (0.5 m from SPW); Day 3

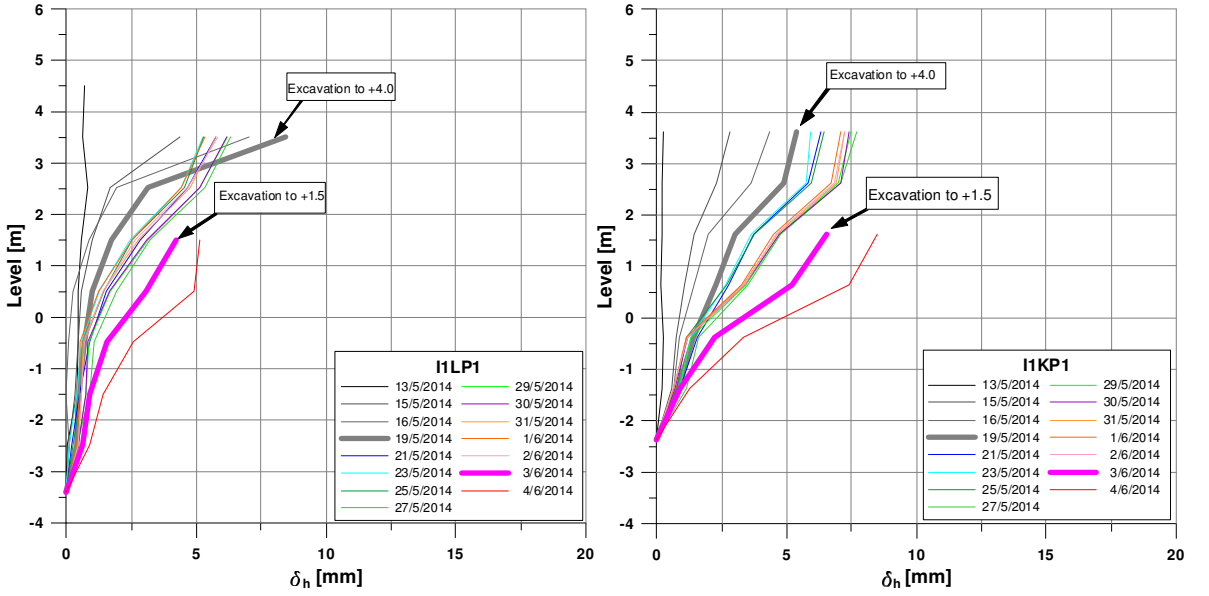

(a) *(b)*

Figure 42: *(a) Test 2: Excavation induced horizontal displacements in clay passive zone (1.5 m from SPW)*
(b) Test 2: Excavation induced horizontal displacements in column passive zone (1.5 m from SPW)

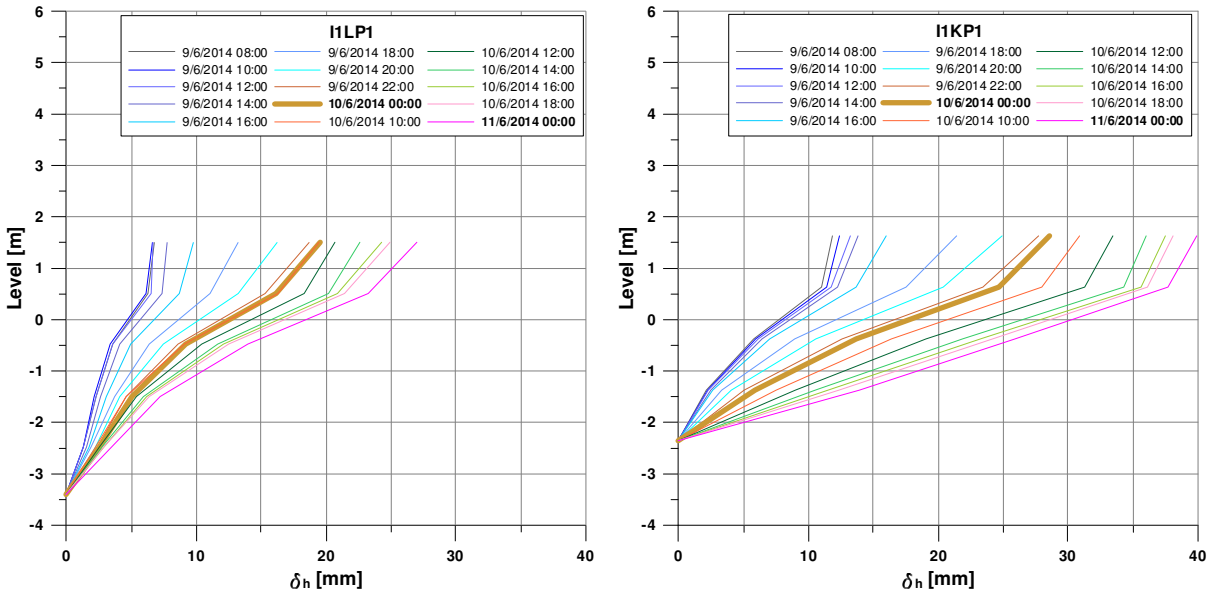

(a) *(b)*

Figure 43: (a) Test 2: Load induced horizontal displacements in clay passive zone (1.5 m from SPW; Day 1+2
(b) Test 2: Load induced horizontal displacements in column passive zone (1.5 m from SPW; Day 1+2

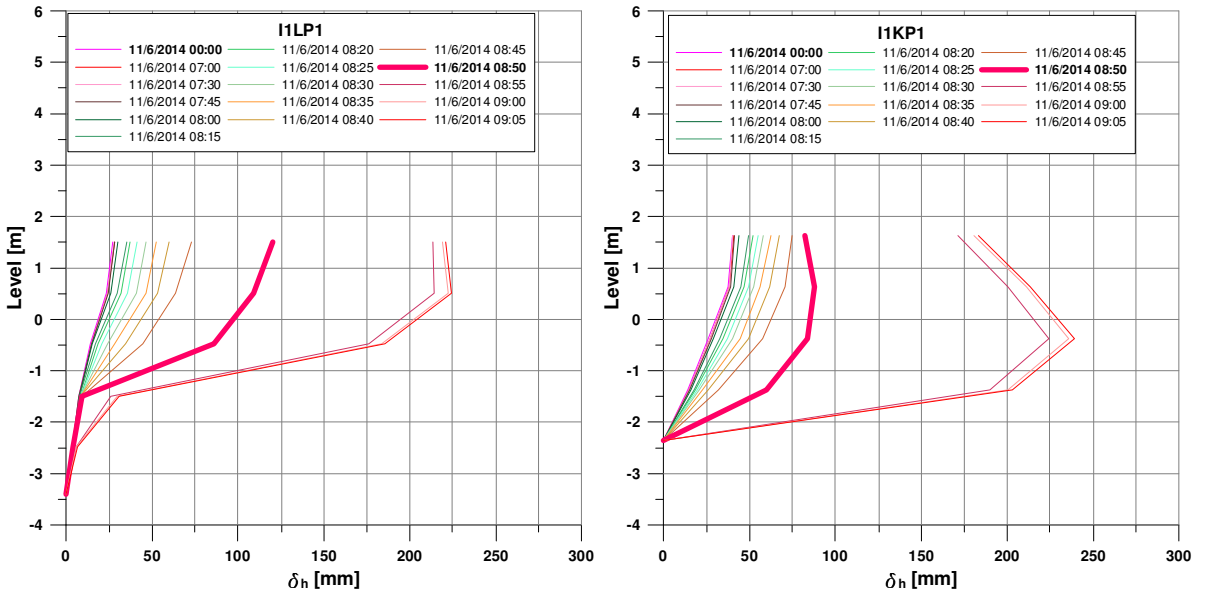

(a) *(b)*

Figure 44: (a) Test 2: Load induced horizontal displacements in clay passive zone (1.5 m from SPW; Day 3
(b) Test 2: Load induced horizontal displacements in column passive zone (1.5 m from SPW); Day 3

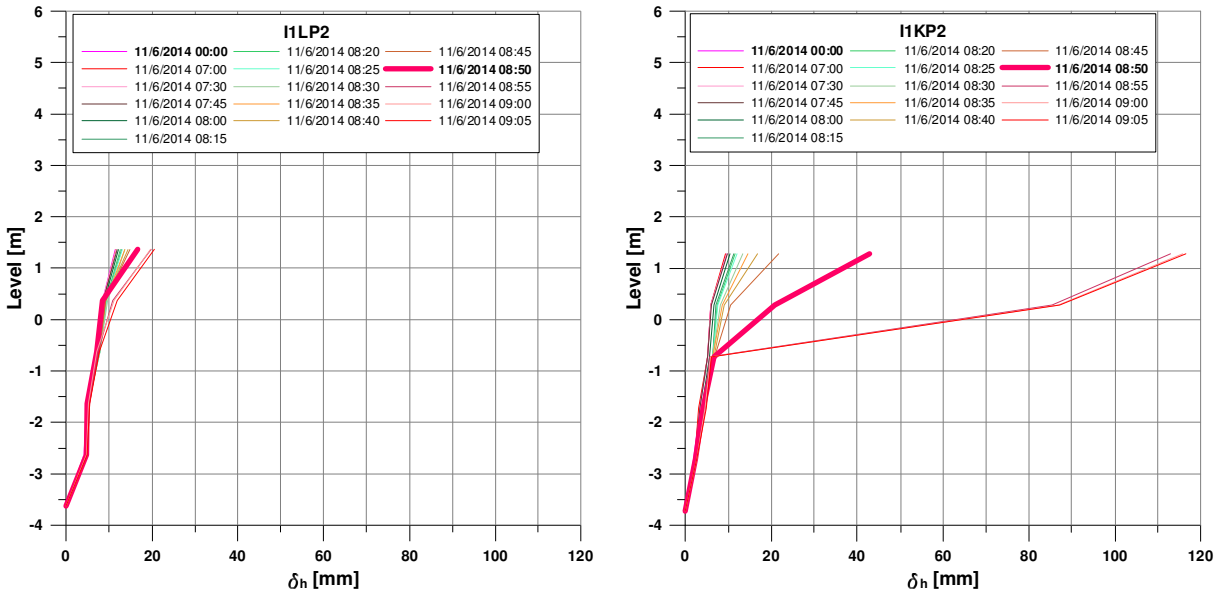

(a) *(b)*

Figure 45: (a) Test 2: Load induced horizontal displacements in clay passive zone (4.0 m from SPW); Day 3
(b) Test 2: Load induced horizontal displacements in column passive zone (4.0 m from SPW); Day 3

5.10.3 Vertical displacements – Test 1

Vertical displacement in the passive zone between columns, B2LP1 and B2LP2, and the passive zone in the columns, B2KP1 and B2KP2, are presented together in the figures below. Measurements were also conducted after failure occurred and the area was secured, in order to obtain additional information about the depth and geometry of the slip failure. The bellow-hose installed in the clay 2.0 m from the SPW, B2LP1, was not accessible after failure.

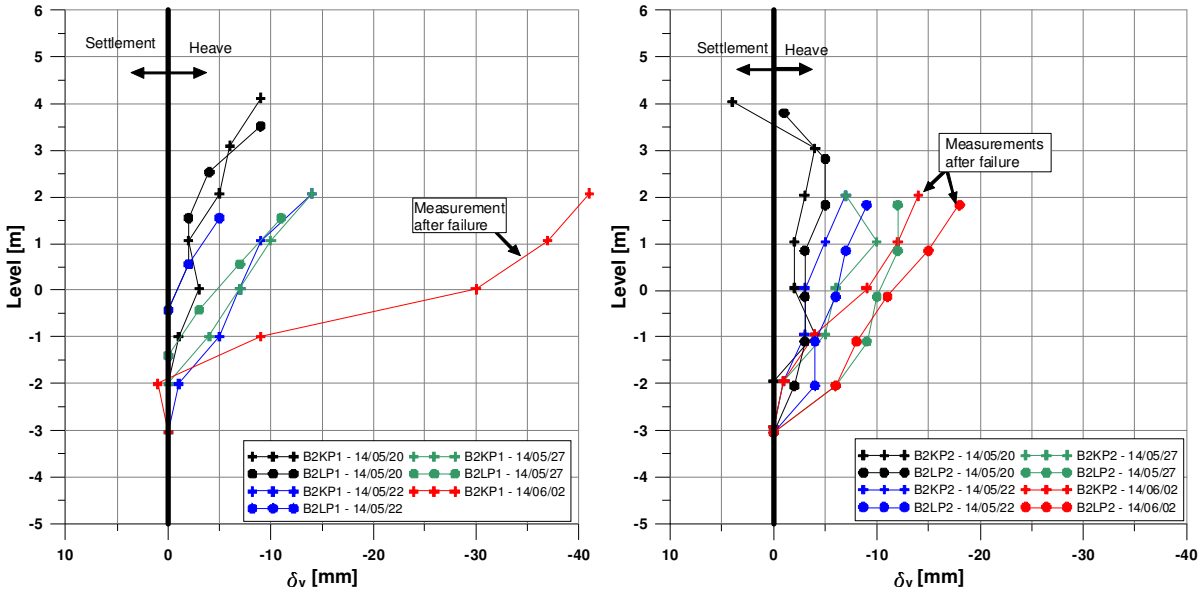

(a) *(b)*

Figure 46: (a) Test 1: Vertical displacements passive zone, clay and column 2.0 m from SPW
(b) Test 1: Vertical displacements passive zone, clay and column 4.5 m from SPW

5.10.4 Vertical displacements – Test 2

Measurements conducted after failure in both of bellow-hoses installed in the columns, B1KP1 and B1KP2 indicated that a failure occurred in both instrumented columns. The measuring tape stopped at level -1.09 for B1KP1 (2.0 m from SPW) and at level +0.99 for B1KP2 (4.5 m from SPW).

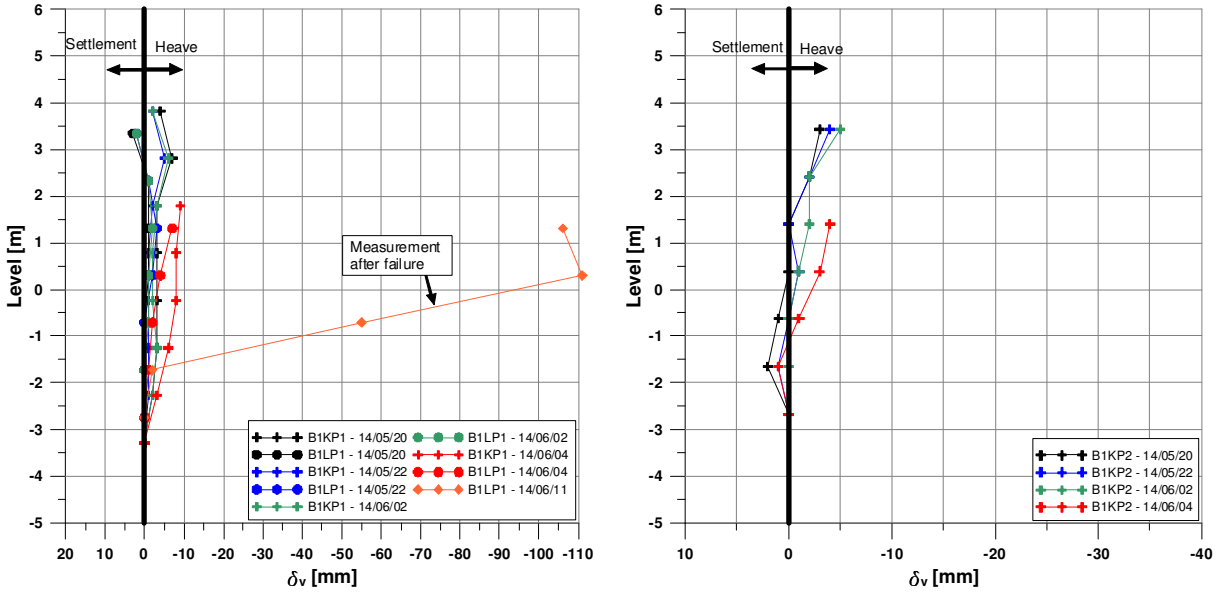

(a) *(b)*

Figure 47: (a) Test 2: Vertical displacements passive zone, clay and column 2.0 m from SPW
(b) Test 2: Vertical displacements passive zone, column 4.5 m from SPW

5.10.5 Horizontal stresses – Test 1

The change in horizontal earth pressure, $\Delta\sigma_h$, during excavation and loading in the active zone, J2LA1 and J2LA2, the passive zone between columns, J2LP1 and J2LP2, and the passive zone in the column wall, J2KP1 and J2KP2, are shown together in Fig. 48 below.

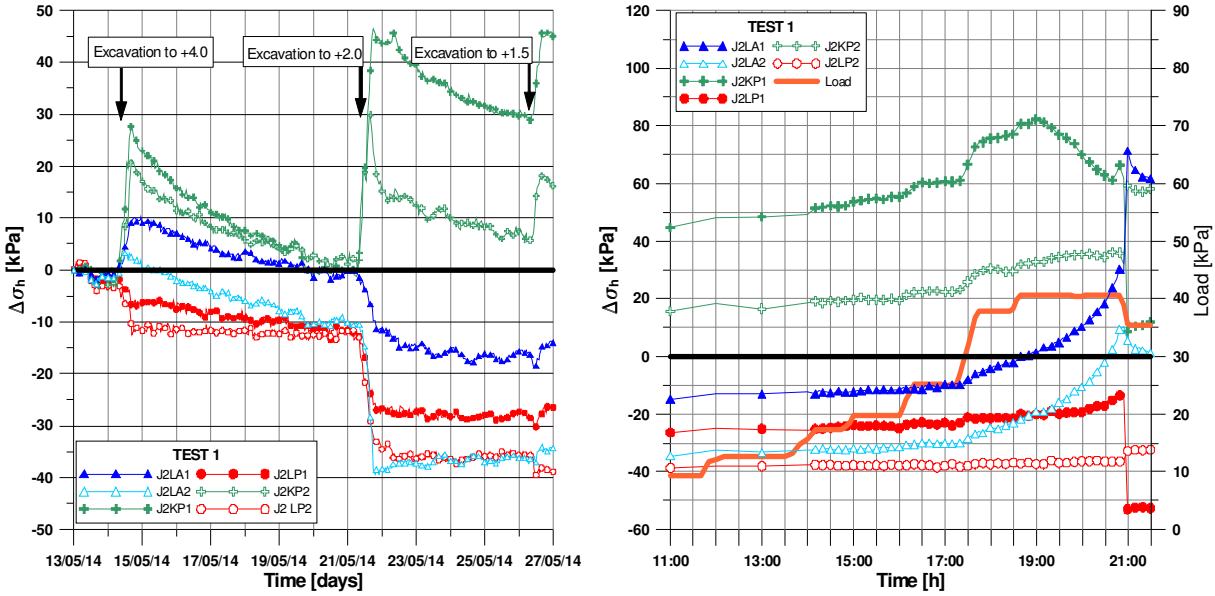

(a) *(b)*

Figure 48: (a) Test 1: Horizontal stress change during excavation stage
(b) Test 1: Horizontal stress change during loading stage

5.10.6 Horizontal stresses – Test 2

The change in $\Delta\sigma_h$ during excavation and loading stage in the active zone, J1LA1 and J1LA2, the passive zone between columns, J1LP1 and J1LP2, and the passive zone in the column wall, J1KP1 and J1KP2, are shown together in Fig. 49 below.

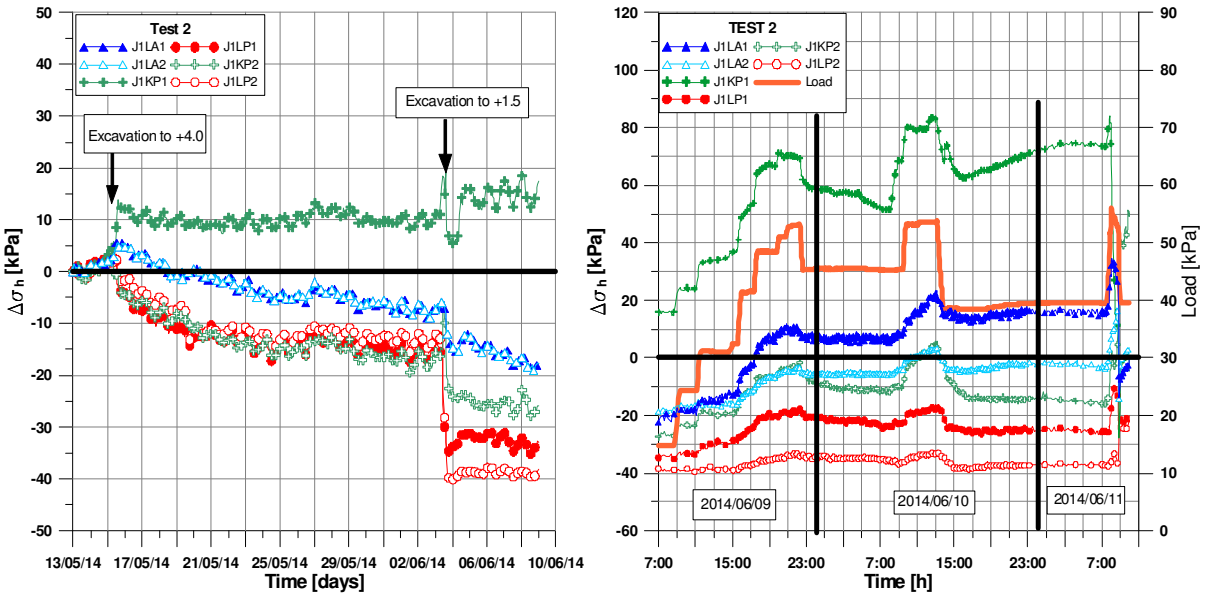

(a) *(b)*

Figure 49: (a) Test 2: Horizontal stress change during excavation stage
(b) Test 2: Horizontal stress change during loading stage

5.10.7 Normal force in strut beams - Test 1

Measurements of normal forces, S2-1 and S2-2, in the two strut beams in front of the LDP during the last excavation stage and the loading stage are presented together with measured daily temperature variations, T2-1 and T2-2, in Fig. 50.

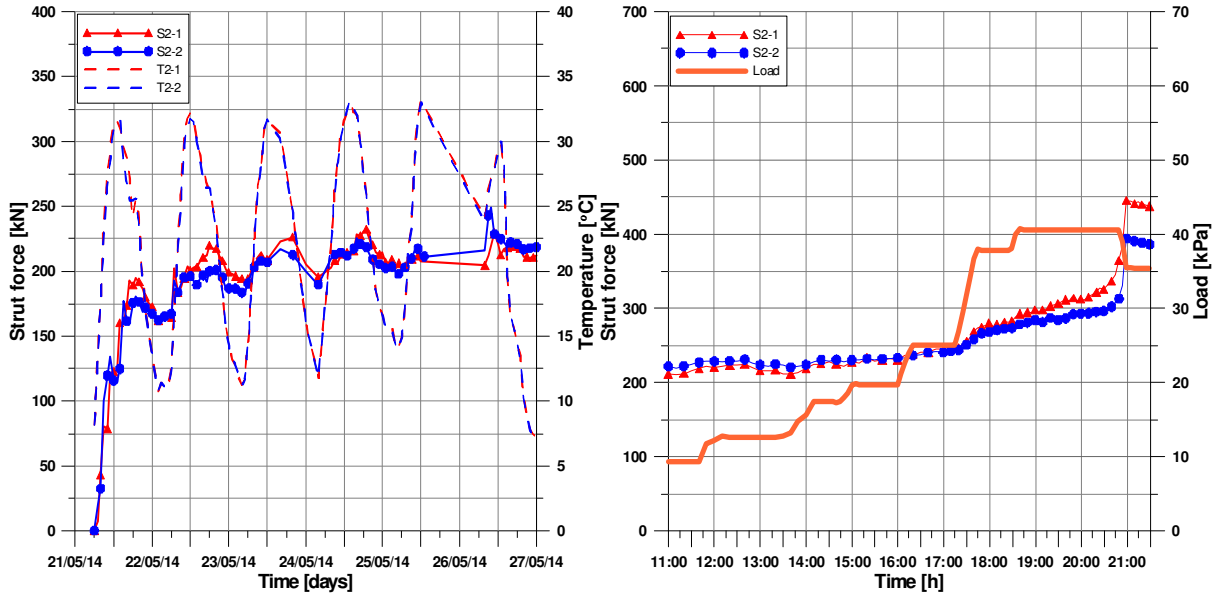

(a) *(b)*

Figure 50: (a) Test 1: Measurement of strut force and temperature during excavation stage
(b) Test 1: Measurement of strut force during loading stage

5.10.8 Normal force in strut beams - Test 2

During the excavation stage conducted on 3 June, two of the four strain gauges installed on strut beam S1-2 were damaged and measurements were thereafter performed with only the remaining two strain gauges, which may have affected the results.

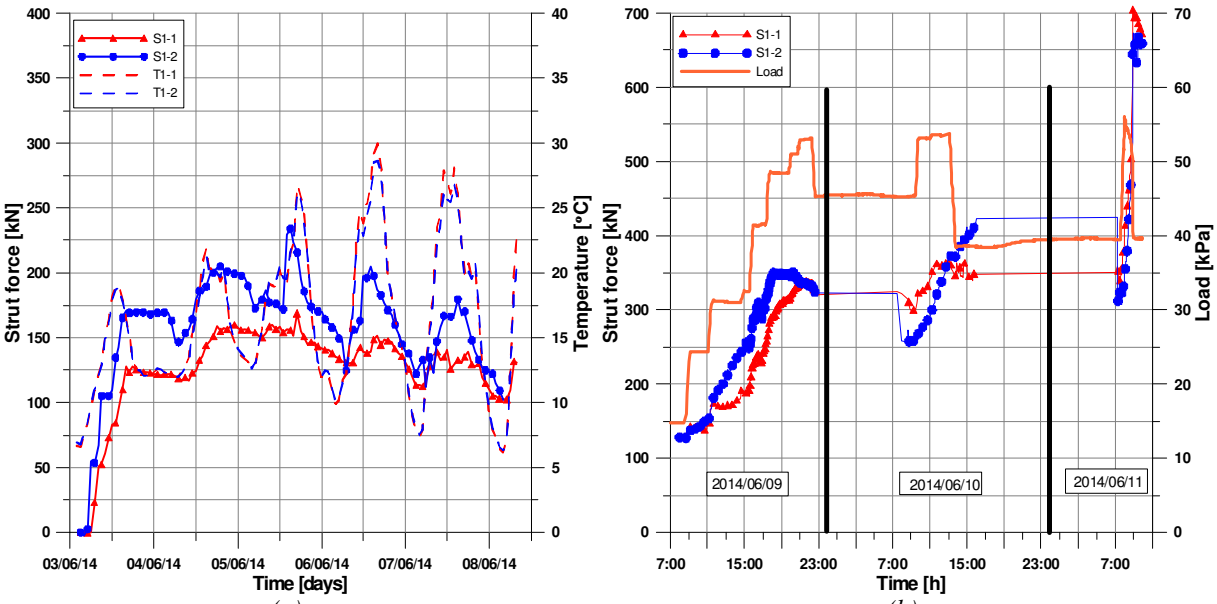

(a) *(b)*

Figure 51: (a) Test 2: Measurement of strut force and temperature during excavation stage
(b) Test 2: Measurement of strut force during loading stage

6 CONCLUSIONS AND FUTURE RESEARCH

The following section is a summary of the major findings and conclusions from this study regarding the laboratory tests on stabilized clay and the field tests. Some suggestions for future research are also presented.

6.1 Conclusions

Laboratory tests show that the natural clay at the site is normally consolidated but its behavior changes to that of an overconsolidated material when the clay is improved with lime/cement. The improved clay exhibits a ductile behavior with a stress-strain relationship similar to a strain hardening material in the case of compression loading and a behavior with a stress-strain relationship similar to linear elastic perfectly plastic material in the case of extension loading. The difference in peak undrained shear strength between tests is much lower in the case of triaxial extension loading compared to triaxial compression loading and the evaluated Young's secant modulus is about 2.2 times larger for the case of extension loading compared to compression loading. Failure in the case of extension loading will occur along a weak zone in the sample, i.e. the weakest link theory where the weakest link determines the strength of the chain, while in the case of compression loading, possible weak zones will not have an equally large impact on the material strength.

Field tests clearly show that column-type ground improvement of the clay installed as rows of overlapping columns in the passive zone of the SPW will significantly increase the capacity of the structure and reduce excavation and loading induced deformations, both in the active and the passive zone. Field measurements indicate that the column rows installed in the passive zone will act as support for the SPW below the bottom of the excavation. Measured horizontal and vertical deformations indicate that failure in Test 1 occurred in the clay between the column rows due to the large distance between the rows while failure of both column rows and clay between the rows occurred in Test 2. A brittle failure with very small deformations measured prior to the failure and a very quick emergence of the failure mechanism was obtained at a large distance between the column rows. Measurements show good agreement with the forecast development of the failure mechanism predicted by the numerical analyses.

Earth pressure measurements showed that excavation and loading induced stress increments are transferred mainly to the column rows even at spacing as large as 3.0 m between the column rows, due to the large stiffness difference between the soft soil and the columns at the interface with the SPW. The measurements also clearly indicate a shear wall effect in the column rows as the stress increment at larger distance from the SPW increases when the load is increased. Development of normal forces in the struts also indicates that the column rows act as support below the bottom of the excavation. After excavation to full depth, the measured normal force in the strut beams of Test 2 was about 60% of the normal force measured for Test 1. A relatively small increase in normal forces was measured during the loading stage in both tests. Although the excavation depth is 0.5 m larger and the applied load is about 40% larger for Test 2, the measured strut forces in the two tests was almost equal. At failure, the increase in normal force in the struts was significantly higher in Test 2, in which failure of the columns occurred (from about 350 kN to 670 kN) compared to Test 1 (from about 320 kN to 410 kN), which is a strong indication that the column rows form a "strut-like effect" below the bottom of the excavation.

Relative horizontal displacements between the column rows and the clay in-between the rows show different trends in the two tests. In Test 1, i.e. with a large distance between the rows, the horizontal displacement in the clay between the rows is larger than the horizontal displacement in the column at the same distance from the SPW and equal depth during the loading stage. In Test 2, i.e. with a smaller distance between the rows, the horizontal displacement in the clay between the rows is smaller than the horizontal displacement in the column at the same distance from the SPW and equal depth during the loading stage. During loading, due to the significantly less stiffness of the SPW in the horizontal plane, deflection of the SPW in the horizontal plane increases as the distance between the supports is

increased and thereby the horizontal displacements between the columns rows will be larger in Test 1 compared to Test 2.

6.2 Future Research

In this study, the behavior of ground improvement with rows of lime-cement columns installed in the passive zone has been documented for the first time. Future research that will be conducted within the scope of this doctoral project is:

- Further investigation of lime-cement improved soil material behavior regarding stress-strain and effective stress paths for different extension loading and unloading conditions that reflects different loading conditions that lime-cement columns installed in shear and passive zone are subjected to.
- Implementation of a material model for lime-cement columns that can adequately describe the material behavior in both loading and unloading situations
- To facilitate implementation of a design model for lime-cement columns in the passive zone, numerical analyses of the field tests will be performed and benchmark calculations will be presented.

REFERENCES

Adams TE., 2011. Stability of levees and floodwalls supported by deep-mixed shear walls: five case studies in the New Orleans area. PhD dissertation, Virginia Polytechnic Institute and State University, Blacksburg VA.

Adams T.E., Filz GM. and Navin M., 2009. Stability of embankments and levees on deep-mixed foundations. In: Proceedings of the international symposium on deep mixing and admixture stabilization, Okinawa; p.305-10.

Adams T.E., Filz GM., Cali PR., Woodward ML., 2008. Stability Analyses of a Levee on Deep-Mixed Columns, Plaquemines Parish, Louisiana. ASCE Geotechnical Special Publication No. 178; p. 708-15.

Baker S., 2000. Deformation behavior of Lime/Cement stabilized clay. PhD thesis, Gothenburg; Chalmers University of Technology.

Balasubramaniam A.S., Li Y.G., 1977. Stress-strain behavior of soft Bangkok clay in triaxial extension. In: proceedings of International symposium on soft clay, Bangkok, Thailand, p. 105-116.

Balasubramaniam A.S., Beunsucesco B.R., 1989. On the overconsolidated behavior of lime treated soft clay. In. Proceedings of 12th Int. conf. Soil Mech. and Found. Engineering; Rio de Janeiro, Brazil; Vol. 2; p.1335-1338.

Balasubramaniam A.S., Bergado D.T., Beunsucesco B.R.,Yang W.C.,1989. Strength and deformation characteristics of lime- treated soft clays. Geotechnical Engineering; Vol. 20; p. 49-64.

Bergado D.T., Balasubramaniam A.S., 2005. Compression behavior of high water content cement – admixed clay. Proceedings of the Int. Conf. on Deep Mixing, Stockholm, Sweden; p.221-230.

Brinch Hansen J., 1948. The stabilizing effect of piles in clay. CN-Post; no. 3.

Broms B.B., 1972. Stabilisation of slopes with piles. In: Proceedings of the 1st international symposium on landslide control, Kyoto; p. 115–23.

Broms B.B., 1999. Progressive failure of lime, lime/cement and cement columns. In: Proceedings of the international conference on dry mix methods for deep soil stabilization. Stockholm; p. 177-84

Filz G.M., Templeton AE., Adams TE., 2011. Stability analyses for levees on deep-mixed shear walls. Ground Improvement; Vol. 164(3); p.117–26

Han J., Chen J., Hong Z., Shen S., 2005. Mitigation of levee failures using deep mixed columns and geosynthetics. Geom Geoeng; Vol. 1; p. 49-55.

Han J., Oztoprak S., Parsons R.L., Huang J., 2007. Numerical analysis of foundation columns to support widening of embankment. Computers and Geotechnics; Vol. 34(6); p.435-48.

Head K., 1998. Manual of soil laboratory testing, 3: Effective stress tests. 2nd edition, John Wiley & sons; Chicester; pp 428.

Huang J., Han J., Porbaha A., 2006. Two and three-dimensional modeling of DM columns under embankments. GeoCongress, Geotechnical engineering in the Information technology age, ASCE, Atlanta, GA

Kitazume M., Maruyama K., 2006. External stability of group column type deep mixing improved ground under embankment loading. Soils and Foundations; Vol. 46(3); p. 323-40.

Kitazume M., Maruyama K., 2007. Internal stability of group column type deep mixing improved ground under embankment loading. Soils and Foundations; Vol. 47(3); p. 437-55.

Kitazume M., 2008. Stability of group column type DM improved ground under embankment loading. Report of the port and airport research institute; Vol. 47; p.1-53.

Kivelö M., 1998. Stabilization of embankments on soft soil with lime/cement columns. PhD thesis, Stockholm: KTH Royale Institute of Technology.

Lacasse S., Berre T., 1988. Triaxial testing methods for soils. Advanced triaxial testing of soil and rock. ASTM Special technical publications, STP 977; p. 264-289.

Ladd C., 1991. Stability evaluation during staged construction. ASCE J. Geotehnical Engineering; Vol. 117 (4); p. 540-615.

Ladd C., Foott R., 1974. New design procedure for stability of soft clays. ASCE J. Geotehnical Engineering Division; Vol. 100 (GT7); p. 763-786.

La Rochelle P., Leroueil S., Trak B., Blais-Leroux L., Tavenas F., 1988. Observational approach to membrane and area corrections in triaxial tests. Advanced triaxial testing of soil and rock. ASTM Special technical publications, STP 977; p. 715-731.

Larsson R., 1977. Basic behaviour of Scandinavian soft clays. Swedish Geotechnical Institute, Linköping; 129 p.

Larsson R., 1981. Drained behaviour of Swedish clays. Swedish Geotechnical Institute, Linköping; pp 157.

Larsson R., 1986. Consolidation of soft soils. Swedish Geotechnical Institute, Linköping; pp 174.

Larsson R., 2006. Deep Mixing – Guidelines, Report 17, Swedish Deep Stabilization Research Centre, Linköping. (In Swedish)

Larsson S., 1999. Shear box apparatus for modeling chemical stabilized soil – introductory tests. In: Proceedings of the international conference on dry mix methods for deep soil stabilization, Stockholm; p. 115-21.

Larsson S., Broms B.B., 2000. Shear box model tests with lime/cement columns – some observations of failure mechanisms. In: Proceedings of geoeng, Melbourne; 2000, 6p.

Larsson S., Malm R., Charbit B., Ansell A., 2012. Finite element modeling of laterally loaded lime-cement columns using a damage plasticity model. Computers and Geotechnics; Vol. 44; p.48-57

Mayne P.W., Kulhawy F.H.,1982. K0-OCR relationship in soil. ASCE J. Geotehnical Engineering Division; Vol. 108 (GT6); p. 851-872.

Mayne P.W., 1985. Stress anisotropy effects on clay strength. ASCE J. Geotechnical Engineering; Vol. 111; p 356-366.

Navin M.P., 2005. Stability of embankments founded on soft soil improved with deep-mixing-method columns. PhD dissertation, Virginia Polytechnic Institute and State University, Blacksburg VA.

Navin M.P., Filz GM., 2006. Numerical stability analyses of embankments supported on deep mixed columns. ASCE Geotechnical Special Publication No. 152; p. 1-9.

O'Rourke T.D., O'Donell C.J., 1997. Field behavior of excavation stabilized by deep soil mixing. Journal of Geotechnical and Geoenvironmental Engineering; Vol.123(6); p.516-524.

O'Rourke T.D., McGinn A.J., 2006. Lessons learned for ground movements and soil stabilization from the Boston central artery, Journal of Geotechnical and Geoenvironmental Engineering; Vol.131; p. 966-989.

Ou C.Y., Wu T.S., Hsieh H.S., 1996. Analysis of deep excavation with column type of ground improvement in soft clay. Journal of Geotechnical Enggineering;Vol. 122(9); p. 709-16.

Ou C.Y., Teng F.C., Wang I.W., 2008. Analysis and design of partial ground improvement in deep excavations. Computers and Geotechnics; Vol. 35(4); p.576-584.

Ou C.Y., Hsieh P.G., Lin Y.L., 2013. A parametric study of wall deflections in deep excavations with the installation of cross walls. Computers and Geotechnics; Vol. 50: p.55-65

SGF, 2012. Triaxial testing – a guidance report. Report 2:2012, SGF, Linköping, Sweden (in Swedish)

SGF, 2004. Direct shear tests – a guidance report. Report 2:2004, SGF, Linköping, Sweden (in Swedish)

SIS, 2005. Geotechnical investigation and testing - Laboratory testing of soil – Part 9: Consolidated triaxial compression tests on water saturated soil (ISO/TS 17892-9:2004)

Sällfors G., 1975. Preconsolidation pressure of soft, high-plastic clay. PhD thesis, Gothenburg, Chalmers University of Technology.

Tanaka H., 1993. Behaviour of braced excavations stabilized by deep mixing method. Soils and Foundations; Vol. 33(2):105-115.

Tatsuoka, F. & Kobayashi, A. (1983). Triaxial strength characteristics of cement-treated soft clay. Proc. 8th European Conf. on Soil Mech. and Found. Engineering, Helsinki 1983, Vol. 1, pp. 421-426.

TK Geo 13, 2014. Technical requirements for geoconstructions (Trafikverkets tekniska krav för geokonstruktioner). The Swedish Transport Administration, Publ. TDOK 2013:0667, Sweden.

Yang T., Tan T.S., Leung C.F., 2011. Mass behaviour of embedded improved soil raft in an excavation. Proc Inst Civ Engrs – Geotechnical Engineering; Vol. 164(GE1); p.11-25.

Yoshida S., 1996. Shear strength of improved soils at lap-joint-face. In: Proceedings of the 2nd international conference on ground improvement geosystems, Tokyo; Vol. 1; p. 461-466.

Yoshizawa H., Okumura R., Hoshia Y., Sumi M., Yamada T., 1997. JGS TC Report: Factors affecting the quality of rested soil during execution of DMM. In: Proceedings of the 2nd Int. conference on ground improvement geosystems, Tokyo; Vol. 2; p. 931-937

Åhnberg H., Johansson S.E., Retelius A., Ljungkrantz C., Holmqvist L., Holm G.,1995. Cement och kalk för djupstabilisering av jord. Report No. 48. SGI, Linköping, Sweden, pp 213. (in Swedish)

Åhnberg H., 2004. Effects of back pressure and strain rate used in triaxial testing of stabilized organic soils and clays. Geotechnical Testing Journal; Vol. 27, No. 3, p. 250-259.

Åhnberg H., 2006. Consolidation stress effects on the strength of stabilized Swedish soils". Ground Improvement, Vol. 10, No. 1, pp. 1-13.

Åhnberg H., 2007. On yield stresses and the influence of curing stresses on stress paths and strength measured in triaxial testing of stabilized soils. Canadian Geotechnical Journal; Vol. 44; p. 54-66.

Paper I

Two- and three-dimensional analyses of excavation support with rows of dry deep mixing columns

Ignat R., Baker S., Larsson S., Liedberg S., 2015. Computers and Geotechnics, 66, 16-30. DOI.org/10.1016/j.compgeo.2015.01.011

Computers and Geotechnics 66 (2015) 16–30

Contents lists available at ScienceDirect

Computers and Geotechnics

journal homepage: www.elsevier.com/locate/compgeo

Research Paper

Two- and three-dimensional analyses of excavation support with rows of dry deep mixing columns

Razvan Ignat [a,*], Sadek Baker [b], Stefan Larsson [a], Sven Liedberg [b]

[a] Department of Civil and Architectural Engineering, Royal Institute of Technology, SE 100 44 Stockholm, Sweden
[b] Skanska Sweden AB, Stockholm, Sweden

ARTICLE INFO

Article history:
Received 7 April 2014
Received in revised form 27 November 2014
Accepted 18 January 2015

Keywords:
Lime
Cement
Deep mixing columns
Finite element analyses

ABSTRACT

In this study, a 2D model of an excavation with a tied back sheet pile wall in interaction with perpendicular rows of deep dry mixed overlapping columns was compared to a 3D model. A method to take into consideration the effect of the overlap zones between columns in a 2D model, where the improved soil was modeled as a composite material, was investigated and the results between the 2D and 3D analyses were compared with focus on predicted failure load, failure mechanism and deformations. The results of this numerical study show that both the area improvement ratio of the improved soil and the quality of the overlap zone has a significant influence on how well a 2D model that incorporates the overlap zone between columns, performs compared to the 3D model.

1. Introduction

Dry deep mixing with lime-cement columns has been used extensively since the mid 1970s mainly to reduce settlement and to some extent to improve stability of road and railway embankments. Deep mixing has been used as reinforced retaining structures [1–5], but one relatively new application is to install columns on the passive side in an interaction with sheet pile walls. Columns are installed in rows or blocks inside the sheet pile wall and thereby increase the passive resistance and after excavation act as a ground improvement of the excavation bottom and foundation of the construction.

Laterally loaded columns have been investigated theoretically, numerically and experimentally by means of model tests by many researchers [6–32]. These studies have mainly considered laterally loaded columns due to embankment loading. The main conclusions are that single columns have limited effect on the improvement of stability and that overlapping columns should be installed in rows perpendicular to the embankment, in order to improve the moment capacity and the interaction with the surrounding soft clay.

A few case studies and numerical analyses of the deep mixing column type of ground improvement in deep excavations have been published [33–38]. In the majority of the numerical analyses that have been made, 2D "plane strain" models or 3D analyses where the improved soil is modeled as a composite material have been used. A study by Yang et al. [39] investigated the behavior of embedded improved soil raft to help restrain the movements of a retaining wall by conducting numerical analyses of a hypothetical case and simulation of a reported case history. An embedded improved soil raft is short soil cement columns that overlap with each other to form a continuously improved composite ground that acts like a strut below the excavated ground level. The authors examined the mechanisms of how the mass properties of the improved soil are mobilized, and how application of different material properties in the horizontal direction within a column and the geometrical arrangement of the columns, affects the degree of mobilization of the mass properties for the raft compared to the elemental properties. Based on these results, Yang et al. suggest that soil–cement columns used to improve the stability of excavations should be constructed with overlap rather than just in contact with each other. The results and conclusions presented by Yang et al. explains how the properties within the columns and how different arrangement of the columns influences the degree of mobilization of the material elemental properties, but when the soil improvement consists of column rows, even the distance between the column rows and the interaction between the columns and the soft soil between the column rows will have a significant effect on the overall behavior of the structure and the type of failure mechanism that will be obtained.

The system of a retaining structure where the soil is improved by deep mixing columns is a complex three-dimensional mechanical system in which the retaining structure, the columns and the soft

* Corresponding author. Tel.: +46 8 7908667, +46 70 8290580 (mobile); fax: +46 8 411 84 32.
E-mail address: razvani@kth.se (R. Ignat).

http://dx.doi.org/10.1016/j.compgeo.2015.01.011
0266-352X/

soil between the columns interact. It has not been investigated how well a 2D plane strain model, where the improved soil is modeled as a composite material, can reflect the interaction between the column rows and the soil between the rows with respect to stress distribution, shear stresses, and relative movements between the columns and the soft soil that is free to move relative to the rows. Due to computational costs there is a great need for 2D analyses that can simulate the mechanical system sufficiently reasonable.

The aim of this study is to investigate if a 2D model can predict the ultimate limit state behavior regarding failure load, failure mechanism, stress–strain relationship, and deformations up to failure load, compared to a 3D model when the columns are subjected to lateral forces. Because several previous studies have shown that the strength properties of the overlapping zone are often lower than the strength of the columns, [26,40–41] the effect of a weak overlapping zone has been included. The paper investigates a method to model the vertical overlap between the columns in a 2D plane strain model compared to a 3D model. The results of the study are intended to provide an insight into the ability of a simplified 2D model to reflect the behavior of a 3D mechanical system consisting of rows of overlapping dry deep mixing columns subjected to lateral loading.

2. Finite element analyses

2.1. General

The finite element program PLAXIS 3D 2012 was used in this study. The soil and the columns were modeled with 10-node tetrahedral elements. Both the 3D model with rows of columns and the 2D plane strain model with a composite soil volume were modeled with PLAXIS 3D in order to eliminate possible sources of uncertainty related to the two principal geometrical problems.

2.2. General geometrical and geological model

The soil consists of 1 m of stiff dry crust overlaying 10.5 m of normally consolidated very soft clay over very stiff frictional soil. The stiff frictional soil was not included in the model. The vertical model boundaries parallel to the *yz*-plane are fixed in *x*-direction and free in *y*- and *z*-directions while vertical model boundaries parallel to *xz*-plane are fixed in *y*-direction and free in *x*- and *z*-directions. The model bottom condition was chosen fixed in all directions while the ground surface is free in all directions. The groundwater table was set at the top of the soft clay, 1 m below the ground surface. In order to avoid boundary effects, the length of the model was chosen to be 35 m and its width, due to symmetrical effects, to be 3 m, Fig. 1. The modeled retaining structure was a steel sheet pile wall with a length of 7 m. The length of the sheet pile wall was chosen such that a rotational stability failure governed the failure mechanism of the wall. The sheet pile wall was horizontally anchored backward with steel wire anchors 1 m below the ground surface with a center-to-center distance of 3 m. The anchors were fixed at the boundary and had a free length of 20 m. A steel whale beam, HEB 300, was modeled at the anchorage level. The adhesion between the soil and the sheet pile wall was taken into account by adding positive and negative interface elements between the sheet pile wall and the soil. The improved soil consists of dry deep mixing columns with a diameter of 0.6 m, installed as overlapping columns perpendicular to the sheet pile wall. The column rows had a width of 7.0–7.2 m and a length of 10 m starting from the upper edge of the soft soil. The simulated width of the excavation was chosen to be 15 m, while the unexcavated side was chosen to be 20 m from side boundary of the model.

2.3. Analyses set-up

In this study, excavation was performed in two steps to a final excavation depth of 4 m below the ground surface, before a uniformly distributed surface load, *q*, was applied from 0 to 5 m behind the sheet pile wall. In the first step, the ground was excavated to a depth of 2 m before the anchor was installed 1 m below the ground surface. The anchors were then prestressed with a force corresponding to 50% of the anchors yield load, 300 kN, before the next excavation step was performed. A prestress force was applied in the anchor element to prevent excessive horizontal deformations at the top of the sheet pile wall. After the second excavation stage, a uniform distributed load, *q*, was applied and increased in constant increments of 10 kPa until a failure collapse mechanism was reached. A dry excavation was assumed in the conducted analyses. In order to eliminate the effect of free water in the excavated region, the water conditions for the excavated soil volumes below the ground water table were set to dry. Due to the excavations, the earth pressure acting on the sheet pile wall increased and the column rows were subjected to an increasing lateral loading and a simultaneously decrease in overburden pressure on the passive side of the retaining structure. In this way, the development of the emerging failure mechanism and the stress–strain relationship

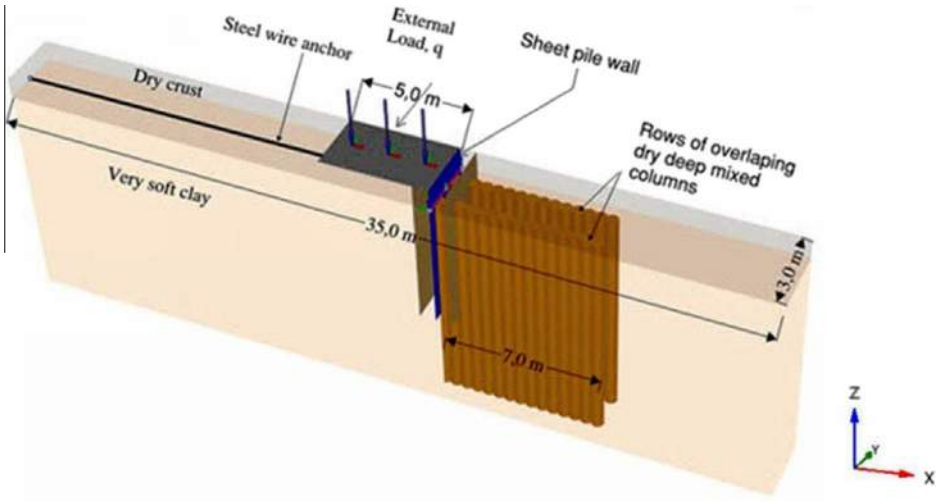

Fig. 1. Model geometry.

in the columns when subjected to laterally loading until failure could be analyzed.

In both the 3D and the 2D models, the effect of the center-to-center distance between the column rows, s_{row}, the center-to-center distance between the columns within each row, s_{col}, the effect of strength and stiffness reduction within the overlapping zone on the calculated deformations, and the evaluated failure load, q_{ult}, were investigated. Some of the parameters in this study such as column length, soil and column properties, and type of retaining structure are very common in Scandinavian country's construction projects involving dry deep mixing and excavations. Varying only parameters related to the stabilized soil, according to Table 1, and holding all other parameters constant, make it possible to draw the conclusions presented in this study. These conclusions are believed to be general for cases where ground improvement installed as rows of overlapping columns is used to sustain horizontal loads.

2.4. 3D geometrical model

Modeling a large number of overlapping circular columns requires a large number of elements, which creates problems related to the mesh generation in numerical simulations. Therefore, the columns were modeled as octagonal cylindrical elements with the same cross-sectional area as cylindrical columns with a diameter of 0.6 m. Full contact was modeled between the column rows and the sheet pile wall. The width of the contact area was chosen to be the diameter of the columns. Full interaction between the columns and the soft clay was assumed. The columns were "wished in place", which implies that no volume strain or disturbance of the clay parameters was taken into consideration. The number of elements in the 3D model ranges between approximately 63,000 for analyses with s_{row} = 3.0 m and s_{col} = 0.6 m, and 150,000 for analyses with s_{row} = 1.0 m and s_{col} = 0.4 m. Because the size of the overlapping zones are very small compared to the size of the model, slender elements will be generated even if a very fine mesh is selected for the elements within the overlapping zones in the columns. This was the case for the analyses performed with s_{col} = 0.4 m. By rotating the columns in the x–y plane, according to Fig. 2, the mesh quality could be improved and no slender elements were generated. Due to this, the ratio of the overlapping area, a_0, between the modeled octagonal shaped columns and the circular columns was a_0 = 0.99 for s_{col} = 0.4 m and a_0 = 0.94 for s_{col} = 0.5 m, which was considered acceptable.

Table 1
Varied parameters for conducted finite element analyses.

Center-to-center distance between the rows, s_{row} (m)	Column center-to-center distance in the row, s_{col} (m)	Reduction of strength and stiffness of overlapping zone (%)
1.0	0.6	0
1.5	0.5	0, 50, 75
3.0	0.4	0, 50, 75

2.5. 2D geometrical model

In order to compare the 3D and the 2D methodologies, the effect of a strength reduction in the overlapping zone between the columns in the rows was taken into account in the 2D model by defining vertical joints in the composite soil volume. Adams [27] used a similar procedure to model vertical joints at column overlap in 2D analyses. The width of the columns excluding the overlap zone, b_{c2D}, and the width of the vertical joints representing the overlap zones, b_{o2D}, were calculated so that the columns' and the overlap zones' respective area replacement ratio in the 2D model, a_{sc} and a_{so}, respectively, is equal to the 3D area replacement ratio, and is described in Fig. 3. The weighted material properties of the composite soil volume were calculated based on a_{sc} and a_{so} as presented in Fig. 3. The number of elements used in the 2D model was approximately 65,000.

2.6. Material properties

In recent years, different advanced models have been proposed that take into consideration the behavior of cemented clay and that include the bonding of the material due to the cementation process and strain-softening behavior beyond yield [42–46]. Even though advanced models like the concrete damage plasticity model that considers stiffness degradation has also been proposed for lime-cement columns [26], which is a less brittle material compared to cement columns, the information available from which the properties of the lime-cement columns can be inferred is limited.

The design procedures [47–49] make use of column strength in terms of cohesion and friction. It is therefore considered appropri-

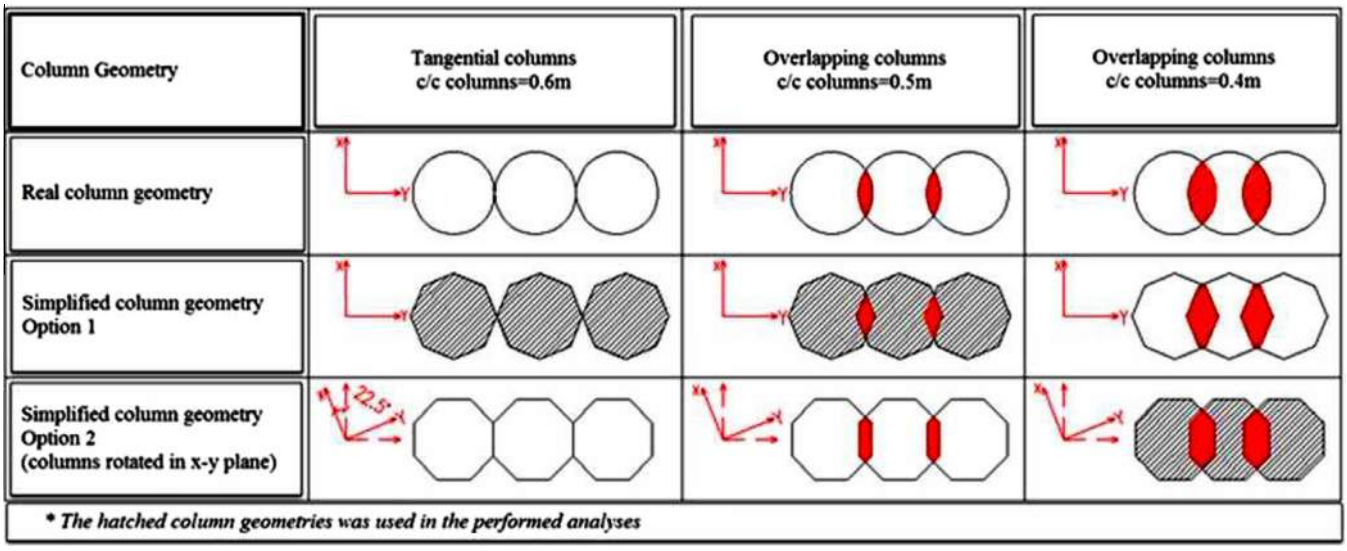

Fig. 2. 3D geometrical model of overlapping columns.

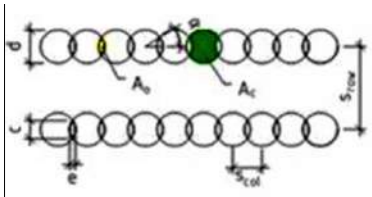

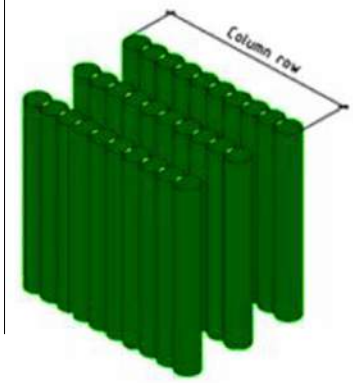

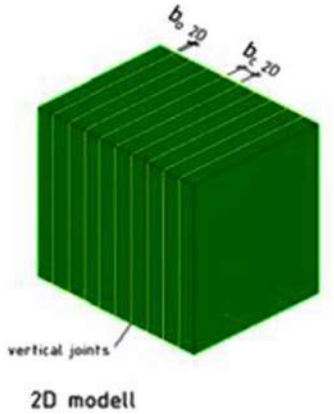

$$A_o = 2\left[\alpha\left(\frac{d}{2}\right)^2 - \frac{((d-e)c)}{4}\right]$$

$$A_c = \pi\left(\frac{d}{2}\right)^2 - 2A_o$$

$$b_{o\,2D} = \frac{A_o}{c}$$

$$b_{c\,2D} = \frac{A_c}{d}$$

$$a_{so} = \frac{c}{s_{row}}$$

$$a_{sc} = \left(\frac{A_c}{s_{row}(d-e-b_{o\,2D})}\right)$$

$$s_{u,o\,2D} = s_{u,o}a_{so} + s_{u,s}(1-a_{so})$$

$$s_{u,c\,2D} = s_{u,c}a_{sc} + s_{u,s}(1-a_{sc})$$

where:

d = column diameter

e = overlap distance between the columns

c = chord length of the overlap

α = one half of the chord angle

s_{row} = center distance between column rows

A_o = area of the overlap zone between columns

A_c = area of columns without overlap

$b_{o\,2D}$ = effective width of overlap zone (vertical joints)

$b_{c\,2D}$ = effective width of columns

a_{so} = area replacement ratio of overlap zone

a_{sc} = area replacement ratio of columns

$s_{u,o}$ = shear strength of overlap

$s_{u,c}$ = shear strength of columns

$s_{u,s}$ = shear strength of soil between column rows

$s_{u,o\,2D}$ = composite shear strength of overlap zone

$s_{u,c\,2D}$ = composite shear strength of columns

Fig. 3. 2D plane strain model of rows with overlapping column with vertical joints.

ate to model the columns using the Mohr–Coulomb model. However, this model provides a crude representation of a quasi-brittle material, but the limited information presently available about the column properties gives no justification for more sophisticated models.

The analysis was performed as an undrained effective stress analysis with undrained strength parameters since the excavation and the loading were executed rapidly and thus the consolidation process is very limited. The undrained strength parameters were chosen according to Table 2. The chosen parameters for the columns are typical of dry deep mixing columns (lime-cement columns) in Sweden [46]. Material properties for the retaining structure, sheet pile wall, whale beam and anchor, was chosen linear elastic and are presented in Table 3.

Table 2
Material property values used for FE analysis.

Material parameter	Dry crust	Soft clay	DM columns
Unit weight, ρ (kN/m^3]	18.0	16.5	16.5
Undrained shear strength, Su (kPa)	40	10 + 1,5z[a]	100
Young's modulus, E (kPa)	8000	250 $S_{u\ clay}$	200 $S_{u\ col}$
Poisson's ratio, v	0.33	0.33	0.33
Compressive strength, σ_c (kPa)	–	–	200
Tensile strength, σ_t (kPa)	–	–	10
Earth pressure at rest, K_0	1.0	0.5	1.0
Interface strength, R_{inter}[b]	0.5	0.6	0.8

[a] z refers to the depth below the top of the clay surface.

[b] R_{inter} accounts for the soil–structure interaction and is defined in Plaxis as reduction of soil strength and stiffness properties at the interface with $0 < R_{inter} < 1.0$. For $R_{inter} = 1.0$ the interface properties are equal to the soil properties.

2.7. Evaluation of ultimate load

In the calculations, the load was increased until a failure mechanism occurs and a soil body collapse message is obtained. This happens in Plaxis when the specified load increment for the actual stage is not reached and the applied load reduces in magnitude in several successive calculation steps whereby the calculation will

Table 3
Material property of structural elements.

Element	Type	Wall thickness (m)	EI (kN m^2/m)	EA (kN/m)
Sheet pile wall	PU12	0.36	4.536×10^4	2.940×10^6
		Area (m^2)	EI_1 (kN m^2)	EI_2 (kN m^2)
Whale beam	HEB300	0.015	5.286×10^4	1.798×10^4
		EA (kN)	Prestress force (kN)	
Anchor	Strand anchor	94.50×10^3	300	

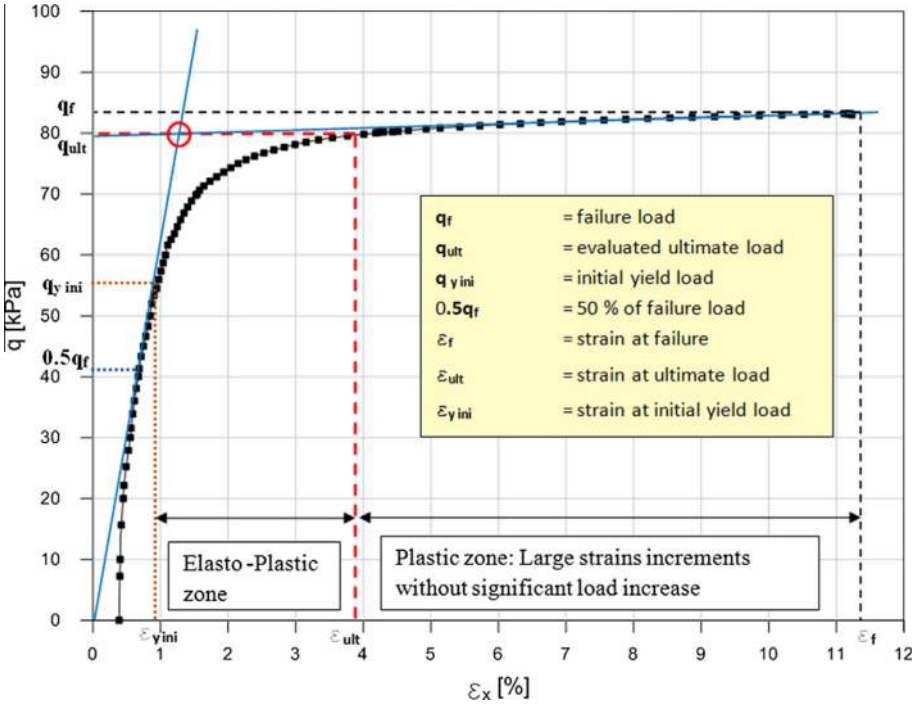

Fig. 4. Simplified approach for evaluation of ultimate load, q_{ult}.

be terminated. The load–strain curves, presented in Fig. 4, largely follow the stress–strain behavior of a linear-elastic strain hardening material, due to increasing yielding in the improved soil volume. Thereby the load–strain curve can be divided in three different parts; an elastic part, an elasto-plastic part and an plastic part. The load applied when soil body collapse occurs is displayed as the failure load, q_f, in Fig. 4. At total collapse of the structure, substantial yielding takes place in the improved soil volume, leading to plastic strains and large deformations in the structure. Initial yielding, or the end of the elastic part, occurs at a load level where further load increment results in non linear strain increment, and is denoted as q_{yini} in Fig. 4. Load increment from the initial yielding point and up to the load level evaluated as q_{ult} results in an elasto-plastic behavior similar to stress–strain relationship for an isotropic hardening material with an expanding yield surface. The evaluation of the ultimate load, q_{ult}, in both the 3D and the 2D calculations was made by choosing q_{ult} as the value at the intersection point of two straight lines that are drawn as a tangent to 50% of q_f, and a tangent to the final part of the load–strain curve. A rather similar approach has been used by Kitazume & Maruyama [9] to describe the embankment pressure at failure.

Further load increase above the load level of q_{ult} is close to the perfect plasticity case with large plastic strains increments for a very low load increment. As the load–strain curve will be close to an asymptote above q_{ult}, comparison of deformations above this load level will make no sense.

Table 4
Evaluation of ultimate load for full overlap strength.

s_{col} (m)	0.6		0.5		0.4	
s_{row} (m)	q_{ult} 3D (kPa)	q_{ult} 2D (kPa)	q_{ult} 3D (kPa)	q_{ult} 2D (kPa)	q_{ult} 3D (kPa)	q_{ult} 2D (kPa)
1.0	(89)	(89)	(89)	(89)	(89)	(89)
1.5	78	78	80	83	81	85
3.0	56	55	58	62	58	62

3. Results and discussion

3.1. Effect of shear wall distance and column distance

The evaluated ultimate load, q_{ult}, is summarized in Table 4 for analyses performed with no reduction of the strength and stiffness material properties for the column overlapping zone in the 3D analyses. In the 2D analyses, the strength and stiffness material properties of the composite soil volume were calculated based on the corresponding area replacement ratio between column overlap and unstabilised soil, a_{so}, respectively the columns and the unstabilised soil, a_{sc}, according to Fig. 3.

Evaluated q_{ult} shows a good agreement between the 3D and 2D analyses for $s_{row} = 1.5$ respectively 3.0 m for both tangential col-

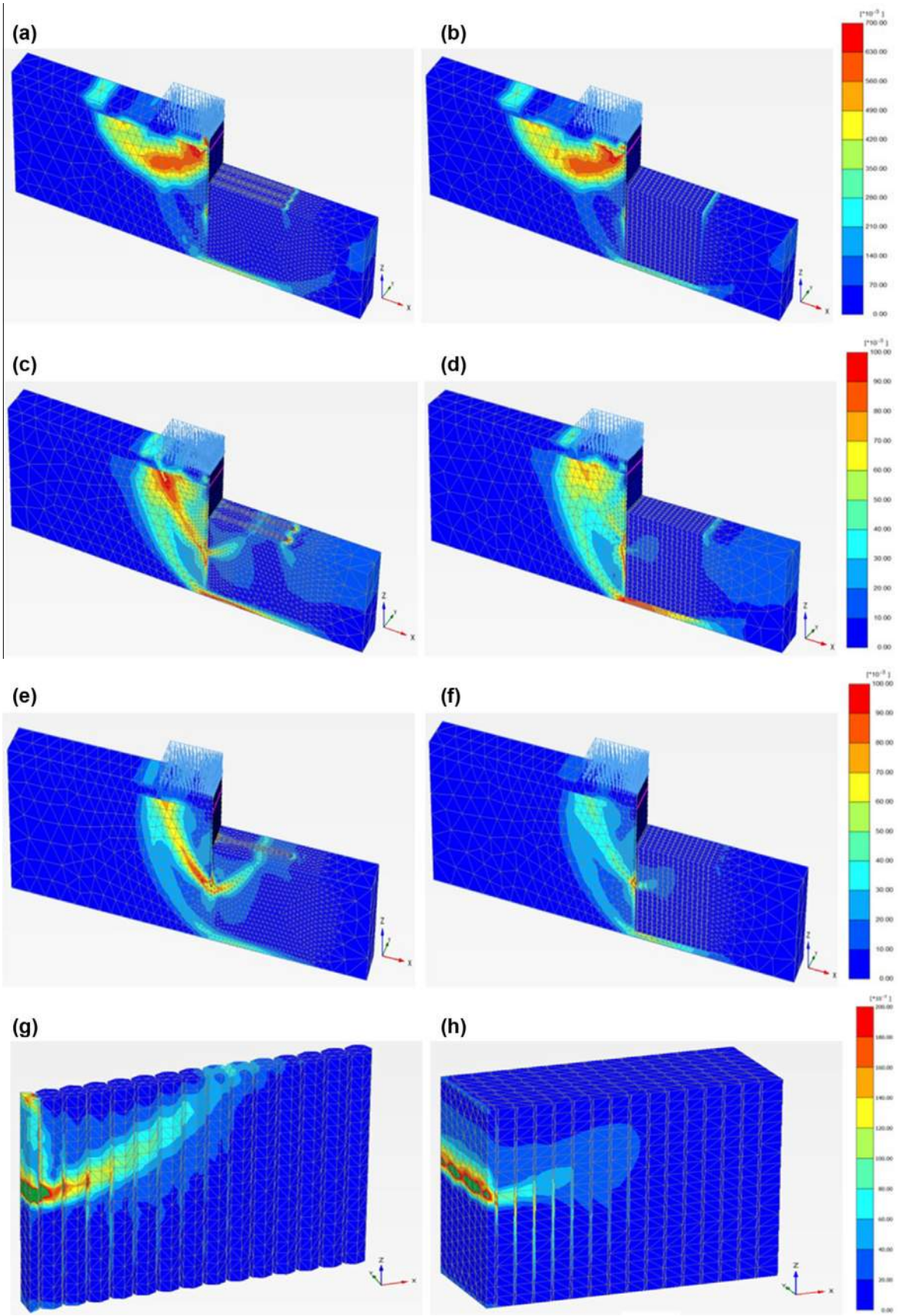

Fig. 5. Deviatoric shear strain at q_{ult} for s_{row} = 1.0–3.0 m and s_{col} = 0.5 m: (a) 3D s_{row} = 1.0 m; (b) 2D s_{row} = 1.0 m; (c) 3D s_{row} = 1.5 m; (d) 2D s_{row} = 1.5 m; (e) 3D s_{row} = 3.0 m; (f) 2D s_{row} = 1.5 m; (g) 3D column row for s_{row} = 3.0 m; (h) 2D composite soil volume for s_{row} = 3.0 m.

umns, s_{col} = 0.6 m, overlapping columns s_{col} = 0.4, and s_{col} = 0.5 m. For s_{row} = 1.0 m, no failure mechanism was induced in the improved soil volume. Instead an identical bearing capacity failure develops for both 2D and 3D analyses, on the active side of the sheet pile wall, due to large q being applied behind the sheet pile wall, that is shown in Fig 5a and b where the deviatoric strain, γ_s, is presented. Thereby the evaluated q_{ult} for s_{row} = 1.0 m have the same value for both the 2D and the 3D analyses and is reported in parentheses in Table 4.

Fig. 5c and f shows the 3D and 2D deviatoric strain at q_{ult} for a configuration of s_{row} = 1.5 and 3.0 m with s_{col} = 0.5 m. It can be observed that in the 3D model, a distinct slip failure under the sheet pile wall has developed through the improved soil volume in both above mentioned cases. The amount of deviatoric strain in the composite soil volume in the 2D model is significantly smaller at the same load level and the largest strain development in the 2D model occurs beneath the improved soil volume. The results of the 3D analysis with s_{row} = 3.0 m also show that a large amount of

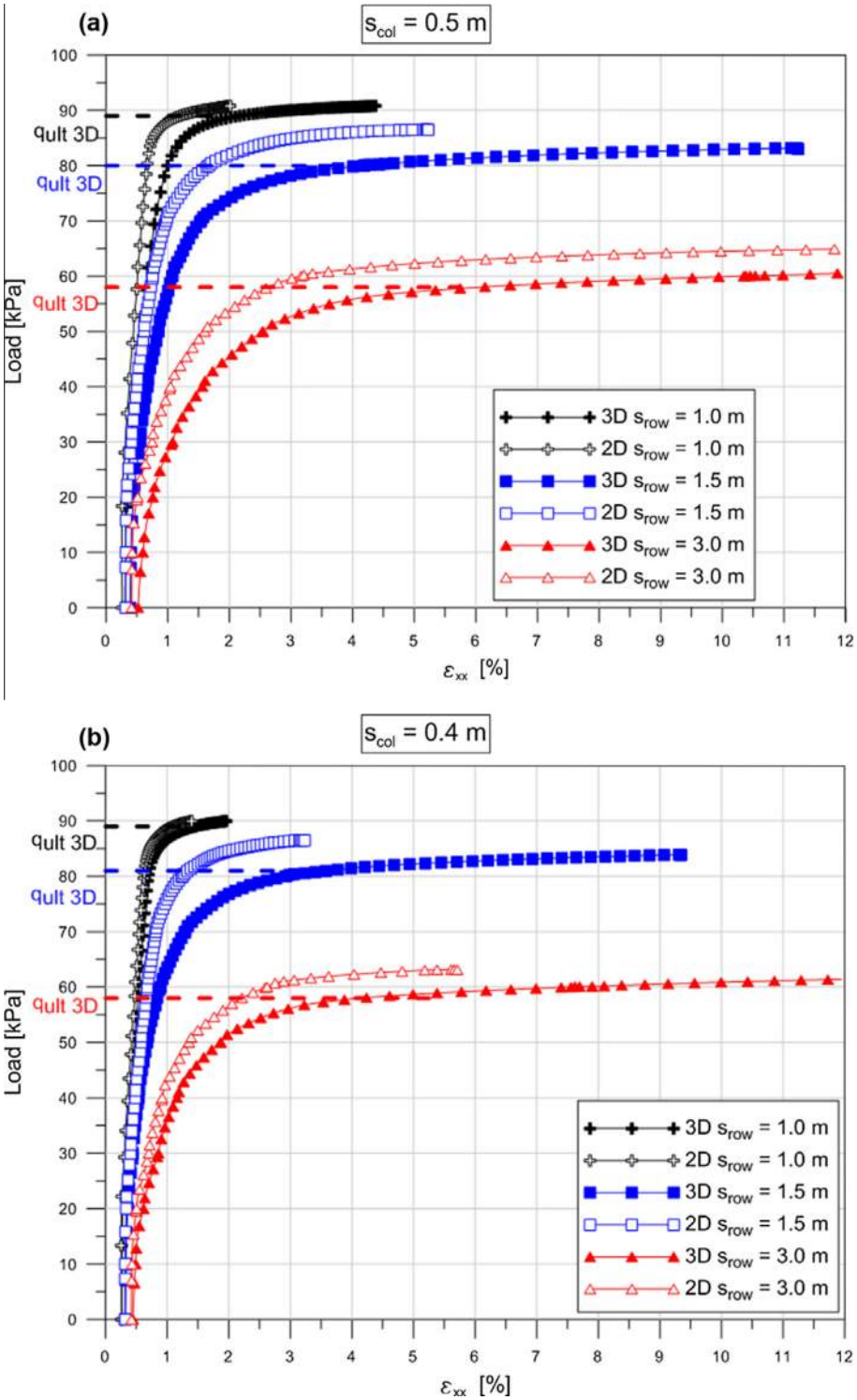

Fig. 6. Load–strain curve: (a) s_{col} = 0.5 m; (b) s_{col} = 0.4 m.

deviatoric strain occurs in the overlap zone in the column closest to the sheet pile wall while the same behavior is not observed in the 2D model, which is displayed in Fig. 5g and h. This is due to a larger stress increment in the stiffer column row that develops as s_{row} is increased.

Fig. 6 shows the horizontal strains, ε_x, in the column row plotted against the applied load, q, until failure mechanism was reached, alternatively up to a strain level of 12% occurs for both the 3D and 2D analyses. In order to compare the 2D and 3D analyses regarding development of strain during loading, Gauss stress point were selected at the same location for both types of calculations. The location of the selected Gauss stress points is 0.5 m inside the excavation pit (the center of the second column in the 3D analyses) and 3 m below the bottom of the excavation (bottom of the

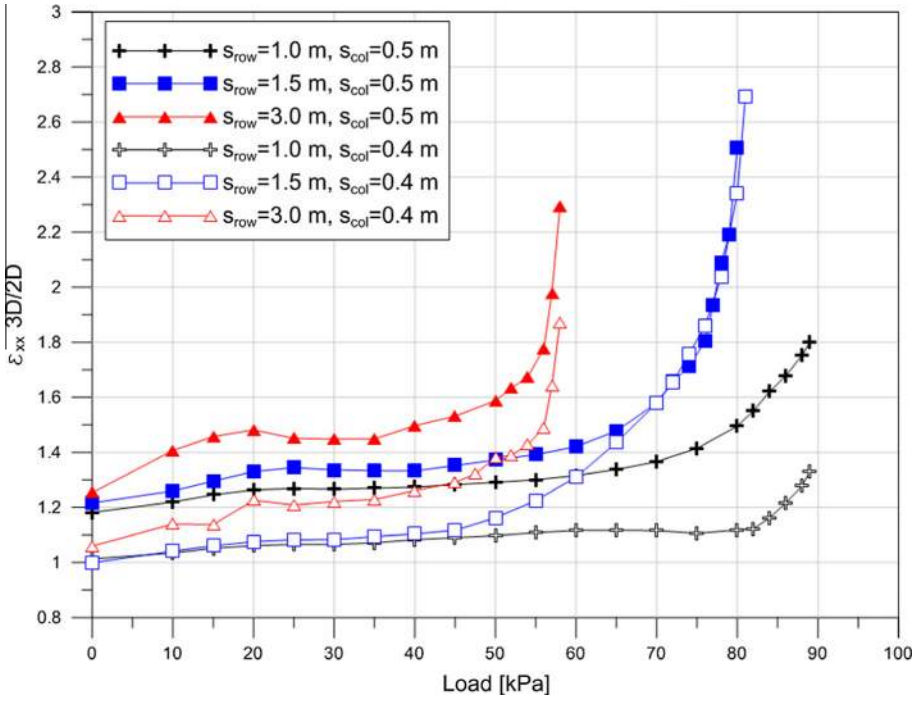

Fig. 7. Horizontal strain ratio, $\varepsilon_{x3D}/\varepsilon_{x2D}$, between 3D and 2D calculations; material properties of overlap zone equal to column material properties.

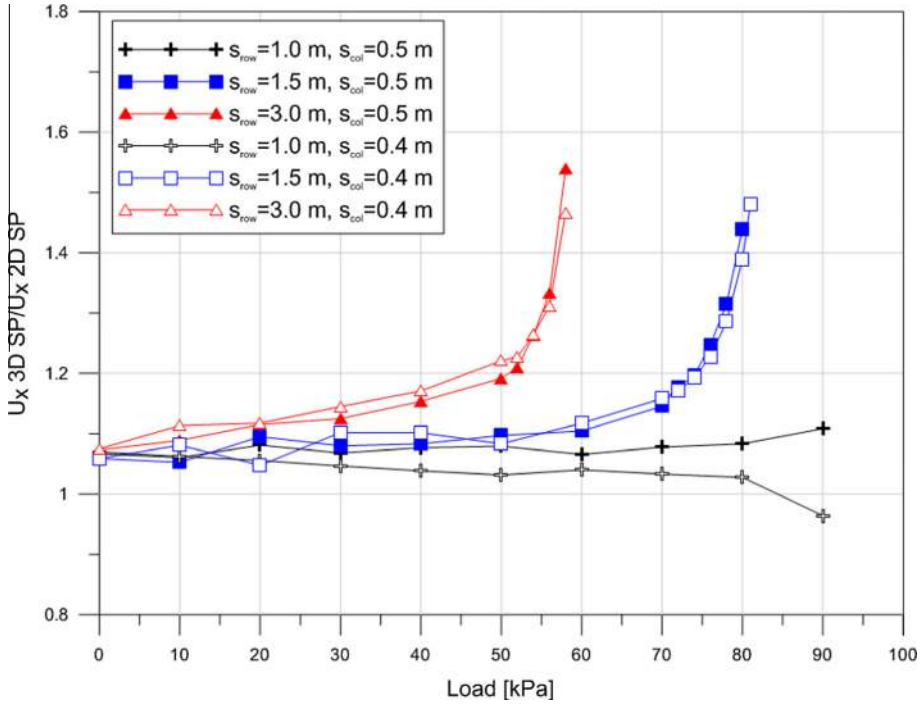

Fig. 8. Ratio between the maximum horizontal deformations of the sheet pile wall between the 3D and the 2D calculations, U_{x3D}/U_{x2D}; material properties of overlap zone equal to column material properties.

sheet pile wall). The results show that ε_x at failure decreases with the decreasing of s_{row} in both the 3D and the 2D analyses, indicating a more brittle failure when s_{row} decreases. The horizontal strain ratio, $\varepsilon_{x3D}/\varepsilon_{x2D}$, between the 3D and 2D analyses as a function of q is presented in Fig. 7 up to the level $q = q_{ult}$. After the excavation and before the load is applied, $\varepsilon_{x3D}/\varepsilon_{x2D}$ is equal to 1.15–1.25 and there

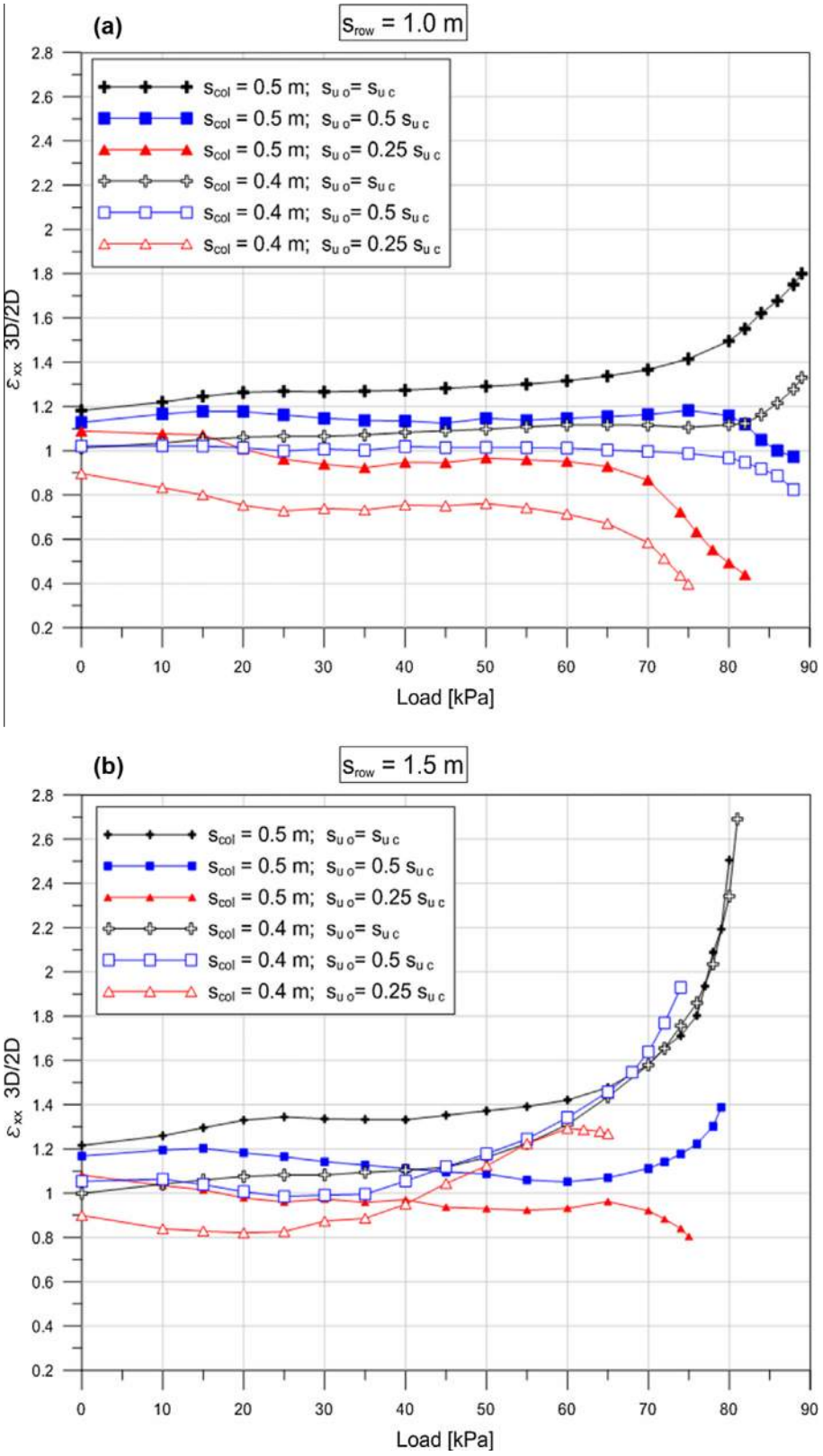

Fig. 9. Horizontal strain ratio, $\varepsilon_{x3D}/\varepsilon_{x2D}$, between 3D and 2D calculations; reduction of material strength properties in the overlap zones according to Table 1; (a) s_{row} = 1.0 m; (b) s_{row} = 1.5 m; (c) s_{row} = 3.0 m.

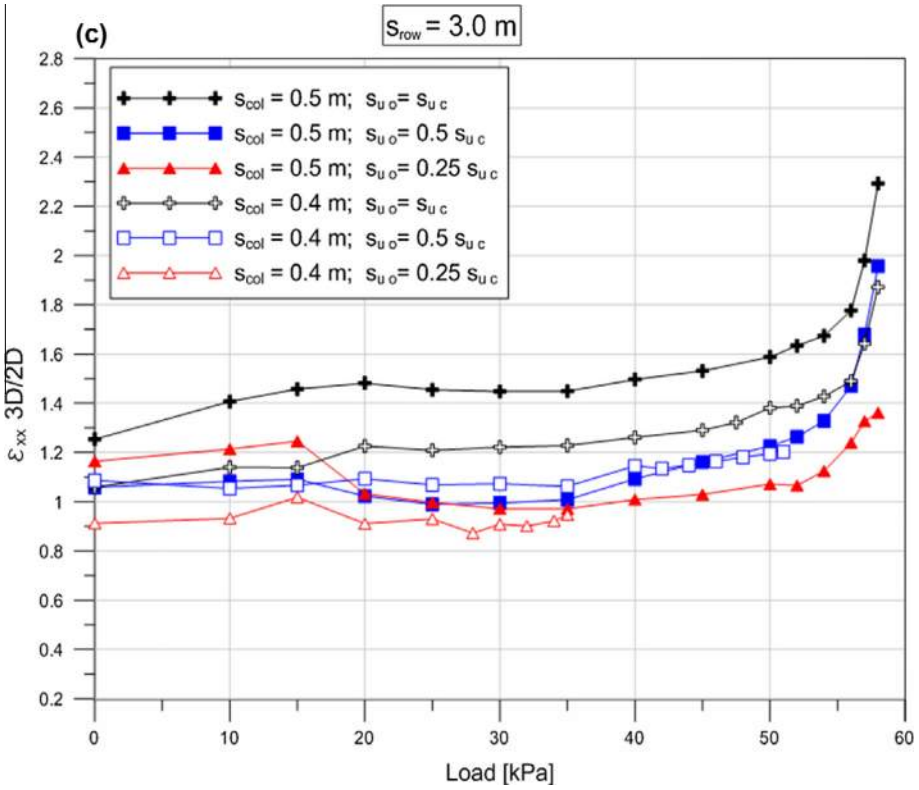

Fig. 9 (*continued*)

is no significant difference regarding s_{row}. After the load is applied, $\varepsilon_{x3D}/\varepsilon_{x2D}$ increases at first almost linearly for all studied cases. For all cases there is a distinct non-linear $\varepsilon_{x3D}/\varepsilon_{x2D}$ increase when q exceeds 65–90% of the evaluated q_{ult}.

The ratio between the maximum horizontal deformations of the sheet pile wall between the 3D and 2D analyses, U_{x3D}/U_{x2D}, as a function of q up to the evaluated q_{ult}, is presented in Fig. 8. The ratio of the horizontal deformations of the sheet pile wall show a similar behavior compared with the results of the horizontal strains ratio in the improved soil.

The results show that the 2D model can predict an q_{ult} that agrees well with the corresponding 3D analyses regardless of s_{row} and s_{col} for full overlap strength. Furthermore, by introducing vertical joints in the composite soil volume, the 2D model can effectively predict the load-induced shear stress in the column rows. This is shown in Fig. 11, where the ratio between the mobilized shear stress, τ_{mob}, and the maximum shear stress, τ_{max}, (where $\tau_{max} = s_u$) in the columns and the composite soil volume for s_{row} = 1.5 m, are displayed at 25%, 50%, 75% and 100% of q_{ult}. For a value of τ_{mob}/τ_{max} = 1.0, the full shear strength of the material has been mobilized and the material behavior changes from linear elastic to perfect plastic as the stated yielding criteria has been reached. The results show that yielding in both columns and composite soil volume is first reached in the overlapping zones closest to the toe of the sheet pile wall. This is due to the failure mechanism that develops where the sheet pile wall rotates around the anchorage level and the largest stress increase will be developed at the toe of the sheet pile wall. As q is increased, yielding will be reached in overlapping zones further and further out in the rows and propagates in a vertical direction. When material yielding is reached in a significant part of the overlap zones, the shear wall effect is lost in the 3D model and the stress in the columns increases until a slip failure mechanism develops. For the 3D model, the applied load is transfered mainly to the column rows due to the large stiffness difference between the soft soil and the columns at the interface with the sheet pile wall. In the 2D case, where the soft soil and the column rows are replaced with a composite soil volume, the stress increment is instead evenly distributed. Even though $s_{u,c}$ is higher than s_u of the composite soil, τ_{mob}/τ_{max} in the columns is significantly higher than in the 2D composite soil volume at q_{ult}. This implies that at q_{ult}, the yielding criterion has been reached in more part of the columns than in the composite soil volume and this is also shown in Fig. 12, where incremental γ_s, Mohr–Coulomb plastic points and deformed mesh at q_{ult} are shown for both the 3D and 2D models. The deformed mesh indicates that columns will fail by bending as two plastic hinges develop above and below the slip surface, starting with the columns closest to the sheet pile wall, and extends until a failure mechanism occurs in the entire structure. Since a large number of columns reach the yielding criteria, the 3D model will predict larger deformations.

The best agreement between the 3D and 2D analyses is, as expected, obtained for the case when s_{row} = 1.0 m. The results also shows that the obtained differences in deformations increases substantially when s_{row} is increased from 1.0 m to 1.5 m, but decreases when s_{row} increases from 1.5 m to 3.0 m. Depending on s_{col} (0.6–0.4 m) the area improvement ratio, a_s, is about 47–56% for s_{row} = 1.0 m, about 31.5–37% for s_{row} = 1.5 m and only about 15.7–18.5% for s_{row} = 3.0 m. The obtained results indicate that for a high a_s, the 3D and 2D calculations will render roughly the same results and this will also be the case when a_s is very low. This can be a subject for further studies by including more sophisticated models considering strength degradations that may drive the progressive failure process.

3.2. Effect of strength and stiffness properties in the overlapping zone

In this study, the effect of reducing the strength and stiffness properties of the column overlap zone by 50% and 75%, respectively, compared to the rest of the columns has been investigated.

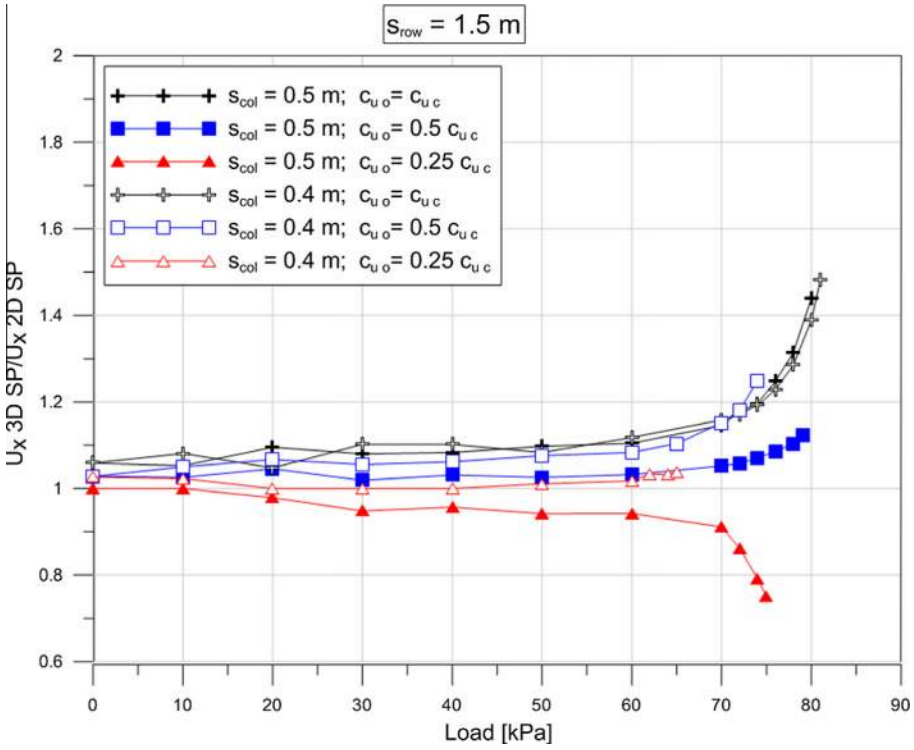

Fig. 10. Ratio of maximum horizontal deformations of sheet pile wall between 3D and 2D calculations, U_{x3D}/U_{x2D}, reduction of material strength properties in the overlap zones according to Table 1.

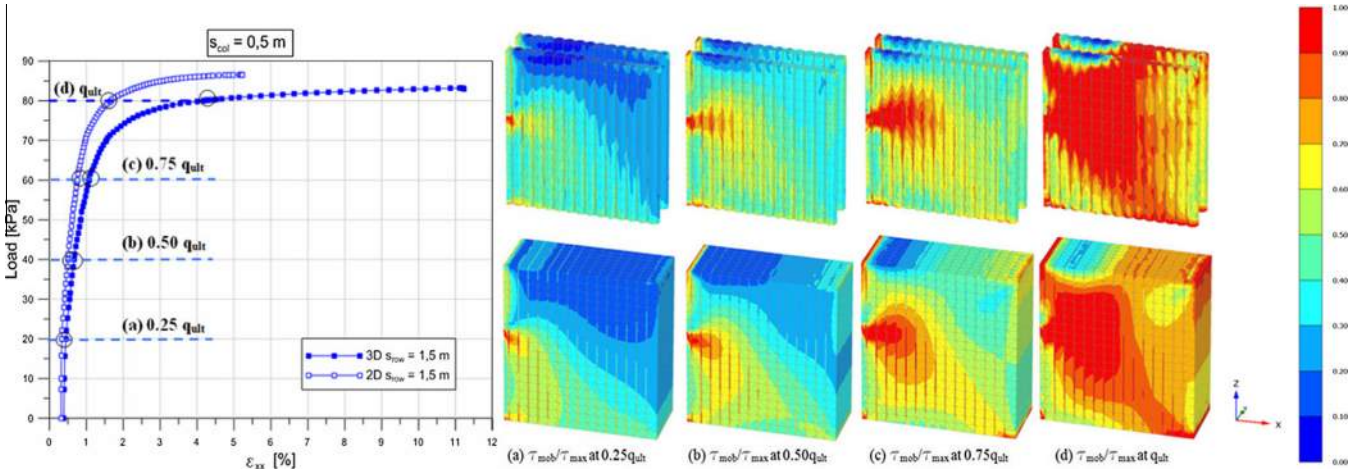

Fig. 11. Load–strain curve of 3D and 2D calculations with s_{row} = 1.5 m and s_{col} = 0.5 m. Snapshots of ratio between mobilized shear stress and maximal shear stress at 25, 50, 75 and 100% of q_{ult}.

The predicted q_{ult} is summarized for the conducted analyses in Table 5.

For 50% reduction of the overlap strength and stiffness properties, the evaluated q_{ult} from the load–strain relationship shows generally a good agreement between the 3D and 2D analyses. For 75% strength reduction of the overlap zones, the results show different trends. For s_{row} = 1.0 m and s_{col} = 0.5 m, the 3D analyses predicts about 7% higher q_{ult} than the 2D analyses and about 15% higher when s_{col} = 0.4 m. The opposite trend is obtained when s_{row} is increased to 3.0 m. For s_{col} = 0.5 m, the 3D analyses and 2D analyses predicts the same q_{ult}, but for s_{col} = 0.4 m the 3D analyses render about 20% lower q_{ult} compared to the 2D analyses.

The obtained results show that the material properties of the columns at the overlaps has a significant effect on the predicted q_{ult}. The results also show that the difference between predicted q_{ult} increases with increasing of the overlap area, A_o, and decreasing $s_{u,o}$. When the overlap distance between the columns, e, is increased from 0.1 to 0.2 m, A_o increases while A_c decreases, see Fig. 3, so the ratio A_o/A_c increases from 9.5% to 39%. A probable explanation is that when e is increased and at the same time $s_{u,o}$ is reduced to such a degree that the strength of the overlap zone is not much higher than the strength in the soft soil, the effect of the column row as a shear wall is lost and the columns will behave as single columns with a much lower stiffness and bending moment capacity compared to the shear wall.

Fig. 9a and c shows $\varepsilon_{x3D}/\varepsilon_{x2D}$ versus q up to the level at which q_{ult} is reached. The results of the calculation performed with no reduction of the overlap's zone strength and stiffness material properties

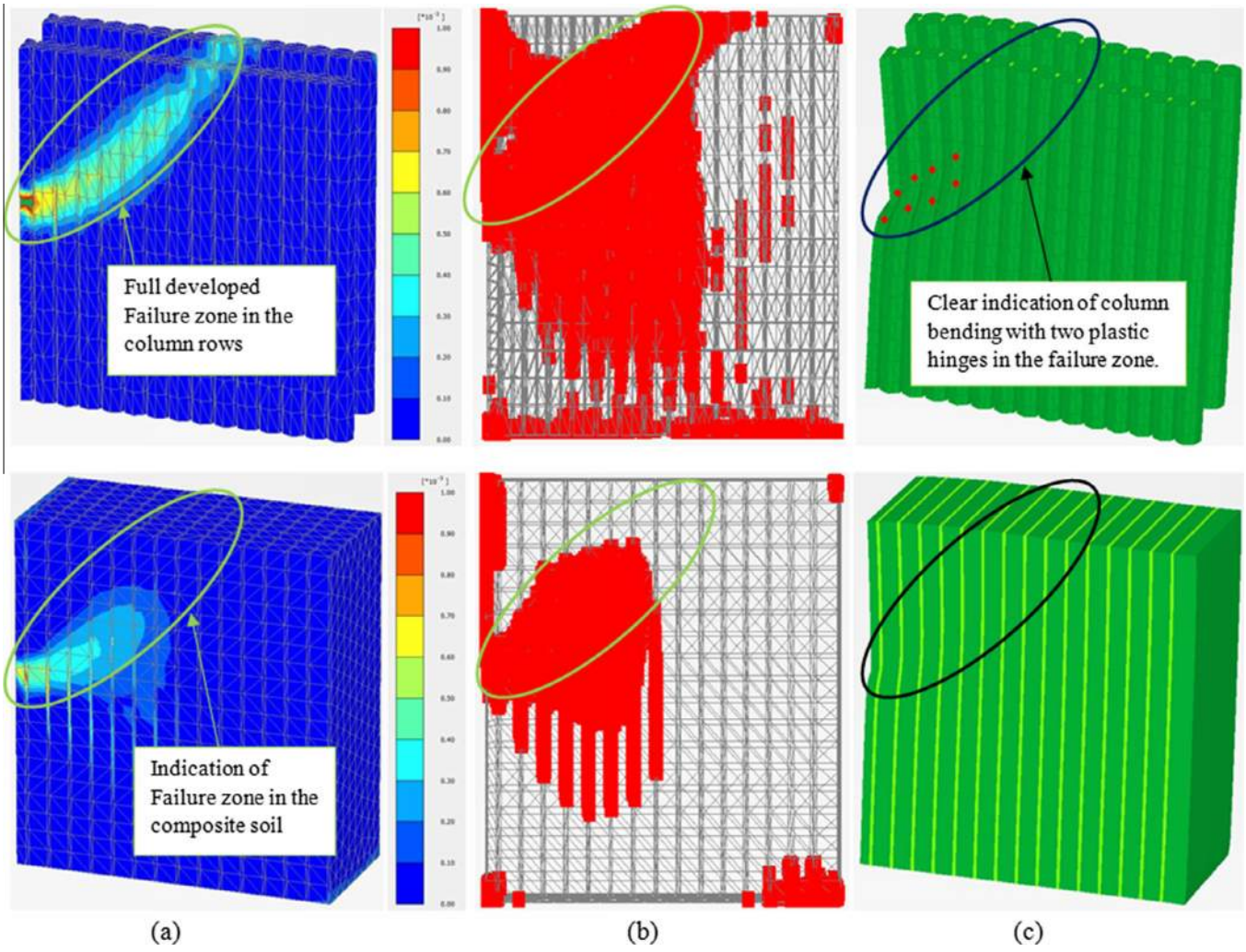

Fig. 12. Incremental deviatoric strain (a), Mohr–Coulomb plastic points (b), and Deformed mesh (c), at q_{ult} for s_{row} = 1.5 m and s_{col} = 0.5 m: Upper images 3D model, lower images 2D model.

Table 5
Evaluation of ultimate load for different shear strength reductions in the overlap zone.

s_{row} (m)	s_{col} (m)	0.5		0.4	
	Reduction of shear strength in overlap zone (%)	q_{ult} 3D (kPa)	q_{ult} 2D (kPa)	q_{ult} 3D (kPa)	q_{ult} 2D (kPa)
1.0	50	88	88	88	88
	75	88	82	86	75
1.5	50	79	79	74	75
	75	78	75	68	65
3.0	50	58	59	51	55
	75	58	58	35	44

has been incorporated for better comparison. For s_{row} = 1.0 m, $\varepsilon_{x3D}/\varepsilon_{x2D}$ is constant until approximately 80–90% of q_{ult} is reached. Above this load level, $\varepsilon_{x3D}/\varepsilon_{x2D}$ increases as q is further increased for an overlap strength equal to the column strength ($s_{uo} = s_{uc}$), but $\varepsilon_{x3D}/\varepsilon_{x2D}$ decreases as the overlap strength is reduced. The results also show that for an equal reduction in overlap strength $\varepsilon_{x3D}/\varepsilon_{x2D}$ decreases faster when the overlap area is increased (s_{col} decreases). For s_{row} = 3.0 m, the overall trend is that $\varepsilon_{x3D}/\varepsilon_{x2D}$ increases when q is increased, i.e. the 3D analysis predicts larger strains at q_{ult} regardless of overlap strength. For s_{row} = 1.5 m there is a much larger discrepancy in the results compared to s_{row} = 1.0 m and s_{row} = 3.0 m especially for s_{col} = 0.4 m and 75% reduction of overlap strength.

Fig. 10 shows the calculated U_{x3D}/U_{x2D} ratio for s_{row} = 1.5 m. The results indicate that U_{x3D}/U_{x2D} follows the same trend as $\varepsilon_{x3D}/\varepsilon_{x2D}$ shown in Fig. 9. Similar results are obtained for s_{row} = 1.0 m and s_{row} = 3.0 m.

The results of predicted strains and deformation of the sheet pile wall show different trends between the 2D and 3D analyses. A possible explanation that the obtained results are pointing in different direction is given here. For the 2D model, $s_{u,c2D}$ and $s_{u,o2D}$ is the calculated weighted shear strength of the composite soil, based on a_{sc} and a_{so}, respectively (Fig. 3). In the 3D model, the stress concentration in the columns at the same q increases with decreasing a_s. For high a_s (s_{row} = 1,0 m), the mobilized shear stress, τ_{mob}, in every individual columns row is below the material shear strength, τ_{max}, ($\tau_{mob}/\tau_{max} < 1.0$) at the load level where a larger part of the overlap zone has reached yielding ($\tau_{mob}/\tau_{max} = 1.0$) for the composite soil in the 2D model. When the yielding criterion in the vertical joints has been reached, further load increase will result in large plastic deformations in the composite soil volume. This is shown in Fig. 13, where it can be observed that for about 25% of q_{ult}, the yielding criterion has been reached in all 2D column overlaps. In the 3D model, however, τ_{mob} have reached τ_{max} only for limited parts of the overlaps zones at this load level. Yielding of a large part

of the vertical joints prevents load distribution through the composite soil volume as q is further increased. In the 2D model, an almost horizontal region, below and above the toe of the sheet pile wall, where the material yielding criterion has been reached, occurs in the entire improved soil volume at q_{ult}. For a high a_s, the calculated strains and deformations in the 2D model will therefore exceed the ones calculated in the 3D model. As s_{row} is increased, the load-induced horizontal stress in the column rows will also increase, which results in increased yielding in the overlap zone in the 3D model. The increased stress concentration in the columns combined with a weak overlap zone results in substantially more utilization of the columns' shear strength that will induce more yielding of the 3D model, especially in the columns closest to the sheet pile wall, as shown in Fig. 14. This implies that the 3D model will predict larger deformations when a_s is decreased and the overlap zones between the columns are weakened.

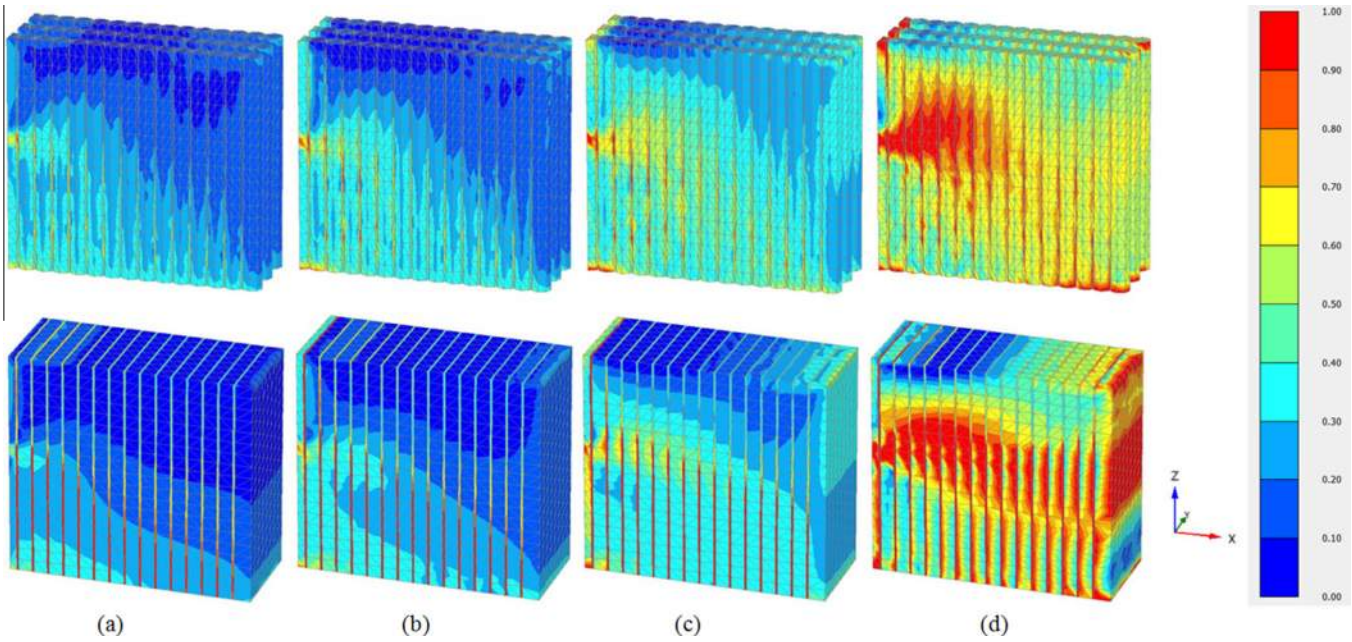

Fig. 13. Ratio between mobilized shear stress and maximal shear stress for s_{row} = 1.0 m and s_{col} = 0.5 m with 75% reduction of overlap strength. Upper images 3D model, lower images 2D model: (a) q = 0 kPa; (b) q = 20 kPa; (c) q = 40 kPa; (d) $q = q_{ult}$ = 82 kPa.

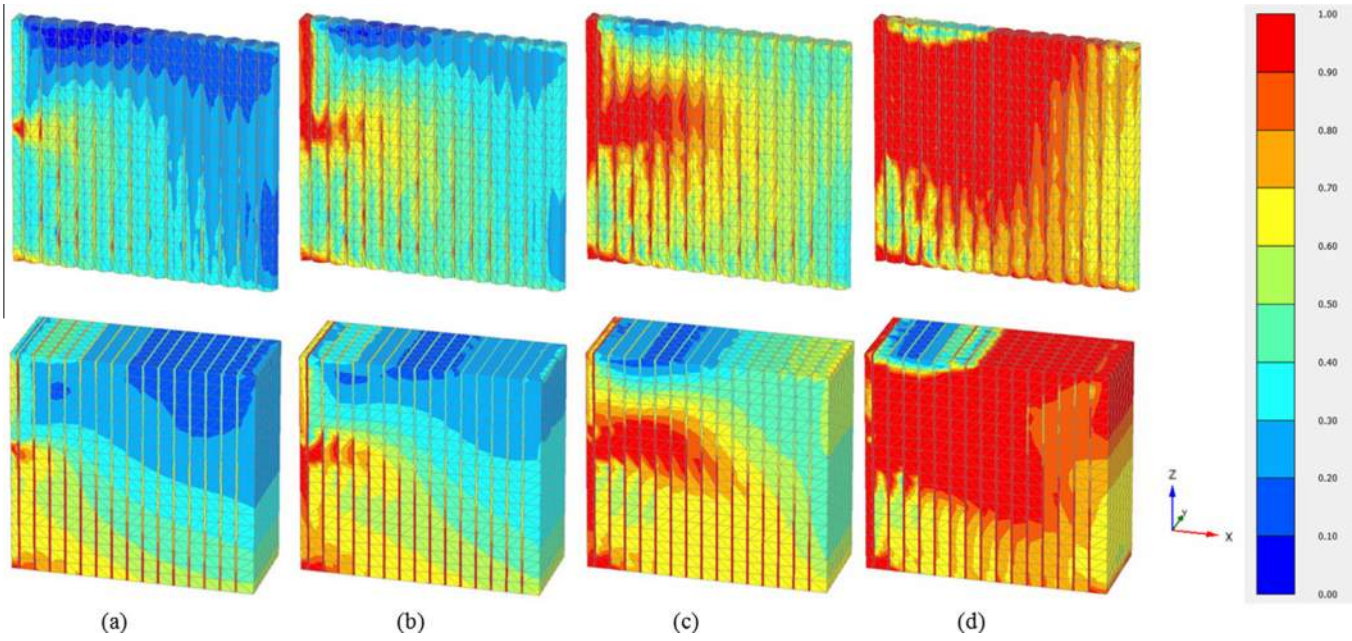

Fig. 14. Ratio between mobilized shear stress and maximal shear stress for s_{row} = 3.0 m and s_{col} = 0.5 m with 75% reduction of overlap strength. Upper images 3D model, lower images 2D model: (a) q = 0 kPa; (b) q = 20 kPa; (c) q = 40 kPa; (d) $q = q_{ult}$ = 58 kPa.

4. Conclusions

The following conclusions could be drawn based on the above analyses.

Regarding full overlap strength, there is good agreement between ultimate load predicted by the 2D and 3D analyses, regardless of spacing between the rows or overlap width. Similar results are obtained as regards reduction of overlap strength by less than 50%. For a width of overlap zone between columns of 0.2 m, the strength properties of the overlap zone have a significant effect on the predicted ultimate load. For a very poor overlap quality, 75% reduction of overlap strength, the 2D model generally predicts a lower ultimate load for a high area improvement ratio and a significantly higher ultimate load for a low area improvement ratio compared to a 3D model.

The results demonstrate that by taking into consideration the effect of the overlap zone between columns installed in a row pattern, a 2D plane strain model shows reasonably good agreement regarding obtained deformations compared to a 3D model, as long as the stress level in large parts of the stabilized soil does not reach the stated yielding criteria. In addition, the development of shear stresses in the overlap zones and columns in the rows due to loading, show good agreement between the 2D and the 3D model. The area improvement ratio has a significant influence on how well the prediction of calculated deformations agrees between the two models. In addition to the area replacement ratio, the quality of the overlap zone between columns has a great influence on the predicted deformation but even predicted ultimate load and the failure mechanism that occurs.

Based on these results, it is recommended that a 2D model should include the overlap zones between columns. For laterally loaded overlapping column rows with area replacement ratio of 15–50% and poor overlap quality, it is recommended that a 3D model should be use instead of a 2D model.

Acknowledgements

This study is part of the BIG (Better Interaction in Geotechnics) project and was funded by Skanska Sweden AB, the Development Fund of the Swedish Construction Industry and the Swedish Transport Administration.

References

[1] O'Rourke T, McGinn A. Lessons learned for ground movements and soil stabilization from the boston central artery. J Geotech Geoenviron Eng 2006;132(8):966–89.
[2] Wang J, Xu Z, Wang W. Wall and ground movements due to deep excavations in Shanghai soft soils. J Geotech Geoenviron Eng 2010;136(7):985–94.
[3] Andromalos K, Bahner E. The application of various deep mixing methods for excavation support systems. ASCE geotechnical special publication no. 120; 2003. p. 515–26.
[4] Mun B, Kim T, Moon T, Oh J. SCM wall in sand: numerical simulation and design implications. Eng Geol 2012;151:15–23.
[5] Gomes Correia A, Tinoco J, Pinto A, Tomásio R. An anchored retaining wall in CSM. In: 18th international conference on soil mechanics and geotechnical engineering (18th ICSMGE). Paris; 2013, p. 1987–90.
[6] Kivelö M. Stabilization of embankments on soft soil with lime/cement columns. PhD thesis. Stockholm: KTH Royale Institute of Technology; 1998.
[7] Broms BB. Stabilization of slopes with piles. In: Proceedings of the 1st international symposium of landslide control, Kyoto; 1972. p. 115–23.
[8] Broms BB. Progressive failure of lime, lime/cement and cement columns. In: Proceedings of the international conference on dry mix methods for deep soil stabilization. Stockholm; 1999. p 177–84.
[9] Kitazume M, Maruyama K. External stability of group column type deep mixing improved ground under embankment loading. Soils Found 2006;46(3):323–40.
[10] Kitazume M, Maruyama K. Internal stability of group column type deep mixing improved ground under embankment loading. Soils Found 2007;47(3):437–55.
[11] Kitazume M. Stability of group column type DM improved ground under embankment loading. Report Port Airport Res Inst 2008;47:1–53.
[12] Kitazume M, Yamamoto M, Udaka Y. Vertical bearing capacity of column type DMM ground with low improvement ratio. In: Proceedings of the international conference on dry mix methods for deep soil stabilization, Stockholm; 1999. p. 245–50.
[13] Horii, N, Toyosawa Y, Tamate S, Hashizume H, Okochi Y. Stability of composite ground improved by deep mixing method. In: Proceedings of the 2nd international conference on ground improvement techniques, Singapore; 1998. p. 193–198.
[14] Terashi M, Tanaka H. Ground improvement by deep mixing method. In: 10th international conference on soil mechanics and foundation engineering (10th ICSMFE), Stockholm; 1981, vol. 3. p. 777–80.
[15] Miyake M, Wada M, Kato Y. A study on horizontal resistance force of the ground improved by cement treated soil columns. Tokyo Construct Techn Res Rep 1996;23:59–64.
[16] Miyake M, Akamura H, Wada M. Deformation Characteristics of Ground Improved by a Group of Treated Soil. In: Proceedings of the international conference on centrifuge, Rotterdam, Balmema; 1991, p. 295–302.
[17] Navin MP, Filz GM. Numerical stability analyses of embankments supported on deep mixed columns. ASCE geotechnical special publication no. 152; 2006. p. 1–9.
[18] Navin MP. Stability of embankments founded on soft soil improved with deep-mixing-method columns. PhD dissertation, Virginia Polytechnic Institute and State University, Blacksburg VA; 2005.
[19] Han J, Chen J, Hong Z, Shen S. Mitigation of levee failures using deep mixed columns and geosynthetics. Geom Geoeng 2010;5(1):49–55.
[20] Han J, Oztoprak S, Parsons RL, Huang J. Numerical analysis of foundation columns to support widening of embankment. Comput Geotech 2007;34(6):435–48.
[21] Han J, Huang J, Porbaha A. 2D numerical modeling of a constructed geosynthetic-reinforced embankment over deep mixed columns. ASCE geotechnical special publication no. 131; 2005. p. 1–11.
[22] Huang J, Han J, Porbaha A. Two and three-dimensional modeling of DM columns under embankments. GeoCongress 2006, Geotechnical engineering in the Information technology age, ASCE, Atlanta, GA.
[23] Voottipruex P, Sukwasat T, Bergado DT, Jamsawang P. Numerical simulations and parametric study of SDCM and DCM piles under full scale axial and lateral loads. Comput Geotech 2011;38(3):318–29.
[24] Larsson S. Shear box apparatus for modeling chemical stabilized soil – introductory tests. In: Proceedings of the international conference on dry mix methods for deep soil stabilization, Stockholm; 1999. p. 115–21.
[25] Larsson S, Broms BB. Shear box model tests with lime/cement columns – some observations of failure mechanisms. In: Proceedings of geoeng 2000, Melbourne; 2000. p. 6.
[26] Larsson S, Malm R, Charbit B, Ansell A. Finite element modeling of laterally loaded lime-cement columns using a damage plasticity model. Comput Geotech 2012;44:48–57.
[27] Adams TE. Stability of levees and floodwalls supported by deep-mixed shear walls: five case studies in the New Orleans area. PhD dissertation, Virginia Polytechnic Institute and State University, Blacksburg VA; 2011.
[28] Adams TE, Filz GM, Navin M. Stability of embankments and levees on deep-mixed foundations. In: Proceedings of the international symposium on deep mixing and admixture stabilization, Okinawa; 2009. p. 305–10.
[29] Adams TE, Filz GM, Cali PR, Woodward ML. Stability analyses of a levee on deep-mixed columns, Plaquemines Parish, Louisiana. ASCE geotechnical special publication no. 178; 2008. p. 708–15.
[30] Adams TE, Filz GM, Cali PR, Woodward ML. Deformation and stability analuses of a pile supported t-wall with deep mixed shear panels in Plaquemines Parish, Louisianna. In: Proceedings of the 2nd International Conference GEDMAR08, Nanjing; 2008. p. 481–86.
[31] Filz GM, Templeton AE, Adams TE. Stability analyses for levees on deep-mixed shear walls. Ground Improvement 2011;164(3):117–26.
[32] Templeton AE, Boehm DW, McGuire MP, Filz GM. Design and construction of deep mixing at orleans avenue canal, New Orleans. ASCE geotechnical special publication no. 231; 2013. p. 2162–76.
[33] O'Rourke T, O'Donell CJ. Field behavior of excavation stabilized by deep soil mixing. J Geotech Geoenviron Eng 1997;123(6):516–24.
[34] Ou CY, Wu TS, Hsieh HS. Analysis of deep excavation with column type of ground improvement in soft clay. J Geotech Eng 1996;122(9):709–16.
[35] Ou CY, Teng FC, Wang IW. Analysis and design of partial ground improvement in deep excavations. Comput Geotech 2008;35(4):576–84.
[36] Ou CY, Hsieh PG, Lin YL. A parametric study of wall deflections in deep excavations with the installation of cross walls. Comput Geotech 2013;50:55–65.
[37] Tanaka H. Behaviour of braced excavations stabilized by deep mixing method. Soils Found 1993;33(2):105–15.
[38] Ruggeri P, Fruzzetti VME, Vita A, Segato D, Scarpelli G. Stiffness of wall-type grouting under transversal loading. Ground Improvement, published Mars 04, 2014, http://dx.doi.org/10.1680/grim.13.00047.
[39] Yang T, Tan TS, Leung CF. Mass behaviour of embedded improved soil raft in an excavation. Proc Inst Civ Engrs – Geot Eng 2011;164(GE1):11–25.
[40] Yoshida S. Shear strength of improved soils at lap-joint-face. In: Proceedings of the 2nd international conference on ground improvement geosystems, Tokyo, vol. 1; 1996. p. 461–66.

[41] Yoshizawa H, Okumura R, Hoshia Y, Sumi M, Yamada T. JGS TC Report: Factors affecting the quality of rested soil during execution of DMM. In: of the 2nd international conference on ground improvement geosystems, Tokyo, vol. 2; 1997. p. 931–37.
[42] Horpibulsuk S, Liu MD, Liyanapathirana DS, Suebsuk J. Behaviour of cemented clay simulated via the theretical framework of the structured cam clay model. Comput Geotech 2010;37(1–2):1–9.
[43] Suebsuk J, Horpibulsuk S, Liu MD. A critical state model for overconsolidated structured clays. Comput Geotech 2011;38(5):648–58.
[44] Yapage NNS, Liyanapathirana DS. Implementation of an elasto-plastic constitutive model for cement stabilized clay in a non-linear finite element analysis. Eng Comput 2013;30(1):74–96.
[45] Yapage NNS, Liyanapathirana DS, Poulos HG, Kelly RB, Leo CJ. Numerical modeling of geotextile reinforced embankments over deep cement mixed columns incorporating strain-softening behavior of columns. Int J Geom, published July 18, 2013, ISSN 1943–5622.0000341.
[46] Arroyo M, Ciantia M, Castellanza R, Gens A, Nova R. Simulation of cement-improved clay structures with a bonded elasto-plastic model: a practical approach. Comput Geotech 2012;45:140–50.
[47] TK Geo 11. Technical requirements for geoconstructions (Trafikverkets tekniska krav för geokonstruktioner). The Swedish Transport Administration, Publ. 2011:047, Borlänge, Sweden; 2011.
[48] Bruce ME, Berg RR, Collin JG, Filz GM, Terashi M, Yang DS. Federal Highway Administration Design Manual: Deep Mixing for Embankment and Foundation Support. Report No. FHWA-HRT-13-046, U.S. Department of Transportation, Federal Highway Administration, Washington; 2013.
[49] Kitazume M, Terashi M. The deep mixing method. CRC Press/Balkema; 2013.

Paper II

FIELD TEST OF BRACED EXCAVATION SUPPORTED WITH ROWS OF DRY DEEP MIXING COLUMNS

Ignat R., Baker S., Larsson S., 2015. Accepted for publication and presentation at Deep Mixing 2015, San Francisco, USA, June 2-5, 2015.
DFI.org/dfieventlp.asp?13237

FIELD TEST OF BRACED EXCAVATION SUPPORTED WITH ROWS OF DRY DEEP MIXING COLUMNS

Razvan Ignat, Skanska Sweden AB/Royal Institute of Technology, Stockholm, Sweden,
Phone: +46-708-290580, E-mail: razvan.ignat@skanska.se

Sadek Baker, Skanska Sweden AB, Stockholm, Sweden

Stefan Larsson, Royal Institute of Technology, Stockholm, Sweden

ABSTRACT
This paper describes the execution of two full-scale field tests where a braced steel sheet pile wall interacting with rows of overlapping dry deep mixing columns was first excavated and then loaded to failure. The aim of the tests is to provide insight of the performance of dry deep mixing column rows located in passive zone and interacting with a retaining structure. The column rows were installed perpendicular to the sheet pile walls with two different area ratios, i.e. different distanced between the column rows. Both tests were extensively instrumented with inclinometers, pore pressure transducers, bellow-hoses, earth pressure gauges and strain gauges mounted on the struts. Results of the performed tests will serve as development of design methods for excavation support with columns.

Keywords: Dry deep mixing, field test, excavation support

INTRODUCTION
Dry deep mixing has been used with good results to strengthen the soil when excavations are to be performed in locations with thick soft clay deposits. An application that has increased in recent years is to install columns on the passive side of the retaining structure. Columns can be installed in different patterns but rows, grids or blocks are the most common arrangement. The use of column type ground improvement installed on the passive side of a retaining structure has been documented for a few field cases, Tanaka (1993), O'Rourke et al. (1997b), O'Rourke and McGinn (2006), Ou et al. (2008). By improving the soil on the passive zone, the passive earth pressure in front of the retaining structure is increased. This has proven to reduce the excavation induced deflections behind the retaining structure, reduce the structural forces (bending moment in the retaining structure, strut and anchor forces) and improve the safety against basal heave failure. The main focus of the conducted measurements within these cases has been on recording deflections and structural forces on the retaining structure and there is very little documentation available of the stress-strain behavior of the improved soil acting on the passive side of the retaining structure.

Two full-scale tests of braced steel sheet pile walls interacting with rows of overlapping dry deep mixing columns were first excavated and then loaded to failure was conducted during the spring-summer of 2014. This paper briefly describes the test set up, instrumentation, test procedure and some selected results from one of the conducted tests.

SITE DESCRIPTION AND SOIL PROFILE
The full scale test was performed on an unexploited open field, with a size of 100x170 m, in the eastern part of Sweden, about 70 km northwest of Stockholm. At the location of the test area, the soil consists of a 1.0-1.5 m thick layer of dry crust followed by a soft post glacial clay layer, silt and sand above a till layer closest to the bedrock. The level of the bedrock varies from 14 to 22 m below the ground level. The thickness of the clay layer beneath the dry crust varies between 7-9 m. The first meter of the soft clay has been classified as gyttja clay and streaks/ shots of sulfide occur to a depth of about 4-5 m. From about 6-7 m depth the clay is varved with thin layers of silt and sand, which is

typical for the region. The undrained shear strength of the clay, s_u, obtained from field vane test is between 10-13 kPa to about 5 m depth and increase below 6 m depth with about 2 kPa/m, see Fig. 1. Performed oedometer tests shows that the clay is normally or slightly overconsolidated. Pore pressure measurements performed in the clay at 2, 5 and 7 m depth, indicates a pore pressure of 3-5 kPa below hydrostatic pressure.

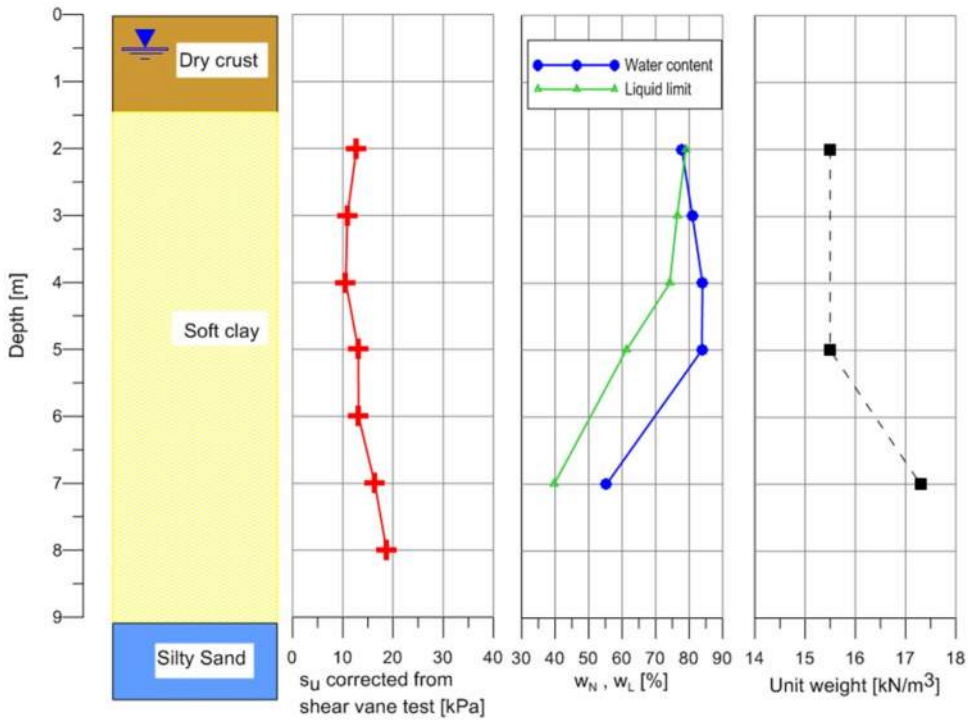

Figure 1: Soil profile and relevant parameters

DESCRIPTION OF TEST SET UP

The geometrical layout of both test areas was chosen identical. For the first test, the distance between the rows was chosen to 3.0 m while for the second test the distance between the rows was chosen to 1.5 m. Each test consisted of a steel sheet pile wall, SPW, with a crest length of 19.8 m installed parallel to each other, as illustrated in Fig 2. The SPW was installed to a depth of 7 m below the ground surface on the loading side and to 7.5 m on the opposite side. The length of the SPW was chosen so that a rotational stability failure was the expected failure mechanism. The SPW was braced at a level of 1 m below the ground surface with steel struts. The size of the excavated area at the bottom of the excavation pit was 14x12 m. The excavation to the planned level of 4.5 m below ground surface between the SPW was performed with open slopes and in order to improve the stability of the slopes, singular columns were installed behind the slope crest.

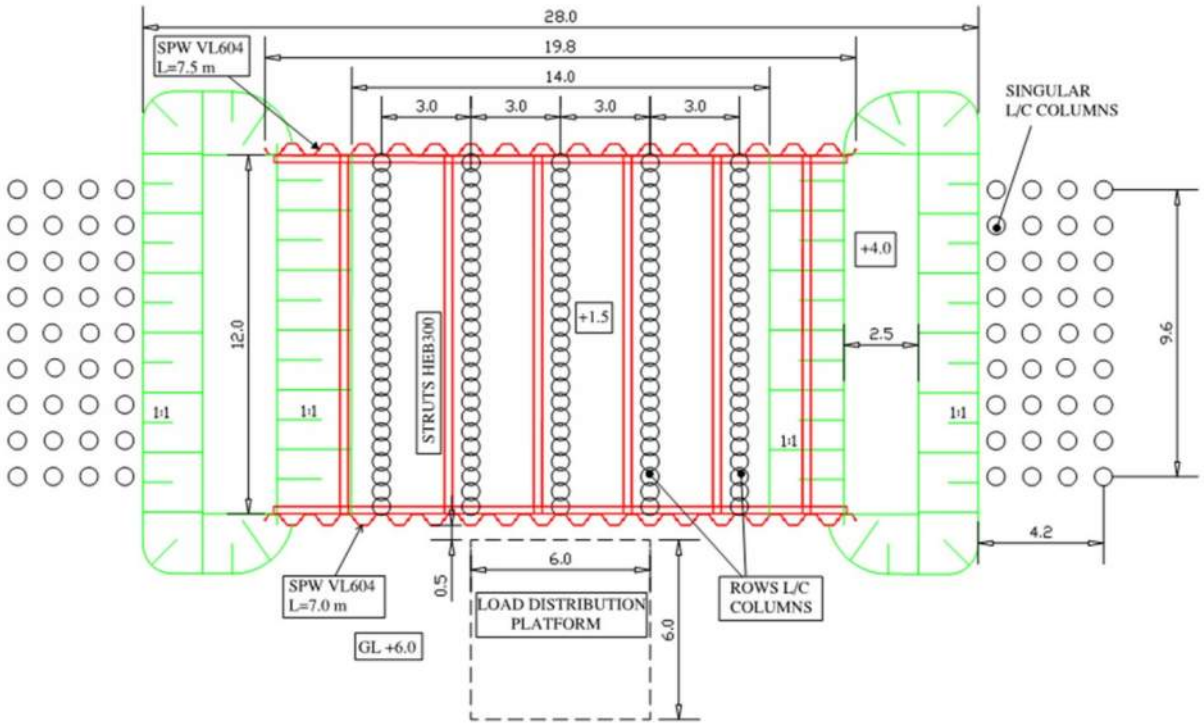

Figure 2: Plan view of geometrical layout for Test 1

INSTALLATION OF LIME/CEMENT COLUMNS

Installation of the columns was performed in April 2014. The binder content was 120 kg/m^3, 50% quicklime and 50% Portland cement. For Test 1, 5 rows of overlapping columns were installed and 9 rows of overlapping columns were installed for Test 2. Every row was composed of 24 columns with a diameter of 0.6 m and a center to center distance of 0.5 m, giving an improvement ratio of 17.5 % for Test 1 and 35% for Test 2. In order to ensure connection between the SPW and the column rows, the SPW in both test areas was installed 4-12 hours after the installations of the columns, in such a way so the SPW was driven through the last column in each row, see Fig. 2 and 3.

TEST PROCEDURE

The general working procedure from the start of excavation works was chosen identical for both Tests and is described below:

1. Excavation to a depth of 2.0 m below the ground surface
2. Installation of whale beams and struts at a level of 1.0 m below the ground surface
3. Excavation to a depth of 4.0 m below the ground surface
4. Excavation to final depth of 4.5 m below the ground surface with exception of a surface of about 0.5 m around the instruments
5. Construction of the load distribution platform and mounting of containers
6. Stepwise loading until a failure mechanism is obtained

Excavation was carried out with a long-range excavator. Due to the long reach of the machine, all the excavation work could be performed from the opposite side of the instrumented sheet pile wall. In order to not damage the instruments installed on the passive zone of the sheet pile wall, excavation closer than 0.5 m from the instruments was conducted with a 8 tons excavator with a very small blade and by hand between the instruments.

The load was applied after the excavation to full depth was performed. Loading was performed by filling two containers, with the size of 6.3x2.6x2.50 (L x B x H). Each container was positioned on steel frames that were placed above a load distribution platform, 6x6 m, see Fig. 4.
For Test 1 excavated clay masses was used as loading material in the containers. The load from the container was calculated as the average load measured by the 4 load cells under each steel frame. Filling in to the containers were performed using a long range excavator, located about 12 m from the loading area.


Figure 3: Photo 1: L/C columns and SPW installation; Figure 4: Photo of mounted container in Test1

INSTRUMENTATION

A total of 6 inclinometers were installed in each test area, two of them on the active side and four on the passive side. Two of the inclinometers on the passive side were installed in the center of the columns while the remaining two inclinometers were installed in between the column rows at a distance of 1.5 and 4.0 m from the center line of the SPW. On the active side the inclinometers were installed 0.5 m from the center line of the SPW and positioned in front of the instrumented column row and in between the column rows.

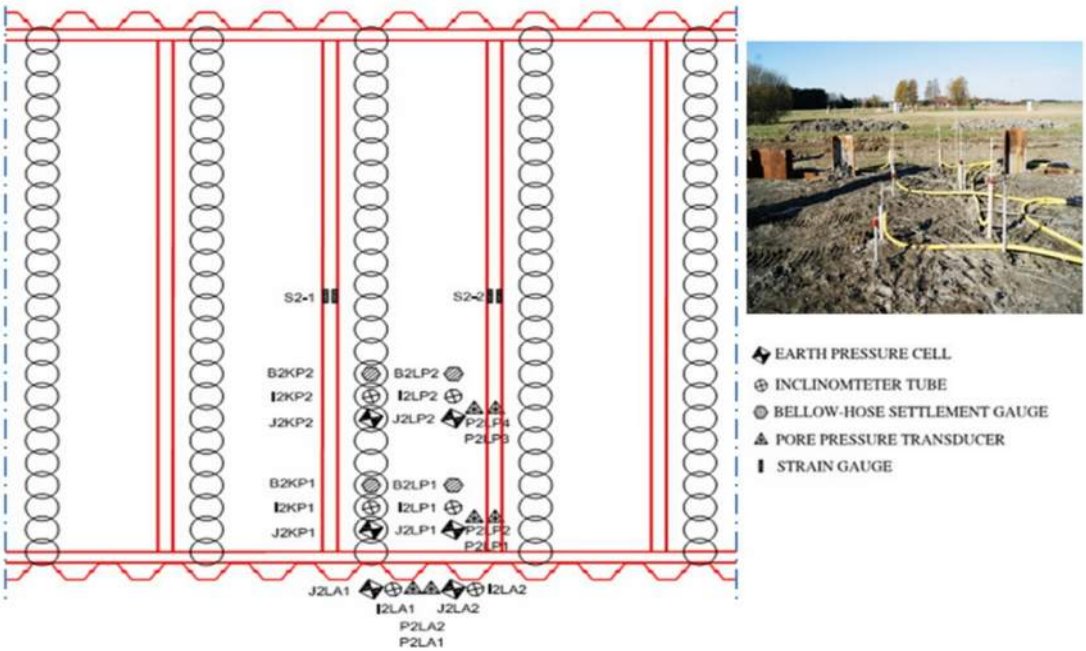

Figure 5: Instrumentation plan and photo of conducted instrumentation for Test 1

Six earth pressure cells with integrated pore pressure measurement were installed in each Test area. Position in plane was chosen very similar to that of the inclinometers, with two cells installed in the lime cement columns.
All the earth pressure cells on the passive side were installed at a depth of 5.5 m which is in between the planned excavation bottom and the toe of the SPW. The earth pressure cells on the active side of the SPW were installed at a depth of 5.5 and 6.5 m. Additional pore pressure measurements were performed through pore pressure transducers equipped with BAT MkIII filter tips installed in the clay on both active and passive zone of the SPW.

Excavation and loading induced vertical displacements in the soil/columns on the passive side of the SPW, was measured through four bellow-hoses installed in each test area. Two of the instruments were installed in the center of the columns and the two in the clay between the rows at a distance of 2.0 respectively 4.5 m from the center of the SPW. Strut forces were measured for two of the struts located in front of the loading area in each Test. Every strut was instrumented with four strain gauges, which were welded to the flanges of the strut. The external load applied on the active side of the SPW was measured by eight load cells.

All measurements, with exception of the vertical deformation measurements performed with bellow-hose settlement gauges, were collected automatically by connecting the measuring devices to GSM data loggers, allowing both the storage of data and transmitting it wireless to a server for near real-time viewing.

SELECTED RESULTS

Some selected results from Test 1 are presented and discussed here. Loading of Test 1 was conducted in 5 load stages, starting from about 12:00 PM, and a failure of the structure occurred at 20:55, about 2 hours and 15 minutes after the last load stage was applied, see Fig. 6.

Figure 6: Picture of failure of SPW

Readings from the inclinometers installed in the active zone and in the passive zone located 1.5 m from the SPW showed that the horizontal displacement, δ_h, start to increase linearly from the start of load step 4 at 17:20 and until about 20:30-20:40, see Fig. 7a-b. The displacement increment rate started to accelerate just prior to the load drop, both in the active zone and in inclinometers installed in the passive zone 1.5 m from the sheet pile wall. The results indicate that the failure is brittle with rather small deformations prior to the failure. The largest horizontal displacement behind the SPW was measured at a level corresponding to approximately 1.0 m above the bottom of the excavation (+2.5). During both the excavation and the loading stage, $\delta_{h\,col}$ is smaller then $\delta_{h\,clay}$ with a ratio $\delta_{h\,clay}/\delta_{h\,col}$ equal to 1.5-1.7 at the end of the excavation stage and 2.3-2.4 just prior to failure. For the inclinometers installed in the passive zone, 4.0 m from the sheet pile wall, δ_h remained constant until failure occurred at 20:55. A small increase of δ_h was measured just prior to the failure but at this distance from the SPW there was almost no difference between $\delta_{h\,clay}$ and $\delta_{h\,col}$.

The earth pressure change in the columns and the clay between the columns during excavation and loading is presented in Fig. 8a-b. During the excavation stages there is a large stress increase in the columns while the horizontal stresses in the clay are decreasing. The stress increase is larger in the column close to the SPW while the stress decrease in the clay is larger at 3.0 m than at 1.0 m from the SPW. These results show that the excavation induced load increment is transfer from the SPW mainly to the column rows, even at a space distance as large as 3.0 m between the column rows. During the loading stage the largest stress increase occurs as expected in the column located 1.0 m from SPW. Around 19:00, about 20 minutes after the last load cycle was applied, the horizontal stress in the column 1.0 m from SPW start to drop indicating that the column started yielding. An accelerating increase of horizontal stress in the clay at 1.0 m from the SPW can be observed from about 20:00 and until failure occurred, indicating a load transfer to the clay due to yielding of the columns.

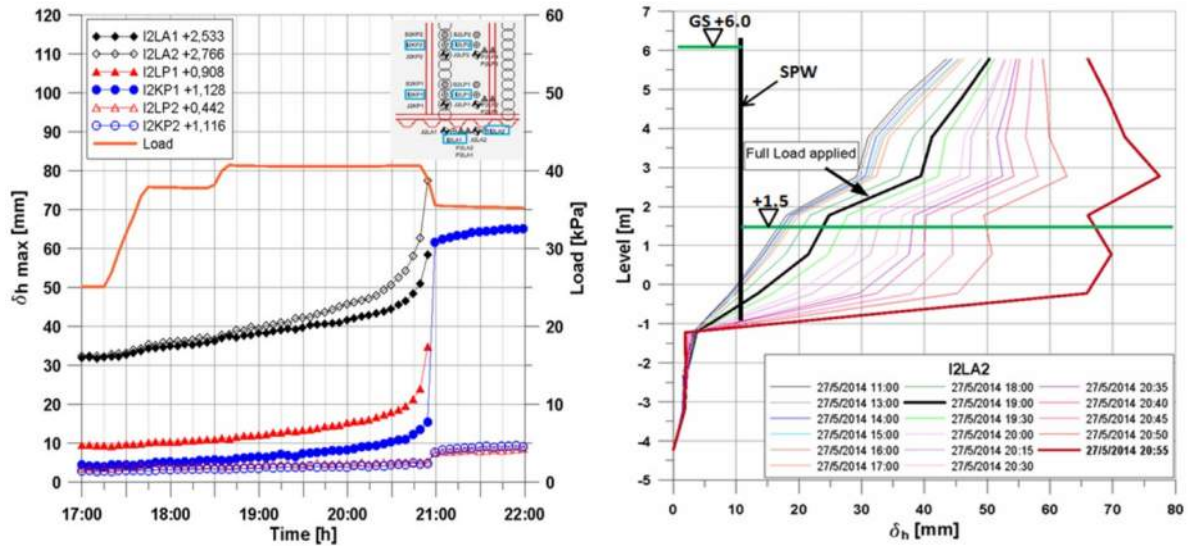

(a) *(b)*

Figure 7: *(a) Test 1: Maximum horizontal displacements and external load at failure*
(b) Test1: Load induced horizontal displacements in active zone (0.5 m from SPW)

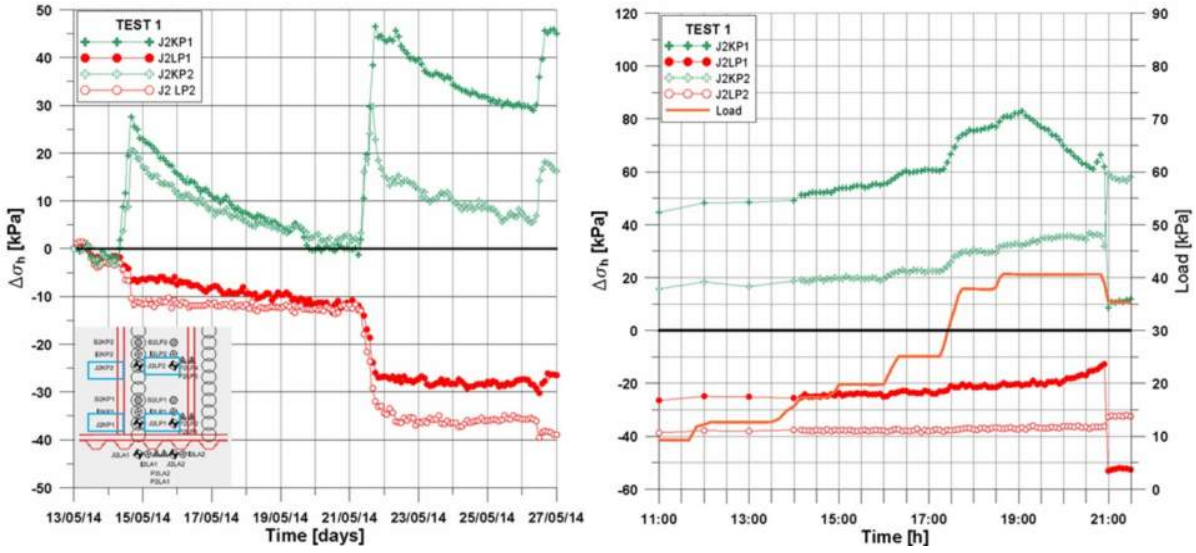

(a) *(b)*

Figure 8: *(a) Test1: Horizontal stress change during excavation stage*
(b) Test 1: Horizontal stress change during loading stage

CONCLUSIONS

This paper briefly describes the performance of two full scale tests for an excavation supported by rows of dry deep mixing columns for the purpose of studying behavior of the improved soil in the passive zone. Selected measurement results from one of the performed tests are presented here in order to illustrate the type of results that were obtained. The results are now being analyzed and in coming publications more detailed results from both tests will be presented.

AKNOWLEDGEMENTS

This study is part of the BIG (Better Interaction in Geotechnics) project. The authors acknowledge the support of Skanska Sweden AB, the Development Fund of the Swedish Construction Industry, the Swedish Transport Administration. The authors also thank Geometrik AB for the provided instruments and support related to the measurements, Ingefors Geoteknik AB for instrumentation help, and Cementa AB and Norkalk AB for the donation of the binders.

REFERENSES

O'Rourke T.D., O'Donell C.J., 1997. Field behavior of excavation stabilized by deep soil mixing. Journal of Geotechnical and Geoenvironmental Engineering; Vol.123(6):516-524.

O'Rourke T.D., McGinn A.J., 2006, Lessons learned for ground movements and soil stabilization from the boston central artery, Journal of Geotechnical and Geoenvironmental Engineering; Vol.131:966-989.

Ou C.Y., Teng F.C., Wang I.W., 2008. Analysis and design of partial ground improvement in deep excavations. Computers and Geotechnics; Vol.35(4):576-584.

Tanaka H., 1993. Behaviour of braced excavations stabilized by deep mixing method. Soils and Foundations; Vol. 33(2):105-115.